Aircraft Integration of Air-Based Thermal Management Systems for Propulsive Fuel Cell Systems

T.L.C. Hoogerdijk

Delft University of Technology

TU Delft

Aircraft Integration of Air-Based Thermal Management Systems for Propulsive Fuel Cell Systems

by

T.L.C. Hoogerdijk

to obtain the degree of Master of Science
at the Delft University of Technology,
to be defended publicly on Thursday the 11th of May 2023 at 09:30.

Student number: 4438329
Project duration: 27th of June 2022 – 11th of May 2023
Thesis committee:

Dr. ir. G. La Rocca,	TU Delft, Chair
Dr. F. Oliviero,	TU Delft, Responsible Thesis Supervisor
Dr. F. Yin,	TU Delft, Examiner

Cover: Fuel cell engine with a ducted heat exchanger retrofitted onto a De Havilland Canada Dash 8-300 by Universal Hydrogen. Photo taken by G. Norris, Senior Editor for Aviation Week & Space Technology. Published with written permission from G. Norris. Modified by D. Steijger.

This document has an equivalent word count of 30,740 words.
An electronic version of this thesis is available at `http://repository.tudelft.nl`.

TU Delft

Preface

This thesis is the culmination of my academic career working towards obtaining a Master of Science degree in Aerospace Engineering from the Delft University of Technology. The work before you presents the development of a thermal management system sizing methodology for propulsive fuel cell systems on 19-passenger commuter aircraft. Any reader with a background in aerospace engineering should be able to follow the report without hinder. A literature study detailing the working principle of fuel cells, fuel cell thermal management and thermal management on commercial aircraft is given to cover any gaps the reader may have in these areas. The thesis shows the importance of considering the design of fuel cell thermal management systems during the conceptual design of commercial fuel cell aircraft.

The topic of fuel cell thermal management is currently a hot topic in the aviation industry and multiple developments occurred during the thesis project. In December Embraer announced their Energia family of hybrid-electric concept aircraft. Though being only a concept, their hydrogen fuel cell aircraft clearly showed that they considered the challenges of fuel cell thermal management. In January ZeroAvia celebrated the first flight of their Dornier 228 aircraft retrofitted with a single fuel cell engine. The size of the aircraft's thermal management system is evident from photos of the aircraft. Not two months later, Universal Hydrogen flew the world's largest aircraft solely powered by hydrogen. The aircraft, a Dash 8-300 was retrofitted with a single fuel cell engine. Images of the aircraft showed the considerable size of the required thermal management system and inspired the system developed in this thesis. For this reason and in celebration of this momentous achievement by the team at Universal Hydrogen an image of their aircraft was chosen for the cover page of this thesis report. The image shows the wing-mounted fuel cell engine with ducted heat exchangers mounted on either side. I would to express my gratitude to G. Norris of Aviation Week & Space Technology for kindly providing permission to use his image.

This thesis project has been quite the journey and I would like to thank everyone who has supported me during this journey. I would like to thank Daniel for setting up the thesis project and providing insight into the fuel cell sizing models developed for the Initiator. I would like to thank Miha for helping me get to grips with the Initiator and providing further insight into Initiator's model. I would like to thank Maurice and Vincent for answering all and any questions I had about the Initiator, its inner workings and the errors that it presented to me. I would like to thank Fabio for providing insight into heat exchanger sizing and helping with the validation of the heat exchanger model. I would like to thank Carlo and Chiara for providing feedback on my work with their backgrounds in heat transfer for aerospace applications during my green light review. Lastly, I would like to thank Fabrizio for supervising me during my master thesis. Your guidance and support helped me greatly in achieving my thesis objective within the planned time.

I would also like to thank Olga, Lucia, Sarah, Sofia, Elise and Marloes with whom I shared a master thesis room. Our lunch breaks together and afternoon walks helped me to take a break, clear my mind and regain focus. I would like to thank all my friends in Delft for helping me wind down in the evenings and focusing my mind on the non-thesis aspects of life. Your support and our friendship during the last eight years have been greatly appreciated. I would like to thank all my friends and colleagues whom I have gotten to know during my time as a student. When I started studying I could never have imagined that I would meet such a great, interesting and inspiring group of friends and colleagues. You all made my time as a student the incredible experience that it was, one that I will never forget and reminisce about for the rest of my life. Lastly, I would like to thank my parents and my two sisters for all their support and following my academic journey no matter the distance between us. Without you, none of this would have been possible.

Tom Hoogerdijk
Delft, April 2023

Summary

Hydrogen is seen as one of the more promising energy carriers for the next generation of aircraft that will be more climate-friendly than the previous generation of kerosene-powered aircraft. Two types of hydrogen-based propulsion systems are currently foreseen for such aircraft: hydrogen combustion and hydrogen fuel cell. In addition to producing useful electrical power, fuel cell systems produce a considerable amount of heat. In proton-exchange membrane fuel cells, the amount of heat produced is of the same order of magnitude as the electrical power produced. This heat must be removed to ensure the continued and efficient operation of the fuel cell stack. A conventional thermal management system consists of a liquid cooling loop and a ducted air-liquid heat exchanger. The modelling of these systems for propulsive fuel cell systems on aircraft has previously been performed to various levels of detail. The objective of this thesis is to continue the development of these models by developing a thermal management sizing methodology for propulsive fuel cell systems on 19-passenger commuter aircraft. A sizing methodology is developed to model the additional mass, parasitic drag and parasitic power attributed to the thermal management system. The methodology sizes a cross-flow single-pass unmixed-unmixed air-liquid plate-fin heat exchanger using the ϵ-NTU method. The core drag is calculated based on the momentum loss through the ducted heat exchanger using isentropic relations. The external drag is modelled by increasing the engine nacelle to accommodate the heat exchanger. The coolant pump mass is empirically modelled using off-the-shelf coolant pumps and the pump power through physics-based equations. The developed sizing methodology is implemented into an aircraft sizing environment to study the characteristics of thermal management systems and their impact on aircraft performance. The Aircraft Design Initiator, developed in-house at the Delft University of Technology, is chosen as the aircraft sizing environment. The thesis goes further than previous literature by implementing an unconventional thermal management system which uses nanofluids as the liquid coolant. The developed and implemented sizing methodology is verified and validated against literature, commercial heat exchanger sizing software, experimental measurements and the propulsive fuel cell system installed on the HY4 fuel cell demonstrator aircraft.

The sizing methodology is run for various configurations of hybrid-electric aircraft based on four 19-passenger commuter aircraft. The Initiator ran smoothly and converged a realistic conceptual design for all aircraft. The results show that the thermal management system has both a direct and indirect effect on aircraft performance. The additional mass, parasitic drag and parasitic power attributed to the thermal management system directly increase the operating empty mass, zero-lift drag and fuel cell power requirement. The mass and drag are found to contribute around 3% to the operating empty mass and zero-lift drag coefficient. The contribution of the coolant pump power is found to be negligible in comparison to the total fuel cell power. The indirect snowball effect of these contributions increases the operating empty mass by around 26% compared to the same aircraft sized without considering the thermal management system. The use of nanofluids showed no considerable improvement in both system and aircraft level performance when compared to the base fluid. This was despite the improved coolant thermal conductivity which was counteracted by the increase in coolant density.

This thesis shows the importance of considering the design of thermal management systems during the conceptual design of fuel cell aircraft. Recommendations for future work include implementing a commercial heat exchanger sizing code, improving the ducted heat exchanger external drag model, developing a physic-based coolant pump model and improving the fuel cell heat model to consider, among other things, all heat sinks with the fuel cell stack. Once implemented, sensitivity studies into the effects of the heat exchanger core type, cooling plate channel geometry and trading-off maximising pressure drop through the heat exchanger to improve heat transfer performance against minimising the pressure drop to minimize core drag can be performed. These studies will provide insight into the optimization of thermal management systems for propulsive fuel cell systems onboard aircraft.

Contents

Preface i

Summary iii

Nomenclature viii

I Introduction 1

II Literature Study 5

II.1 Introduction 7

II.2 Fundamental Working Principle and Operation of Fuel Cells 9
II.2.1 Working Principle . . . 9
II.2.2 Heat Sources . . . 11
II.2.3 Operating Temperature Range of PEMFC . . . 11

II.3 Fuel Cell Thermal Management Techniques 12
II.3.1 Edge cooling . . . 12
II.3.1.1 Heat Spreaders . . . 12
II.3.1.2 Heat Pipes . . . 13
II.3.2 Air Cooling . . . 13
II.3.2.1 Cooling with Cathode Air flow . . . 14
II.3.2.2 Cooling with Separate Air flow . . . 14
II.3.3 Liquid Cooling . . . 14
II.3.3.1 Liquid Metal Cooling . . . 16
II.3.4 Two-phase Cooling . . . 16
II.3.4.1 Cooling through Boiling . . . 17
II.3.4.2 Evaporative Cooling . . . 17
II.3.5 Summary of Thermal Management Techniques . . . 18

II.4 Heat Sinks on Commercial Aircraft 19
II.4.1 Ambient Air . . . 19
II.4.1.1 Ram Air Cooling . . . 20
II.4.1.2 Surface Heat Exchanger . . . 22
II.4.1.3 Novel Skin Integrated Heat Exchangers . . . 23
II.4.1.4 Other . . . 23
II.4.2 Fuel . . . 24
II.4.3 Other Heat Sinks . . . 25

II.5 Current State of Fuel Cell Thermal Management Systems onboard Aircraft 27
II.5.1 Demonstrator Aircraft . . . 27
II.5.2 Conceptual Commercial Aircraft . . . 29

II.6 Effects of Fuel Cell Thermal Management Systems on Aircraft Performance 31
II.6.1 Modelling of Fuel Cell Thermal Management Systems for Aircraft . . . 31
II.6.1.1 Summary . . . 35
II.6.2 Parasitic Drag . . . 35
II.6.3 Additional Weight . . . 36
II.6.4 Parasitic Power . . . 37

II.7 Formulation of Research Objective and Research Questions 38

III Scientific Paper **41**

IV Supporting Work **75**

IV.1 Methodology **76**
IV.1.1 Nusselt Number . . . 76
IV.1.2 Colburn Factor and Fanning Friction Factor . . . 77
IV.1.3 Overall Heat Transfer Coefficient . . . 77
IV.1.4 Heat Exchanger Core Geometry . . . 78
IV.1.5 Heat Exchanger Geometric Relations . . . 79

IV.2 Verification and Validation **81**
IV.2.1 Validation of Thermophysical Properties of Water Ethylene Glycol Mixtures . . . 81
IV.2.2 Visual Comparison with Universal Hydrogen Dash 8 . . . 81

IV.3 Results and Discussion **84**
IV.3.1 Comparison of CS-23 Commuter Aircraft . . . 84
IV.3.2 Sensitivity Studies . . . 84
IV.3.2.1 Heat removed by the thermal management system . . . 84
IV.3.2.2 Heat exchanger design methodology inputs . . . 87
IV.3.3 Results of the Baseline Hybrid-Electric Aircraft Based on the Metro 23 . . . 87
IV.3.4 Answers to the Thesis Research Questions . . . 88

References **92**

List of Figures

II.2.1 Schematic diagram of a single proton-exchange membrane fuel cell. Public domain. . 10

II.3.1 Schematic of various fuel cell thermal management techniques by Hashmi [36] 13
II.3.2 Schematic of an example liquid cooling system by Fly [41] 15
II.3.3 Schematic of an example evaporative cooling system by Fly [41] 17

II.4.1 Graph of ambient air temperature as a function of altitude for various atmospheric models by van Heerden et al. [2] 20
II.4.2 Schematic of an example ram air cooling system by Nøland et al. [51] 21
II.4.3 Tail cone heat exchanger from Patent US 8,794,571 B2 23
II.4.4 Laminar flow control system with an integrated heat exchanger in vertical stabilizer from Patent US 10,618,636 B2 24

II.5.1 Images of flown fuel cell demonstrator aircraft 27
II.5.2 Schematic of the fuel cell thermal management, air delivery and hydrogen delivery systems on the ENFICA-FC Rapid 200FC by Romeo et al. [68] 29
II.5.3 Schematic of the fuel cell thermal management system proposed for the UNIFIER19 PVS1 concept aircraft by Eržen et al. [53] 30

IV.1.1 Colburn factor and Fanning friction factor as a function of Reynolds number for plate-fin type 12.00T from Kays and London [88] 77
IV.1.2 Thermal circuit (own work based on work by Shah and Sekulić [90]) 77
IV.1.3 Schematics of the heat exchanger core [88] 79

IV.2.1 Thermophysical properties of aqueous ethylene glycol as a function of mass fraction of ethylene glycol in water 82
IV.2.2 Comparison of the heat exchanger sized by the Initiator through the developed thermal management sizing methodology and the heat exchanger mounted on a fuel cell engine 83

IV.3.1 Comparison of thermal management system and aircraft level performance of four CS-23 commuter aircraft 85
IV.3.2 Selected plots from the sensitivity study of the percentage of stack heat removed by the thermal management system 86
IV.3.3 Colour plots of heat exchanger properties as function of allowable pressure drops on air side during take-off and coolant side 89
IV.3.4 Zero-lift drag coefficient breakdown of the baseline hybrid-electric aircraft 90
IV.3.5 Comparison of OEM for the baseline aircraft sized with and without considering the thermal management system 90
IV.3.6 Views of the baseline hybrid-electric aircraft based on the Metro 23 sized by the Initiator 91

List of Tables

II.5.1 Thermal management system data for the UNIFIER19 concept aircraft configurations from Eržen et al. [53] 30

II.6.1 Summary of fuel cell thermal management system modelling considering parasitic power, parasitic drag and system weight 35

IV.1.1 Dimensions of heat exchanger core based on plate-fin type 12.00T from Kays and London [88] 78

Nomenclature

List of Symbols

Symbol	Definition	Unit
A	Area	m^2
A_0	Free flow area	m^2
AR	Aspect ratio	-
b	Plate spacing	m
C	Heat capacity rate	W/K
$C_{D,0}$	Zero-lift drag coefficient	-
c_p	Specific heat capacity	J/kgK
C_r	Ratio of heat capacity rates	-
D	Drag force	N
D_h	Hydraulic diameter	m
e_0	Oswald efficiency factor	-
f	Fanning friction factor	-
f	Fin pitch	m
f_{Darcy}	Darcy friction factor	-
$F_{T,split}$	Temperature splitting factor	-
g	Acceleration due to gravity	m/s^2
$\bar{g}_f$	Molar Gibbs free energy of formation	J/mol
G	Mass velocity	kg/m^2s
h	Heat transfer coefficient	W/m^2K
h	Height	m
$\bar{h}_f$	Molar enthalpy	J/mol
j	Colburn factor	-
k	Thermal conductivity	W/m/K
K_c	Entrance loss coefficient	-
K_e	Exit loss coefficient	-
L	Length	m
L	Lift force	N
L/D	Lift to drag ratio	-
M	Mach number	-
m	Mass	kg
$\dot{m}$	Mass flow rate	kg/s
Nu	Nusselt number	-
N_p	Number of passages	-
p	Power	W
P	Pressure	Pa
Pr	Prandtl number	-
$\dot{Q}$	Heat transfer rate	W
$\dot{Q}/m$	Heat rejection parameter	kW/kg
R	Range	m
R	Thermal resistance	K/W
R_o	Total thermal resistance	K/W
$R_{specific}$	Specific gas constant	J/kgK
Re	Reynolds number	-
r_h	Hydraulic radius	m
S	Surface area	m^2

Symbol	Definition	Unit
SFC	Specific fuel consumption	g/Ns
t	Thickness	m
T	Temperature	K
U	Overall heat transfer coefficient	W/m^{2}K
v	Velocity	m/s
V	Volume	m^3
w	Width	m
W	Weight	N
α	Surface area density w.r.t. V_{tot}	m^2/m^3
β	Surface area density	m^2/m^3
γ	Heat capacity ratio	-
γ	Installation angle	rad
ϵ	Heat exchanger effectiveness	-
η	Efficiency	-
θ	Fin angle	rad
μ	Dynamic viscosity	Pas
ρ	Density	kg/m^3
ρ_{fin}	Fin density	1/inch
σ	Ratio of free flow area to frontal area	-
σ	Stefan-Boltzmann constant	W/m^{2}K^4
ϕ	Volume concentration	-
Ω_{mass}	Mass fraction	-
Ω_{vol}	Volume fraction	-

List of Subscripts and Superscripts

Symbol	Definition
∞	Freestream
0	Free flow
aw	Adiabatic wall
bf	Basefluid
CP	Coolant pump
cr	Cruise
EM	Electric motor
ext	External
FC	Fuel cell
FCS	Fuel cell system
HEX	Heat exchanger
LH_2	Liquid hydrogen
max	Maximum
nf	Nanofluid
np	Nanoparticle
ref	Reference
req	Required
to	Take-off
tot	Total
TMS	Thermal management system
$''$	Fouling factor

Introduction

Hydrogen is seen as one of the more promising energy carriers for the next generation of aircraft that will be more climate-friendly than the previous generation of kerosene powered aircraft[1,2,3]. Two types of hydrogen-based propulsion systems are currently foreseen for such aircraft: hydrogen combustion and hydrogen fuel cell. Hydrogen fuel cells have been found to have a greater *climate impact reduction potential* than hydrogen combustion[1]. This is mainly due to the low-temperature electrochemical reaction in which no CO_2 or NO_x is emitted during operation. In addition to producing useful power, fuel cells produce a considerable amount of heat. For proton-exchange membrane fuel cells (PEMFC) the heat produced is of the same order of magnitude as the electrical power produced [1]. This heat must be removed from the fuel cell stack to ensure its continued and efficient operation. Due to the low operating temperature of PEMFC (around 80°C), the heat to be removed is considered 'low quality' or 'low grade' [2]. This makes the heat transfer more challenging and limits the number of possible heat sinks [2]. The thermal management system is the sub-system tasked with removing heat from the fuel cell stack and dissipating it to a heat sink. The topic of thermal management is not only an important design challenge for fuel cell systems onboard aircraft but also for electrical systems (including battery systems) on more electric aircraft (including the Boeing 787), hybrid-electric aircraft and full-electric aircraft. In their review paper on the topic, van Heerden et al. state these *thermal management challenges are so severe that they are becoming one of the major impediments to improving aircraft performance and efficiency* [2]. Similarly, Schiltgen et al. state that *the heat rejection capability of an aircraft is an often understated limiting factor on performance which can have a significant impact on the design of the* aircraft [3]. The United Kingdom's Aerospace Technology Institute has specified developing *lightweight thermal management systems for hybrid- and all-electric aircraft as a priority activity* [2]. Due to the identified impact on aircraft design and aircraft performance, the design of thermal management systems (TMS) should be adequately considered during the conceptual design of such aircraft.

Literature was studied on fuel cell thermal management, aircraft thermal management and conceptual design methods of thermal management systems for propulsive fuel cell systems onboard aircraft. These conceptual design methods aim to model the effects of the additional mass, parasitic power and parasitic drag attributed to the thermal management system on aircraft design and aircraft performance. The additional mass directly affects the operating empty mass (OEM) and maximum take-off mass (MTOM). Increased aircraft mass increases the amount of lift required which increases the lift-induced drag and increases the power requirement from the fuel cell system requiring larger fuel cell systems. Increased aircraft weight also increases take-off and landing distances and decreases the rate of climb. The parasitic power of the thermal management systems increases the power requirement of the fuel cell increasing the system size and weight. The parasitic drag directly affects the zero-lift drag further affecting the power requirement of the fuel cell system. As presented in the following paragraphs the modelling of these contributions in literature has been performed to various levels of detail.

Kožulović [4] considered a water cooling system with a wing-mounted ducted counter-flow liquid-air heat exchanger sized for cruise in his preliminary design of a fuel cell thermal management[4]. The mass of the heat exchanger, coolant pipes and pumps were considered, the latter two indirectly through a factor applied to the heat exchanger mass. The parasitic power associated with the coolant pump was neglected due to its low power consumption when compared to the required aircraft power. The core drag was calculated using the momentum theorem and the ramjet effect was taken into account. The external drag of the ducted heat exchanger was estimated based on a drag coefficient value from Hoerner [5] for a wing-mounted nacelle close to the wing trailing edge. The author stated *that the external drag estimation was the element with the largest uncertainty in the current study, an issue which has to be addressed much more intensely in the future* [4]. Furthermore, the author recommends focusing on *aircraft-level integration of the large heat exchanger system, together with heat transfer enhancement methods* [4]. Guida and Minutillo [6] analyze the use of a PEMFC as an auxiliary power unit (APU) for a two-person light aircraft [6]. The mass of the heat exchanger is taken into account by multiplying the heat transferred by the specific power of an off-the-shelf heat exchanger [6]. It is inferred

[1] *Hydrogen-powered aviation. A fact-based study of hydrogen technology, economics, and climate impact by 2050.* McKinsey & Company, May 2020. URL: https://www.fch.europa.eu/sites/default/files/FCH%20Docs/20200507_Hydrogen%20Powered%20Aviation%20report_FINAL%20web%20%28ID%208706035%29.pdf Date accessed: 7 Mar. 2023.

[2] *Airbus reveals new zero-emission concept aircraft.* Airbus, September 2020. URL: https://www.airbus.com/en/newsroom/press-releases/2020-09-airbus-reveals-new-zero-emission-concept-aircraft Date accessed: 7 Mar. 2023.

[3] *Hydrogen | A future fuel for aviation?.* Roland Berger, March 2020. URL: https://www.rolandberger.com/publications/publication_pdf/roland_berger_hydrogen_the_future_fuel_for_aviation.pdf Date accessed: 7 Mar. 2023.

that the parasitic power and parasitic drag of the thermal management system are not considered in the sizing methodology. Snyder et al. [7] investigate the use of fuel cells in aircraft propulsion systems to further understand these systems and guide future research and analysis. The overall heat transfer coefficient and area-to-volume ratio were kept fixed in their modelling. The heat exchanger mass was found to be 16.3% of the complete fuel cell system [7]. Parasitic drag was not considered because *drag reduction and optimization were beyond the scope of this study* [7]. Commenting on this the authors state that preliminary analyses performed yielded designs that reduce parasitic drag to a *less than a 10 per cent increase in total drag* [7]. It was inferred that the parasitic power and mass of the rest of the thermal management system were not considered. Inacio et al. [8] study the use of liquid hydrogen storage on a PEMFC hybrid-electric aircraft by conceptually retrofitting a one-person crop dusting aircraft. The mass of the total cooling system was determined using the specific power of a single off-the-shelf PEMFC fuel cell. The cooling subsystem specific power of this PEMFC fuel cell was 2.27 kW/kg [8]. It was unclear whether the drag of the heat exchanger was considered in the aerodynamic modelling of the aircraft. Vredenborg and Thielecke [9] investigated the thermal management implications of a PEMFC APU on a commercial aircraft. The system mass, parasitic power and parasitic drag were all said to be considered. However, which specific components were considered was unclear from the paper. The mass of the pumps, pipes and fittings are also said to be considered in the model however which specific components are considered was not clear from the paper. Thirkell [10] modelled a propulsive fuel cell system to explore the use of fuel cells in aircraft. Though the topic of thermal management system was discussed, which thermal management system components were modelled was not discussed beyond stating that *simplified modelling strategies have been developed*, *that the fuel cell stack [was] treated as a single control volume* and *average stack thermal properties* were used [10]. It is inferred that because the topics of parasitic drag and heat exchanger sizing were not discussed in detail that these were not modelled. The variation in ambient air properties with regards to geographical location, altitude and time was discussed in some detail and specifically included in the model.

In Comincini's master thesis [11] a design methodology for propulsive PEMFC systems onboard aircraft was developed and analysed. No fuel cell thermal management system was defined in the design methodology. Commenting on the temperature of the fuel cell stack Comincini states that it *is supposed stable, but the way how this characteristic is achieved [...] is not defined* [11]. In Vonhoff's master thesis on the *Conceptual Design of Hydrogen Fuel Cell Aircraft* [12] the fuel cell thermal management system was considered in some detail. The design methodology was based on a methodology proposed by Chapman et al. [13]. This work presented the thermal design of a turboelectric 15-passenger vertical take-off and landing (VTOL) aircraft consisting of a liquid cooling system and a ducted heat exchanger [13]. In Vonhoff's model, cooling fan and coolant pump power were considered using equations adapted from correlations in Chapman et al. [13]. The mass of the cooling system was determined through an empirical equation adapted from Chapman et al. [13]. The mass of the coolant line, cooling fan, coolant pump and 'wet' heat exchanger were included in this mass calculation. A factor of 1.2 was included by Vonhoff on the powertrain mass calculation to *take into account auxiliary components, mounting and cables*. The parasitic drag was neglected as it was reasoned that *due to the action of the cooling fan pulling the air through the* heat exchanger there is a net zero thrust/ drag. Juschus [14] developed a propulsive PEMFC system sizing methodology for an aircraft sizing environment known as the Initiator. Concerning the fuel cell thermal management system, only the effects of the heat exchanger mass were considered. The heat exchanger was sized using the simplified model developed by Kožulović [4]. Furthermore, Juschus sized the thermal management system for cruise and not take-off which is seen as more challenging for the thermal management system.

A lot of research has been done into the modelling of thermal management systems for fuel cell systems onboard aircraft and understanding the effects on aircraft performance. No model found in open literature adequately considers all the effects of parasitic drag, additional weight and parasitic power on aircraft performance during the conceptual design phase. The objective of the thesis is to continue the development of these fuel cell thermal management system sizing models by modelling the parasitic drag, additional weight and parasitic power associated with air-based fuel cell thermal management systems. The focus will be on commuter aircraft in the aircraft category governed by the Certification Specifications for Normal-Category Aeroplanes (CS-23). This model will be implemented into an aircraft sizing environment to determine and understand the characteristics of fuel cell thermal management systems and their effects on aircraft performance. The model will go further than previous

literature by developing and implementing an unconventional thermal management system which uses nanofluids as the liquid coolant. This objective is formulated into the following research question:

"How can the parasitic drag, additional weight and parasitic power of air-based fuel cell thermal management systems be modelled during the conceptual design of CS-23 commuter aircraft and how do these contributions affect the performance of these fuel cell aircraft?"

This thesis contributes directly to the field of thermal management system modelling for propulsive fuel cell systems onboard aircraft by continuing the development of fuel cell thermal management system sizing methods for the conceptual design of CS-23 commuter aircraft. It directly continues to the development of the Initiator by improving the fuel cell sizing methods. For the first time a thermal management system using nanofluids as the liquid coolant is modelled and its effects on aircraft design and aircraft performance are studied.

The thesis is structured into four parts. Part II presents the literature study carried out on the topic of fuel cell thermal management with specific attention on the thermal management of propulsive fuel cell systems onboard aircraft. Topics include an introduction to the working principle of fuel cells, fuel cell thermal management techniques and the current state of fuel cell thermal management systems onboard aircraft. The subsequent thesis work is summarised in the scientific paper presented in Part III. The developed fuel cell thermal management system sizing methodology, verification and validation of the sizing methodology, main results, conclusions and recommendations are all given in this paper. Additional explanations of the developed sizing methodology, verification, validation and results omitted from the paper for conciseness and coherency are presented in part IV. Concise answers to the thesis research questions are also given in this final part.

II

Literature Study

Literature Study Summary

Sustainable aviation is the largest research field currently being worked on in the aerospace industry. The collective aim is to reduce the climate impact of the aviation industry. This is in part done by researching and developing aircraft with a significantly lower climate impact than current kerosene powered aircraft. Hydrogen is seen as one of the more promising energy carriers for this next generation of aircraft. Two types of hydrogen based propulsion systems are currently foreseen for such aircraft: hydrogen combustion and hydrogen fuel cell. The latter will be the focus of this report and subsequent thesis due to its larger impact on aircraft design and aircraft performance. The design and production of hydrogen powered aircraft is not without its challenges. One major challenge in using fuel cell systems is the thermal management of the heat released during operation. The heat released during operation of the fuel cell is of the same order of magnitude as the electrical power produced. One of the most promising fuel cell types for aviation is the proton-exchange membrane fuel cell (PEMFC) type. For a PEMFC to operate optimally the operating temperature of the stack must be kept within a certain temperature range. If the stack temperature is allowed to rise or fall outside this operating temperature range it will lead to performance loss and permanent damage.

It is the responsibility of the fuel cell thermal management system (TMS) to maintain the stack operating temperature within the operating temperature range. A TMS is based around a thermal management technique which transfers the heat produced within the stack to a coolant medium. The heat is then transferred away from the stack where the heat is dissipated to a heat sink. Many thermal management techniques are presented in literature and can be grouped into four categories: edge cooling, air cooling, liquid cooling and two-phase cooling. The most promising thermal management techniques for application in fuel cell systems on commercial aircraft are liquid cooling and two-phase cooling. Two main heat sinks exist on aircraft: the ambient air surrounding the aircraft and the fuel (liquid hydrogen). Other heat sinks proposed in literature include synergies with anti-icing systems, passenger services, phase change materials and thermoelectric generators. The ambient air heat sink with its various integration means, including ram air cooling and skin integrated heat exchangers is seen as the more promising heat sink for fuel cell thermal management systems. The other proposed heat sinks either can not provide the required amount of cooling or have a low technology readiness level (TRL). A fuel cell TMS may make use of a combination of heat sinks and/ or in conjunction with the TMS of other systems (e.g. electric motors).

Several fuel cell demonstrator aircraft have flown including the Boeing Fuel Cell Demonstrator, Antares DLR-H2 and ENFICA-FC Rapid 200-FC. These demonstrator aircraft all used a form of liquid cooling with an ambient air-liquid heat exchanger. Several concept fuel cell aircraft have been presented in open literature. These are the CHEETA concept aircraft and the UNIFIER19 concept aircraft. One thermal management system proposed for the CHEETA concept aircraft makes use of a coolant and ducted heat exchanger. Concept PVS1 presented in the UNIFIER19 project uses a liquid cooling system with a ducted heat exchanger. The conventional fuel cell thermal management system consists of a water cooling loop and a ducted heat exchanger.

Various efforts in open literature have modelled fuel cell thermal management systems. These models attempt to consider the effects of the fuel cell thermal management system on aircraft design and aircraft performance. These effects include the contribution of parasitic drag to total aircraft drag, the additional weight on OEM and the parasitic power on the aircraft's fuel cell power requirement. No model studied as found in open literature adequately considers the effects of parasitic drag, additional weight and parasitic power on aircraft performance during the preliminary and conceptual design phases. This is identified as a research gap in the field of fuel cell thermal management systems for commercial aircraft. These effects must be adequately considered during the preliminary and conceptual design phases as it affects aircraft performance including aircraft range, MTOM and fuel cell power requirement.

The objective of the subsequent master thesis is hence to **model the parasitic drag, additional weight and parasitic power associated with air-based fuel cell thermal management systems on CS-23 commuter fuel cell aircraft and determine their effects on aircraft performance**.

II.1

Introduction

Sustainable aviation is the largest research field currently being worked on in the aerospace industry. The aim is to reduce the climate impact of the aviation industry. This is in part done by researching and developing aircraft with a significantly lower climate impact than current kerosene powered aircraft. Hydrogen is seen as one of the more promising energy carriers for this next generation of aircraft[1,2,3]. Two types of hydrogen based propulsion systems are currently foreseen for such aircraft; hydrogen combustion and hydrogen fuel cell. The latter will be the focus of this report and subsequent master thesis due to its larger impact on aircraft design and development. The design and production of hydrogen powered aircraft is not without its challenges.

In addition to producing useful electricity, fuel cells produce a considerable amount of heat. This heat must be removed from the fuel cell in order to ensure continued and efficient operation. The thermal management system is tasked with removing heat from the fuel cell and dissipating it to a heat sink. The topic of thermal management is not only an important design challenge for fuel cell systems on aircraft but also for electrical systems (including battery systems) on more electric aircraft (including the Boeing 787) and hybrid electric aircraft. In one review paper on the topic the authors state that these *thermal management challenges are so severe that they are becoming one of the major impediments to improving aircraft performance and efficiency* [2]. In another paper the authors state that *the heat rejection capability of an aircraft is an often understated limiting factor on performance which can have a significant impact on the design of the* aircraft [3]. The United Kingdom's Aerospace Technology Institute has specified *the development of lightweight thermal management systems for hybrid- and all-electric aircraft as a priority activity* [2]. Due to the identified consequences at aircraft level and effects on aircraft performance it is vital that fuel cell thermal management systems are adequately considered during the preliminary and conceptual design phases of aircraft. In previous master theses completed at the TU Delft on the preliminary and conceptual design of fuel cell aircraft, including [14, 12], the parasitic drag, additional weight and parasitic power associated with fuel cell thermal management systems are inadequately taken into consideration.

The purpose of this report is to summarize the studied open literature on fuel cell thermal management systems. Specific attention is given to the topics of thermal management techniques, heat sinks on aircraft, the modelling of thermal management systems and the effect on aircraft performance. Based on the studied literature a research gap for a subsequent master thesis will be identified. Though the report is written to include as much background information as possible the reader is expected to have a background in (aerospace) engineering.

Chapter II.2 in this literature study report presents the working principle and operation of fuel cells in relation to heat generation and thermal management. Chapter II.3 presents and discusses a number

[1] *Hydrogen-powered aviation. A fact-based study of hydrogen technology, economics, and climate impact by 2050.* McKinsey & Company, May 2020. URL: https://www.fch.europa.eu/sites/default/files/FCH%20Docs/20200507_Hydrogen%20Powered%20Aviation%20report_FINAL%20web%20%28ID%208706035%29.pdf

[2] *Airbus reveals new zero-emission concept aircraft.* Airbus, September 2020. URL: https://www.airbus.com/en/newsroom/press-releases/2020-09-airbus-reveals-new-zero-emission-concept-aircraft

[3] *Hydrogen | A future fuel for aviation?.* Roland Berger, March 2020. URL: https://www.rolandberger.com/publications/publication_pdf/roland_berger_hydrogen_the_future_fuel_for_aviation.pdf

of techniques in which the heat generated within the fuel cell stack is removed from the stack. Chapter II.4 presents and discusses the various heat sinks available on an aircraft. A number of demonstrator aircraft have flown using fuel cell propulsion systems and a number of concept fuel cell aircraft have been proposed in open literature. These aircraft are discussed and presented in Chapter II.5 with specific attention given to the thermal management systems used. Chapter II.6 presents various efforts in the modelling of fuel cell thermal management systems from open literature. This chapter also discusses the effects of drag, weight and power on overall aircraft performance. The final chapter in this literature study report presents the research objective and research questions of the forthcoming master thesis in the field of fuel cell thermal management systems for commercial aircraft.

II.2

Fundamental Working Principle and Operation of Fuel Cells

Fuel cells are electrochemical devices that convert chemical energy into electrical energy. At the core of the fuel cell system is the fuel cell stack. This is where the electrochemical reactions take place and electricity is produced. The fundamental components of a fuel cell stack are the anode, cathode and electrolyte. Many different types of fuel cells exist. The major differences between the types are the electrochemical reactions taking place and the materials used within the stack. The most common type of fuel cell used in transport applications is the proton-exchange membrane fuel cell (PEMFC). Extensive reasoning for the use of PEMFC in transport applications is given in literature. A non-exhaustive list of these reasons is given below.

- High specific power [1, 7]
- Able to operate in dynamic environments (vibration and shock) [15]
- Quick start up time [1, 6, 7, 15]
- High technology readiness level (TRL) [1]
- Low noise [6]

Disadvantages of other fuel cell types for transport applications include longer start up times, use of corrosive and hazardous fluids and the production of greenhouse gases [15, 16]. The main focus of this literature study will hence be on the PEMFC type. This is not to discredit the potential use of different fuel cell types in aviation. Solid-oxide fuel cells (SOFC) are considered in literature as a potential alternative to PEMFC [1], including in combination with a gas turbine in a SOFC-GT system [17]. With continued research and development into the other types fuel cell may become applicable for aircraft.

This chapter presents the fundamentals of fuel cells with respect to thermal management. Section II.2.1 presents the fundamental working principle of PEMFC. Section II.2.2 briefly discusses the heat production mechanisms and spatial heat sources in PEMFC. The last section discusses the operating temperature range of PEMFC.

II.2.1 Working Principle

The fundamental working principle and components of a PEMFC are shown in Figure II.2.1. Gaseous hydrogen enters the cell on the anode side of the membrane electrode assembly (MEA). An oxidation reaction of hydrogen occurs at the anode side, aided by a catalyst (not shown in Figure II.2.1). The resulting electrons from the reaction are conducted into the anode and the H^+ ions (protons) pass through the electrolyte towards the cathode. This is why this type of fuel cell is called the 'proton exchange membrane' fuel cell. The oxidation reaction is shown in Equation II.2.1 [18]. The electrons pass via the conductive anode through the electric load generating an electric current. The electrons then pass on to the cathode side of the MEA. Here the electrons react with the oxidant (oxygen) and the H^+ ions which have passed through the electrolyte. The result of this reduction reaction is water

and is shown in Equation II.2.2 [15]. As on the anode side, the cathode reaction is aided by a catalyst. The reactions taking place at the anode and cathode are referred to in literature as half reactions [19].

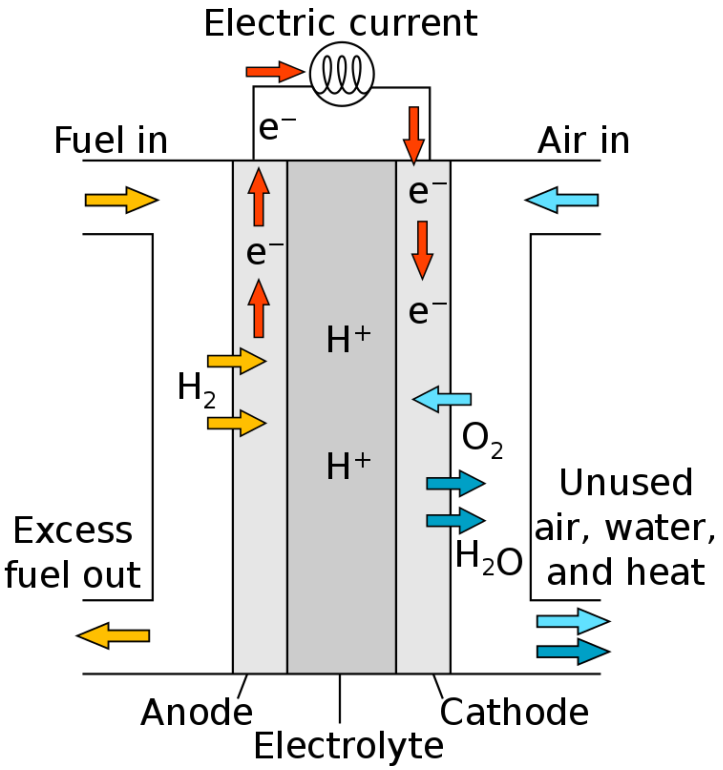

Figure II.2.1: Schematic diagram of a single proton-exchange membrane fuel cell. Public domain.

$$H_2 \longrightarrow 2\,H^+ + 2\,e^- \tag{II.2.1}$$

$$\frac{1}{2}\,O_2 + 2\,H^+ + 2\,e^- \longrightarrow H_2O \tag{II.2.2}$$

The complete chemical reaction taking place within a cell is given in Equation II.2.3 [15].

$$2\,H_2 + O_2 \longrightarrow 2\,H_2O \tag{II.2.3}$$

This electrochemical reaction has two byproducts; electrical work (electrical energy) and heat (thermal energy). The magnitude of each byproduct produced in the electrochemical reaction is indicated in the efficiency. The efficiency of a fuel cell is *the fraction of the energy in the fuel that is converted into useful electrical output* [15]. The thermodynamic efficiency of a fuel cell, as adapted from literature, is shown in Equation II.2.4 [15, 18]. This thermodynamic efficiency is the theoretical maximum efficiency of a fuel cell η_{max}.

$$\eta_{max} = \frac{\Delta\bar{g}_f}{\Delta\bar{h}_f} \tag{II.2.4}$$

$\Delta\bar{g}_f$ is the change in the molar Gibbs free energy of formation between the reactants (oxygen and hydrogen) and the product (water). $\Delta\bar{h}_f$ is the change in molar enthalpy. This last value depends on the state of the product water. If the water produced in the reduction reaction is in a gaseous state the lower heating value (LHV) of water is used. If the water produced condenses into a liquid state the higher heating value (HHV) of water is used.

The theoretical maximum efficiency for a PEMFC operating at 25°C is calculated to be 83% (HHV) [15]. This means that in an ideal PEMFC 83% of the chemical energy is converted into electrical energy. The remaining energy is converted into thermal energy i.e. waste heat [15]. The non-ideal practical efficiency of fuel cells is always lower than the theoretical maximum efficiency. The practical efficiency

of PEMFC is stated in literature to be in the 40-60% range [1, 18, 20] with 50% often quoted as the baseline [18, 20]. The difference between the theoretical maximum efficiency and practical efficiency is due to a number of irreversibilities. The four major irreversibilities as stated in literature are activation losses, internal currents & fuel crossover, Ohmic losses and concentration losses [1, 15].

II.2.2 Heat Sources

In the practical operation of fuel cells a large portion of the chemical energy that is not converted into electrical energy is converted into thermal energy. Literature states that the thermal energy produced in a PEMFC is approximately equal to the electrical energy produced i.e. an efficiency of around 50% [15, 21, 22]. Zhang and Kandlikar [23] state that there are four sources of heat generation during the operation of a PEMFC. These are *the entropic heat of reactions, the irreversible heat of electrochemical reactions, heat from the Ohmic resistances and heat from the condensation of water vapor* [23]. Rashidi et al. [24], Afshari et al. [25] and Huang et al. [26] concur with Zhang and Kandlikar [23] on these heat sources in a PEMFC. Huang et al. [26] in their review on the thermal management of PEMFC state that the entropic heat of reactions account for ~30% of the heat generated, the irreversible heat of electrochemical reactions for ~60% and heat from the Ohmic resistances for ~10%. The small remaining source of heat generated is attributed to the phase change of water. These values differ from values presented in a survey completed by Bargal et al. [27] on liquid cooling techniques in PEMFC. Here the values are given as 55%, 35% and 10% respectively [27]. Ramousse et al. [19] in their discussion and analysis on heat sources in PEMFC show that the contribution of heat sources varies with current density. This explains the discrepancy in heat sources values between Huang et al. [26] and Bargal et al. [27]. Ramousse et al. [19] go on to state that the irreversible heat of electrochemical reactions, referred to as activation overpotentials, generate the majority of the heat, regardless of the current density considered. This conclusion along with the values stated in Chen et al. [28] support the values presented by Huang et al. [26]. The heat sources are also distributed over the different components within the fuel cell stack [19, 28]. Though there may not be a complete consensus on the heat generation mechanism and heat source spatial locations, the complexity of the topic is acknowledged. This complexity adds to the complexity of modelling heat sources within PEMFC, especially when considering the conductive heat transfer between heat sources within the stack. This is important in the accurate thermodynamic modelling of fuel cell stacks and their thermal management systems.

II.2.3 Operating Temperature Range of PEMFC

In order for a PEMFC to operate optimally, the operating temperature of the fuel cell stack must be kept within a certain temperature range [24]. Low temperature PEMFC (LT-PEMFC) are stated in literature to have an operating temperature range of 60°C to 80°C [1, 20, 23, 29]. High temperature PEMFC (HT-PEMFC) are stated in literature to have an operating range of 160°C to 180°C [20]. If the stack temperature is allowed to rise above this range it will lead to material degradation [20, 23] and a loss of the self-humidification function of the cell [30]. This will lead to stack performance losses [20, 23]. If the stack temperatures decrease below the specific operating range it will lead to non favourable reaction kinetics [23, 24, 26] and flooding within the fuel cell [20, 23, 24, 29]. Both lead to reduced stack performance.

It is the responsibility of the thermal management system (TMS) of the fuel cell system to maintain the operating temperature within the specified temperature range. Different thermal management systems employ different thermal management techniques and heat sinks. Both of these will be discussed in the following chapters. The topic of thermal management is considered by many in literature as one of the most important technical challenges to be overcome in the wide scale adoption of PEMFC [29, 26]. That said not all of the heat generated within a fuel cell stack needs to be removed by the thermal management system. A small portion of the heat is used in the evaporation of water within the stack, is removed by the reactants or is removed through natural convection to the surrounding environment [26, 27, 31]. The total magnitude of these heat sinks are small [31] meaning the largest portion remains to be removed by the thermal management system, emphasising the importance of this system.

II.3

Fuel Cell Thermal Management Techniques

In the previous chapter the heat sources within a PEMFC were discussed. This chapter presents the various means by which this heat is removed from the fuel cell stack in order to maintain an acceptable fuel cell operating temperature. These means are referred to as thermal management techniques. In the studied literature numerous thermal management techniques for fuel cell systems are presented and discussed. Each technique has a range of different fuel cell power applications, advantages and disadvantages. The thermal management techniques have been grouped into four categories namely; edge cooling, air cooling, liquid cooling and two-phase cooling. This categorisation is based on the medium whereby the heat is removed from within the fuel cell stack. Edge cooling (Section II.3.1) makes use of highly thermally conductive materials and heat pipes to remove heat from the core of the stack and transport it to the edge of the stack. In air cooling and liquid cooling (Sections II.3.2 and II.3.3) the respective mediums are circulated through the fuel cell stack generally in an open loop and closed loop respectively. In two phase cooling (Section II.3.4) the coolant undergoes a phase change within the cooling loop. In the last section a summary and comparison of the thermal management techniques is given.

II.3.1 Edge cooling

In edge cooling the heat generated within the stack is transferred to the edge of the stack where it is convected to the ambient air. Two different heat transfer mechanisms were found in literature. The first uses highly thermally conductive materials known as heat spreaders [20, 26]. The second uses heat pipes [26]. In both techniques the heat is passively transferred from within the stack to the edge of the stack. In some applications the heat transfer from the edge of the stack to the ambient air is through forced convection through the use of fans. This would make such a system an active system.

II.3.1.1 Heat Spreaders

Heat spreaders use highly thermally conductive materials to transfer heat to the edge of the stack as shown in Figure II.3.1. Here the heat is convected to air through specially designed cooling fins [32]. Though this technique does not require cooing channels within the stack (reducing stack volume) it does require extra material adding weight to the stack [32]. The convection taking place at the edge of the stack may be natural, not requiring any parasitic power [20] or forced through the use of a powered fan. The highly thermally conductive materials required in these systems are costly [24, 32]. Wen and Huang [33] propose the use of pyrolytic graphite sheet (PGS) as heat spreader material. This material has a thermal conductivity of 600 to 800 W/mK [33]. Burke [34] analysed and studied what would be required to improve the performance of this thermal management technique. Burke [34] concluded that even with the use of materials with very high thermal conductivities such as highly oriented pyrolytic graphite (HOPG) (1500-1700 W/mK [34]) the maximum distance that the heat can be conducted remains below 10 cm. Tolji et al. [32] identified the need for meticulously designed cooling fins in order to *achieve uniform temperature distribution inside and along the stack* when designing an edge cooling thermal

management system for a 1 kW PEMFC. This may lead to increased design and manufacturing costs contradicting the low cost advantage of edge cooling as stated by Flückiger et al. [35].

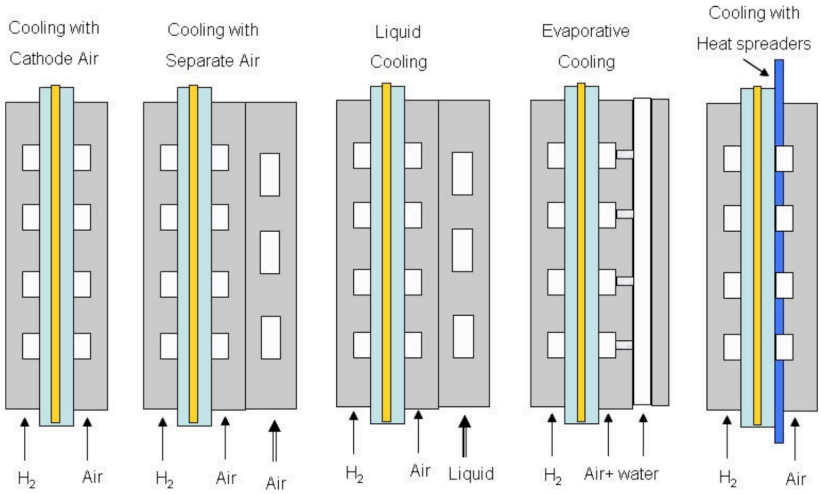

Figure II.3.1: Schematic of various fuel cell thermal management techniques by Hashmi [36]

II.3.1.2 Heat Pipes

Another means to transfer the heat from within the stack to the edge of the stack is through the use of heat pipes. These heat pipes have an extremely high effective thermal conductivity meaning small cross sectional pipes can be used [23]. The effective thermal conductivity of heat pipes ranges from 2100 to 50000 W/mK [37], much higher than the materials used as heat spreaders [26, 28]. Heat pipes are closed tubes containing a fluid that undergoes a phase change [37]. At the evaporator section of the pipe (hot side) heat is absorbed by the fluid resulting in evaporation [26]. The vapour is convected towards the condenser side of the pipe (cool side) where it releases the heat to ambient air condensing the fluid. The liquid is then transported back to the warm side through passive capillary action (commonly known as wicking) through a special coating at the circumference of the pipe [28, 37]. The condensed liquid can also be returned to the evaporator section by means of a pump or by gravity [26, 28]. The heat pipes are installed within the bipolar plates of the stack [37]. Different fluids and materials yield different effective thermal conductivities. Heat pipes are generally manufactured as cylindrical tubes. Other heat transfer devices making use of the same working principle but different geometrical sizes also exist and are referred to as vapour chambers. Vapour chambers often take the form of thin planar sheets. Zhang and Kandlikar [23] comment on an experiment completed by Burke et al. [38] which found that the measured effective thermally conductivity of the planar heat pipes were *an order of magnitude higher than that of HOPG composite* heat spreaders. Leakage of the fluid into the stack will lead to a reduction in cooling performance and may damage other components within the fuel cell stack [28]. The two-phase flow within the heat pipe may lead to instabilities and flow maldistribution leading to nonuniform temperatures within the stack, directly affecting fuel cell performance [26, 28].

Afshari et al. [25] state that edge cooling is employed in *low-power fuel cells* without specifying a magnitude. Rasidi et al. [24] state the upper power output limit to be 1 kW. Tolji et al. [32] detail a design with heat spreaders for a 1 kW PEMFC and Flückiger et al. [35] have verified their model using heat spreaders with a 0.5 kW PEMFC. Wen and Huang [33] tested their edge cooling design with heat spreaders on a 1 kW PEMFC. Zhang and Kandlikar [23] in their review of thermal management techniques say that different types of heat pipes can be used in PEMFC up to 1 kW. In summary, edge cooling is used in fuel cell stacks with quite low power outputs.

II.3.2 Air Cooling

Air cooling thermal management techniques cover all techniques where ambient air is the medium used to remove heat from within the stack. These thermal management techniques are generally used in lower power fuel cell stacks. The main advantage of air cooling is the low complexity. The main

disadvantage is that due to the low specific heat of air compared to liquids these thermal management techniques are not applicable in PEMFC with a high power output [26].

II.3.2.1 Cooling with Cathode Air flow

For lower power applications the cathode air flow (containing the oxidant) can be used to cool the cell. This is shown in Figure II.3.1. A major advantage of this thermal management technique is its simplicity [39]. If natural convection is used through the cathode it is referred to in literature as an air breathing fuel cell [22]. No active components are required with natural convection which reduces the weight and size of the system [24]. This also reduces the complexity of the system. To improve the cooling performance of this technique, a fan can be used to ensure forced convection between the cell and the cathode air flow [15]. Further improvement of this technique can be obtained by increasing the size of the cathode air flow fields. This however comes at a cost of cell size [22] which affects the power density. Because this thermal management technique occurs directly at the cathode it directly affects the reactions taking place and in turn, the electrochemical performance of the fuel cell [25]. Increasing the cathode airflow may be required for increased cooling performance but will lead to reduced humidity within the cell through the removal of water [26]. This drys out the membrane which reduces cell performance [15, 23, 24, 26, 39]. Decreasing the cathode airflow may not be sufficient in the cooling of the cell leading to an increasing temperature [39], also reducing cell performance. At a certain power level it is beneficial to separate the cooling airflow from the cathode airflow. This thermal management technique is presented in the following section.

Dicks and Rand [15] state that natural convection using cathode airflow can be used in PEMFC below 100 W. Islam et al. [39] states that cathode air cooling through forced convection is used in fuel cells with a power output in the range of 100-1000 W. Faghri and Guo [22] when discussing cathode air flow cooling conclude that if *the power of the fuel cell is higher than a few hundred watts, a more effective cooling approach must be applied*. In summary, edge cooling is used in fuel cell stacks with quite low power outputs.

II.3.2.2 Cooling with Separate Air flow

A separate airflow channel can be incorporated into the bipolar plates or as an additional separate cooling plate to increase the cooling performance of the stack [23, 26]. This thermal management technique is shown in Figure II.3.1. Hereby the cathode reactions can take place optimally without the influence of excess air and higher cathode air flow rates. A cooling fan is used to force air through the air cooling channels [23].

A large temperature gradient through the cooling channel is identified in literature as a big issue for this thermal management technique. Different flow orientations and flow speeds have been studied to minimize the thermal gradients within the cooling channels [26]. Optimizing these flow fields leads to improved cooling performance [26] and hence improved stack performance. Hmad and Dukhan [40] propose the use of metal foam through which air is circulated within the stack. In a study by Odabeaee et al. as discussed by Hmad and Dukhan [40] a water cooling system was compared with a metal-foam air-cooling system. It was found that the metal-foam air-cooling system required half the power of the water cooling system to remove the same amount of heat. Hmad and Dukhan [40] concluded in their own study that the use of a metal-foam air-cooling system *can be used for cooling fuel-cell stacks for a reasonable pumping power* and that further research is required to make a complete comparison between the two.

Dicks and Rand [15] state that air cooling with a separate channel is used in fuel cells with power outputs between 100 W and 1 kW. Xu et al. [21] and Bargal et al. [27] state that the applicability range of this technique is between 200 W and 2 kW. Zhang and Kandlikar [23] state this range to be between 100 W and 2 kW. For PEMFC with power outputs of greater than 5 kW Zhang and Kandlikar [23] state that liquid cooling may become more advantageous and provide the required cooling. In summary, edge cooling is used in fuel cell stacks with low power outputs.

II.3.3 Liquid Cooling

The most common thermal management technique used in higher power PEMFC is liquid cooling. The main reason for this is due to the higher heat capacity and thermal conductivity of liquids compared to air [23, 26, 39]. The resulting size of a liquid cooling system will be therefore smaller than an air cooling

system for the same cooling performance [15]. Coolants which are often used include deionized water [23] and mixtures of ethylene glycol and water [23, 26]. The heat generated within the stack is convected to the liquid coolant passing through cooling channels within the bipolar plates or dedicated cooling plates [23, 37] as shown in Figure II.3.1.. The heated liquid is then passed through a heat exchanger where the heat is rejected to a heat sink, usually ambient air. An example liquid cooling system is shown in Figure II.3.2 [41]. The hot liquid coolant can be transported over some distance allowing for the heat exchanger to be placed some distance away from the stack. The heat is not dumped in the proximity of the stack as is the case with edge cooling. Liquid cooling uses an active control system to alter the inlet coolant temperature and coolant flow rate to control the stack temperature [41, 42]. The active system consists of a coolant pump and a flow regulation valve [39]. This control system adds to the cost, weight, size and complexity of the complete system. Control methods for liquid cooling systems for PEMFC is an active research area [41]. Another issue in liquid cooling systems is the coolant becoming electrically conductive. This ionization of the coolant results from the uptake of ions on the bipolar plates or through oxidation of the coolant [23, 43]. An electrically conductive coolant can lead to current leakage, reducing stack efficiency and leading to bipolar plate damage, reducing stack performance [23]. Liquid cooling systems therefore include de-ionization filters in the coolant loop or add specific substances to the coolant to minimize the electrical conductivity. A drawback of using liquid cooling is that a large frontal area of the heat exchanger is required (if using ambient air as the heat sink). This is because of the small temperature difference between the stack and the ambient air [23, 42, 44].

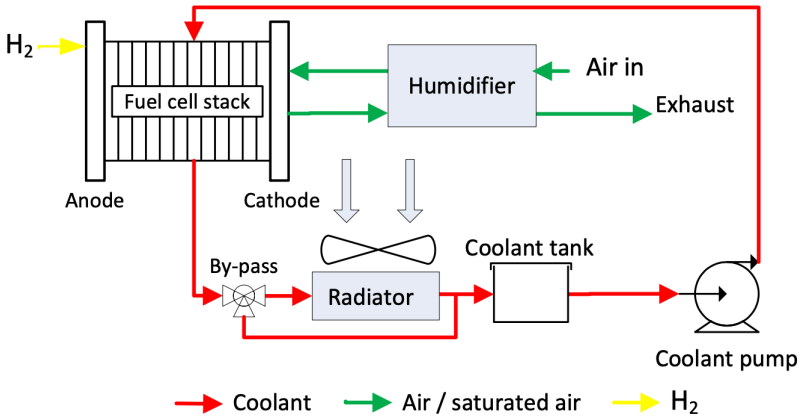

Figure II.3.2: Schematic of an example liquid cooling system by Fly [41]

Zhang and Kandlikar [23] state that liquid cooling is the most widely used thermal management technique in fuel cell stacks with a power output of greater than 5 kW. Zakaria et al. [43] and Dicks and Rand [15] concur with this statement. Zhang and Kandlikar [23] go on to say that this technique is extensively used in PEMFC vehicles where power outputs reach 80 kW or higher. Bargal et al. [27] in their survey of liquid cooling techniques do not state an upper fuel cell power limit for the use of a liquid cooling system in PEMFC. Most of the fuel cell vehicles using a PEMFC employ a liquid cooling system including both versions of the Toyota Mirai [21]. Because of this wide application range and large potential market liquid cooling systems for PEMFC is an active research area with the aim in improving cooling performance whilst reducing overall systems size and weight. This research and development is especially present in the automotive industry [23, 39, 44]. Research is specifically ongoing into optimizing coolant flow channels, development of coolants (high heat capacity and low electrical conductivity) and optimization of the complete liquid cooling system [23, 26, 27, 42, 43].

In the optimization of the flow fields within the coolant channels the main parameters considered are the uniformity of the temperature profile across the cooling plate and the pressure drop [23, 26, 27]. Attention is also given in literature to the geometry of the coolant channel in order to improve heat transfer between the cooling plates and the coolant [23]. Zhang and Kandlikar [23] and Bargal et al. [27] in their reviews of thermal management techniques address the design of chaotic laminar flow through the coolant channels. They concluded that chaotic laminar flow improved heat transfer between the cooling plates and the coolant. Chaotic flow channels do increase pressure losses but

Zhang and Kandlikar [23] state that the improved heat transfer outweighs the pressure losses.

Islam et al. [39] propose the use of nanofluids as coolants in PEMFC due to their superior heat transfer properties. The main advantages of nanofluids are stated to be the improved heat transfer performance, self de-ionizing mechanism, and lower freezing point [26, 37, 39]. The first two points mentioned lead to a smaller and lower weight overall system and lower parasitic power for the same cooing performance [39]. In a later article Islam et al. [45] model the use of nanofluids in PEMFC and claim that *by adding only 0.05 vol% of nanoparticles with 50/50 water/[ethylene glycol] mixture, the frontal area of the [heat exchanger] can be reduced by ~21% compared with the base fluid for same coolant mass flow rate*. Bargal et al. [27] and Huang et al. [26] in their reviews state that with the use of nanofluids the frontal area of heat exchangers are able to be reduced by up to ~30%. Challenges in using nanofluids mentioned by Islam et al. [39] include ensuring long-term stability and electrical conductivity. Possible solutions to this include adding inhibitors to the nanofluids to increase stability and decrease electrical conductivity [39]. Zakaria et al. [43] propose the use of Al_2O_3 in water ethylene glycol mixtures to improve the convective heat transfer coefficient of the coolant. In their experimental work they did notice an increase in required pumping power due to a higher pressure drop through the cooling channels [43].

II.3.3.1 Liquid Metal Cooling

Huang et al. [26] discuss the use of liquid metal as a coolant in PEMFC. The use of liquid metals in cooling applications has been used in other industries including computer chips and high power LEDs [26]. The major advantage of liquid metals is their very high thermal conductivity compared to water. Liquid metals also decrease the thermal resistance between components in the thermal management system. The major drawback of using liquid metals is the high density of these liquids leading to higher system weight. There are numerous challenges to the use of liquid metal cooling in PEMFC. Huang et al. [26] list the following; *exorbitant price, high pressure drop, the poor performance of the cold start, corrosion between common metals and liquid metal among others*. Despite the acknowledged challenges Huang et al. [26] merit research into the development of liquid metals with optimal properties for use in PEMFC.

II.3.4 Two-phase Cooling

Like liquid cooling, two-phase cooling consists of a fluid passing through a coolant loop. However in two-phase cooling the fluid undergoes a phase change. In literature this category of thermal management technique is also referred to as phase change cooling [23]. There are two thermal management techniques within this category; cooling through boiling and evaporative cooling. In the first, the boiling temperature of the coolant is below the stack operating temperature [23]. The opposite is true for the second technique [23, 26]. A major advantage of using these thermal management techniques is that the heat absorbed by a fluid, for example water, during a phase change (latent heat of vaporization) is far greater than what is absorbed by water without a phase change (sensible heat) [23, 26]. For reference the heat absorbed during vaporization (the latent heat of evaporation is 2250 kJ/kg) is over 500 times the sensible heat absorbed by liquid water leading to a temperature increase of 1°C [23]. This results in a lower required coolant flow rate to remove the same amount of heat as compared to water cooling [23, 46, 47]. This leads to the systems being more compact and cheaper [47].

Another advantage of these two thermal management techniques is the simplification of the complete cooling system when compared to liquid cooling [26, 28]. Coolant pumps are not required as other means can be utilized to pump the two phase fluid around the cooling loop. One such means is using the difference in density between the two phases of the coolant [23, 47]. Other means include by a difference in pressure through the loop or through hydrophilic wicking [23]. This reduces the size and parasitic power required by the cooling system increasing the specific power of the PEMFC. Another advantage presented by Baroutaij et al. [37] of this thermal management technique is the ability for two-phase cooling to provide a more uniform temperature distribution within the cell. This is beneficial for overall stack performance. As with liquid cooling, a disadvantage of two-phase cooling is coolant leakage and corrosion of materials [28].

II.3.4.1 Cooling through Boiling

In this two-phase thermal management technique, the coolant is required to have a boiling point below the operating temperature of the PEMFC [23]. This operating temperature range is 60°C to 80°C for LT-PEMFC [1, 20, 23, 29]. Water can hence not be used as a coolant unless the pressure is decreased within the fuel cell system [23]. A suitable coolant often mentioned in literature is HFE-7100 which has a boiling temperature of 61°C at 1 atm [23]. A disadvantage of this thermal management technique is two-phase flow instabilities [23, 28].

In studies completed by Choi and Park and discussed in Huang et al. [26] cooling through boiling with HFE-7100 was compared with single phase water cooling. They found that *better temperature maintenance and temperature uniformity was achieved by adopting the two-phase HFE-7100 cooling method as compared to the single-phase water-cooling method* [26]. Fly and Thring [42] state that cooling through boiling has the potential to reduce heat exchanger size due to the high heat transfer coefficients seen in the condenser. In a study into cooling through boiling Soupremanien et al. [48] conclude that the heat transfer performance of cooling through boiling is better than liquid cooling.

Cooling through boiling cooling systems are stated to be used in PEMFC with power outputs of greater than 10 kW [24, 37].

II.3.4.2 Evaporative Cooling

In evaporative cooling, the boiling temperature of the coolant must be above the operating temperature of the PEMFC. Water has a boiling point around 100°C and is hence a suitable coolant for evaporative cooling in LT-PEMFC. Another major advantage of using water is the synergy between the humidification of the membrane and the thermal management of the cell [23, 26]. This synergy is often utilized in evaporative cooling systems [42] as it removes the need for a separate humidification system [41]. Zhang et al. [23] state there are three main approaches in evaporative cooling systems for PEMFC. These are: *a) direct introduction of the liquid water into the reactant gas channels, (b) bipolar plates with in-plane wicking material, or (c) porous water transport bipolar plates*. Approach (b) and/ or (c) is shown in Figure II.3.1. An example evaporative cooling system is shown in Figure II.3.3 [41].

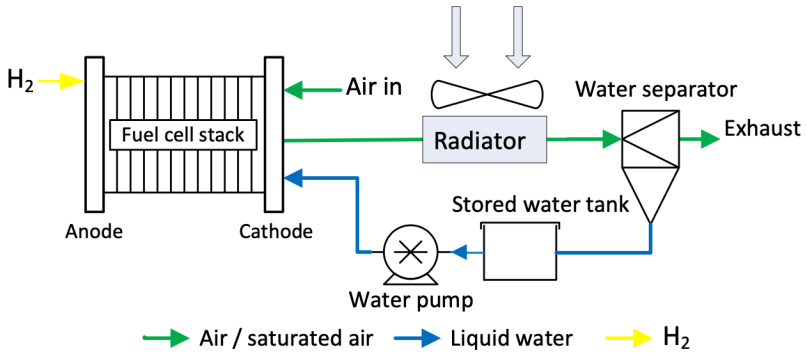

Figure II.3.3: Schematic of an example evaporative cooling system by Fly [41]

Approach (a) is used in a comparison made between thermal management techniques by Fly and Thring [42]. In this approach liquid water is added to the cathode flow stream where it evaporates, removing heat from the cell. In this process the water vapour also humidifies the membrane improving stack performance. The cathode exhaust includes both the water produced in the electrochemical reaction and water which was added into the stream for cooling but didn't. This exhaust is condensed and the liquid water is separated from the air and remaining water vapour. This liquid water is reused in the evaporative cooling system. In Fly's PhD thesis [41] it is stated that for the specific system considered *over 90% of the condensed liquid water needs to be extracted from the exhaust stream* in order to remain beneficial over a liquid cooling system. Fly and Thring [42] found that the radiator frontal of the evaporative cooling system (concept B in [42]) was 27% smaller than that of the liquid cooling system (concept A in [42]). Fly [41] states that in using an evaporative cooling system the *overall heat exchanger area can be reduced up to 40% compared to a liquid cooled system*. This is attributed to the *presence of phase change within the vehicle radiator improving heat transfer coefficients* [41]. As with liquid cooling it is important in approach (a) that the coolant remains non conductive in order to

prevent degradation [10]. Perry et al. [46] state that a drawback of approach (a) is that it may lead to local fuel starvation on the anode side or flooding on the cathode side. Commenting on approach (b) they state that the water transport rates required for adequate cooling are difficult to maintain through wicking [46].

Evaporative cooling systems are stated to be used in PEMFC with power outputs of greater than 10 kW [24, 37].

II.3.5 Summary of Thermal Management Techniques

After analysing all the thermal management techniques found in literature it is identified that the major differentiator between techniques is the applicable PEMFC power output range. Secondary differentiators include cooling system weight, size, complexity and parasitic power. A lot of ideas and methods to improve the cooling performance of the thermal management techniques were found in open literature. It is expected many more ideas exist in closed literature. The aim of this research is to decrease cooling system weight, volume, complexity and parasitic power whilst improving the heat transfer performance. This will expand the power output range to which the thermal management techniques can be applied to. As this is an active area of research future thermal management techniques will have better performance. This will likely affect the choice of thermal management technique to be used for the PEMFC system on an aircraft. The following down selection is made with the current understanding of thermal management techniques for PEMFC.

For the thermal management of PEMFC for commercial aircraft application the most promising thermal management techniques are liquid cooling and evaporative cooling. The main reason behind this down selection is the applicability of these thermal management techniques in high power systems as expected in fuel cell aircraft. Liquid cooling systems are often stated in literature to be used when the PEMFC power output is above 10 kW [33, 37]. Liquid cooling is often used in commercially available fuel cell vehicles [21] meaning it has a high technology readiness level. The Toyota Mirai II fuel cell vehicle, which has a power output of 128 kW makes use of a liquid cooling system [21, 49]. Liquid cooling has been extensively used in fuel cell demonstrator aircraft as will be discussed in Section II.5.1. In Thirkell's doctoral thesis on fuel cell aircraft [10] the choice is made for liquid cooling in *higher power fuel cell systems* despite acknowledging the numerous advantages of evaporative cooling over liquid cooling. The reasons for this choice is the *higher technology maturity and more robust nature* compared to evaporate cooling systems and that a lot of research and development on evaporative cooling systems is proprietary [10]. This opinion is shared with Huang et al. [26] who state that *liquid cooling is still the primary choice for practical applications in recent years*. In the design of a 20 kW PEMFC system for onboard power on a Boeing 787 the authors conclude that air cooled PEMFC systems are not preferred due to additional weight and volume and the performance penalties [50]. A water cooled PEMFC is chosen in this study [50].

Evaporative cooling is a newer thermal management technique with a number of advantages over liquid cooling including *lower coolant flow rate, simplified system layout, and eliminated coolant pumps* [37]. Literature suggests that employing this thermal management technique leads to a reduced frontal heat exchanger area compared to liquid cooling [41, 42]. This thermal management technique has however not yet been used practically applied in fuel cell vehicles yet [37] however has potential. Hence this thermal management technique is selected for consideration.

II.4

Heat Sinks on Commercial Aircraft

Once the heat has been removed from the fuel cell stack through one of the thermal management techniques the heat must be dissipated into a heat sink. This chapter presents and discusses the various heat sinks available on commercial aircraft. The two main heat sinks found in literature are ambient air surrounding the aircraft and the onboard fuel [2]. These are discussed in Sections II.4.1 and II.4.2 respectively. Other heat sinks available on aircraft and innovative heat sinks including ice-protection systems, thermodynamic cycles and thermoelectric generators are discussed in Section II.4.3. A fuel cell thermal management system may make use of a combination of heat sinks.

II.4.1 Ambient Air

The most widely used and well documented heat sink available on aircraft is ambient air [2]. This is due to the relatively low temperatures experienced at cruise altitudes [2] and it being always present around the aircraft. In their survey on the topic of aircraft thermal management van Heerden et al. [2] state the three main means to use ambient air as a heat sink are ram air cooling, surface heat exchangers and gas turbine bleed air. The first two will be discussed in this section. The last is omitted as gas turbines are not present on fuel cell aircraft. Novel skin integrated heat exchangers are also discussed in this section.

The ambient air temperature is not equal to the cooling air temperature experienced by these systems. For ram air cooling the ram air temperature T_{ram} is to be considered and for skin heat exchangers the adiabatic wall temperature T_{aw} [2]. These temperatures are calculated using the formulae in Equation II.4.1 and II.4.2 adapted from [2].

$$T_{ram} = T_\infty \left(1 + \frac{\gamma - 1}{2} M^2\right) \tag{II.4.1}$$

$$T_{aw} = T_\infty \left(1 + \frac{\gamma - 1}{2} \sqrt{Pr} M^2\right) \tag{II.4.2}$$

The properties of the ambient air vary greatly with geographical location, altitude and time. These differences should be considered when designing a thermal management system using ambient air as the heat sink [10]. Thirkell [10] discusses the effect of altitude on the ability of the ambient air to remove heat. He states that at increasing altitudes the heat transfer coefficient decreases requiring a large heat exchanger frontal area for the same heat transfer [10]. On the other hand, the mass flow rate of air required decreases due to the increase in temperature difference between the stack and the ambient air [10]. The importance of considering the varying properties of ambient air is also discussed by van Heerden et al. [2]. Figure II.4.1 from [2] clearly shows the variation in temperature with altitude for a variety of models. They stress the importance of not only considering the Internal Standard Atmosphere (ISA) but state that *when designing thermal management systems, the interest is usually more on the extreme climatic conditions that an aircraft may experience during its operational lifetime* [2]. The additional hot and cold day models shown in Figure II.4.1 are from MIL-HDBK-310. Other ambient air properties to be considered are air density, thermal diffusivity and thermal conductivity [10].

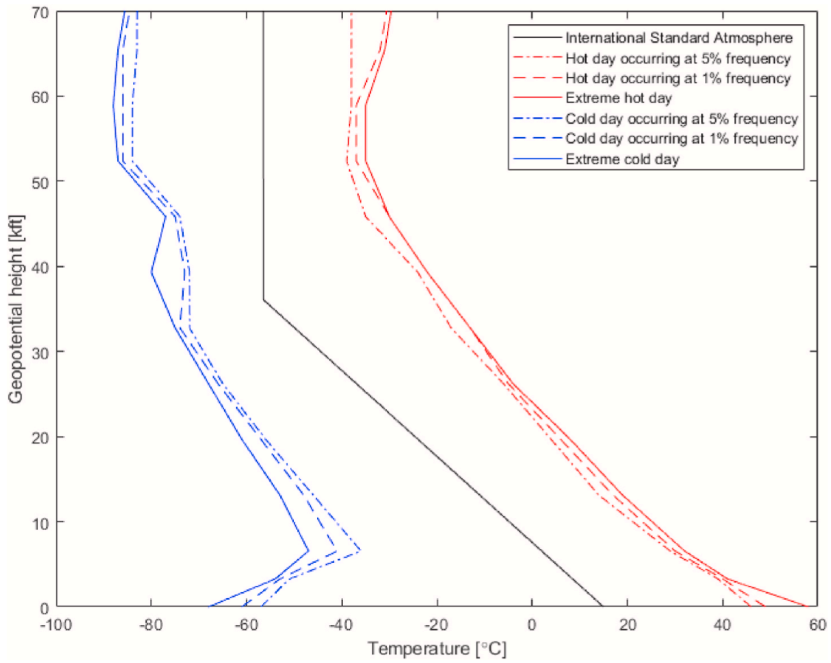

Figure II.4.1: Graph of ambient air temperature as a function of altitude for various atmospheric models by van Heerden et al. [2]

As the heat is transferred from the aircraft to the ambient air the temperature of the air aft of the aircraft will increase. For a single aircraft over a single flight, this may be minimal. But considering many aircraft with such propulsion systems the increase in ambient air temperature may have a measurable climate effect. This should be nevertheless quantified in a separate study.

II.4.1.1 Ram Air Cooling

Ram air cooling systems, also know as ducted heat exchangers use the dynamic pressure of the free stream to intake ambient air into a duct. The air then flows through a heat exchanger cooling the coolant. The air exits the duct via the outlet. A schematic of a ram air cooling system is shown in Figure II.4.2 [51]. Some of the first aircraft to utilize ram air cooling were World War Two era piston aircraft including the Mustang P-51D and Messerschmitt Bf 109 [52]. Ram air cooling systems are still used in modern aircraft including in environmental control systems [52]. Ram air cooling systems for fuel cell systems and HEA have been proposed extensively in literature. Open literature includes van Heerden et al. [2], Kellermann et al. [52] and Vredenborg and Thielecke [9]. The three demonstrator aircraft presented in Section II.5.1, the H2FLY HY4 and at least the UNIFIER19 PVS1 concept aircraft [53] all use some form of ram air cooling in their thermal management system.

When the aircraft is stationary or travelling at low speeds e.g. waiting at the gate, taxi or initial take off run there is little to no airflow through the ram air cooling system. For instances like these air can be pulled through the duct by installing a puller fan behind the heat exchanger [2] as shown in Figure II.4.2 [51]. The fan pulls air through the duct creating a cooling airflow over the heat exchanger [2]. The addition of a puller fan adds to the weight, power requirement and complexity of the thermal management system [2]. Including a puller fan is often proposed in literature and is proposed in numerous concept aircraft [51, 52, 53, 54]. The major disadvantage of ram air cooling is the additional drag, referred to as cooling drag [2]. This cooling drag is the accumulation of a number of drag components. One component is the loss of momentum the air experiences through the duct, referred to as core drag by Kožulović [4]. Other components of cooling drag include external drag associated with the duct itself and drag associated with the additional weight of the thermal management system [4]. Another drag component is interference drag. A number of alterations can be performed to minimize drag. The inlet geometry can be designed to minimize momentum loss and hence minimize drag. The standard inlet for these applications is the submerged NACA duct [2, 55] however other inlets exist including circular and semi-circular scoop intakes. The duct outlet can be designed to employ the Meredith effect, a way

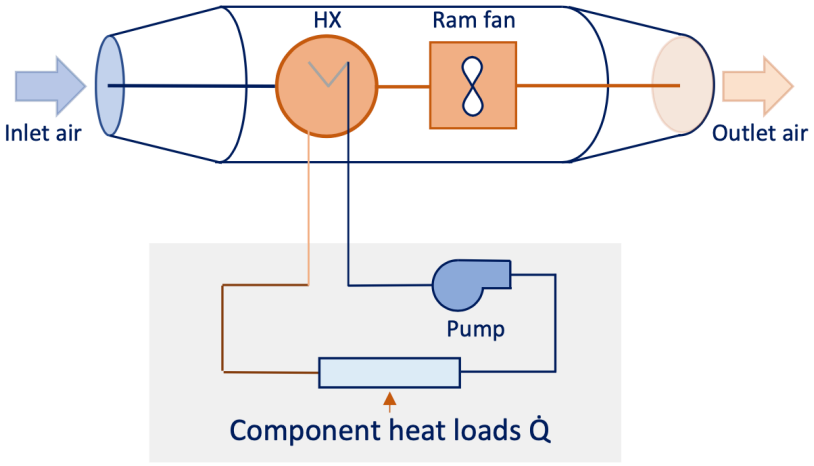

Figure II.4.2: Schematic of an example ram air cooling system by Nøland et al. [51]

in which cooling drag can be offset. As explained by R.S. Capon in [56] the Meredith effect is attributed to the thrust produced by a pressure jet created in a ram air cooling system. This pressure jet is created by partially closing the outlet which creates a higher pressure region behind the heat exchanger. This aft pressure is still lower than the pressure in front of the heat exchanger. The pressure jet is created as the air exits the duct through the nozzle and exerts a force on the aircraft which is considered as thrust. The increase in the air temperature due to the heat exchanger additionally contributes to the thrust force. The Meredith effect is similar to the ramjet, albeit a weak ramjet [54]. This effect has been employed on the Mustang P-51D, Messerschmitt Bf 109 and the 1996 Ferrari Formula One car [56]. In the Messerschmitt Bf 109 the ram air cooling system is installed within the aft section of the main wing of the aircraft [56]. It is expected by van Heerden et al. [2] that *electrified propulsion aircraft will rely more extensively on the use of ram air systems for cooling than current aircraft*. They go on to state that thermal management system needs to be *designed with great care* as parasitic drag, parasitic power and weight *could significantly diminish the efficiency gains these propulsion concepts offer* [2]. Ram air cooling systems can be installed in the aircraft in various locations for example underneath the wings as external nacelles, integrated within the wing or integrated within the fuselage. Each installation will have different inlet flow properties and cooling drag. Ahlers [57] states that ram air cooling systems reject more heat per volume than skin heat exchangers.

Kellermann et al. [52] performed a study into the *Design and Optimization of Ram Air–Based Thermal Management Systems for Hybrid-Electric Aircraft*. Though the focus of their study was on HEA using batteries, the ram air cooling section of the thermal management system can be applied to the thermal management system of a PEMFC system. Ambient air enters the ram air cooling duct through a diffuser to *reduce cooling air speed and thereby the cold-side pressure loss* of the heat exchanger [52]. A puller fan is located behind the heat exchanger in order to create a cooling airflow when the aircraft velocity is low or additional cooling is required. The airflow exits the duct through a nozzle to *recover some of the momentum [loss] of the cooling air* thereby partially offsetting the drag penalty [52]. Kellermann et al. [52] develop a thermal management system model in order to estimate the effects of drag, mass and fuel burn on hybrid-electric aircraft. In the discussion of future work it is recommended to consider the *integration of the thermal management system, including secondary mass and drag increases* in the thermal management system model [52]. It is inferred that these components are not included in the current model. In the current study an equation for the spillage drag is given. It is mentioned that the internal drag of the duct is calculated using the conservation of momentum however no calculation is given in the article. Kellermann et al. [52] state that the *integration of the thermal management system seems to be one of the largest challenges* in the design of such an aircraft. It is also recommended to consider the installation of the ram air cooling duct behind an open rotor and use a nozzle with adaptive geometry to improve performance [52]. This adaptive geometry can be used to change the mass flow rate for off design cases to meet the cooling requirement [9] and employ the Meredith effect.

Brelje et al. [54] present two models for the calculation of cooling drag through a ram air cooling

system for unconventional propulsion systems. The first is an incompressible approximation adapted from Theodorsen's method presented in [58]. For a detailed explanation of the first model the reader is directed to section 2.6 in [54]. The second is *a more sophisticated 1D thermodynamic cycle modelling approach* which considered compressible flow [54]. The models are open-source and implemented in the OpenConcept toolkit[1], an alpha level software using the OpenMDAO framework[2] developed by NASA.

II.4.1.2 Surface Heat Exchanger

A surface heat exchanger makes use of the aircraft skin as an intermediary in the heat transfer between the coolant and the ambient air flowing over the outer aircraft skin [2, 59]. Such a system has considerable less parasitic drag than a ram air cooling system as no ducts or heat exchangers are located in the airflow. The pre-World War Two Supermarine S.6b racing seaplane required surface heat exchangers covering *much of the wings, some parts of the fuselage, and even the top surfaces of the floats* to meet the cooling requirements [2]. For more on the history of surface heat exchangers the reader is directed to Wang et al. [60]. Surface heat exchangers are also used on current aircraft including the Airbus A320 which uses a surface heat exchanger for the cooling of the avionics compartment [2]. Like the ram air cooling system, the heat transfer rate of the surface heat exchanger is dependent on the aircraft's velocity. When the aircraft is stationary, only natural convection can occur if a sufficient temperature difference is present. This heat transfer is considered irrelevant by Vredenborg and Thielecke [9] and hence another cooling system for this phase of flight is recommended.

The drag of surface heat exchangers is not necessarily zero as the heated aircraft skin affects the boundary layer which may *lead to earlier transition and separation of the flow, leading to an increase in drag* [2]. In their review van Heerden et al. [2] comment on a study completed by Kallath et al. [61] which found that heating a wing through such a skin heat exchanger may lead to improved aerodynamic performance. Their study found that with an optimal combination of *heat flux, the angle of attack, and the Reynolds number [and] surface heating at the best locations* the lift coefficient increased by 2.5% and drag coefficient decreased by 1.6% [61]. The *installation area, the heated aircraft skin area and the fluid temperature* all affect the heat transfer [9]. In order to improve heat transfer is has been proposed to increase the surface area by altering the aircraft skin with protrusions as presented in Anibal et al. [62]. These protrusions will directly affect the drag of the skin section and should be traded off with the increased heat transfer. Anibal et al. [62] present an aerodynamic heat transfer optimization of a surface heat exchanger for an electric motor. The optimized fuselage shapes yield such protrusions.

Of importance in surface heat exchangers is the thermal conductivity of the aircraft skin. Older aircraft extensively use metals often aluminium alloys. Modern aircraft use composites which have different thermal conductivities than aluminium alloys [2]. This should be taken into account when designing surface heat exchangers as the trend in the aerospace industry is towards the use of lighter materials including composites.

Kellermann et al. [59] assess the potential of use surface heat exchangers to avoid the drag associated with ram air cooling systems. A thermodynamic model of a surface heat exchanger is developed for a wide range of aircraft as a function of MTOW. Empirical correlations are derived to determine an aircraft's wetted area based on its MTOW. The model uses *flat plate models with uniform temperature distribution* for the heat transfer calculations. The available cooling power Q_{av} is determined and relations between aircraft MTOW and Q_{av} are given for four different flight cases (take-off, hot day take-off, climb and cruise) and three surface temperature levels. These relations as shown in figure 7 in [59] and are applicable for aircraft with an MTOW of up to around an Airbus A380. The study finds *that surface heat exchangers can provide cooling power in the same order of magnitude as the waste heat expected from (hybrid-) electric drive trains for all sizes of considered aircraft* [59]. This study is hence not specific for fuel cell aircraft. Drag is qualitatively assessed in the study. It is found that heating in laminar boundary layer regions leads to earlier transitions, hence an increase in total drag. Kellermann et al. [59] refer to wind tunnel experiment and flight test performed by Kramer et al. who found that increasing turbulent boundary layer temperature reduces skin friction drag. It is hence recommended to install surface heat exchangers in the turbulent boundary layer regions of the aircraft in order to *make use of [this] beneficial effect of wall heating on the turbulent drag force* [59]. Quantification of the drag is left for future work.

[1] OpenConcept `https://openconcept.readthedocs.io/en/latest/`
[2] OpenMDAO `https://openmdao.org/`

II.4.1.3 Novel Skin Integrated Heat Exchangers

A novel use of the ambient air heat sink is the integration of the heat exchanger into the skin of the aircraft. This is different from the surface heat exchanger discussed above because the ambient air enters the aircraft through the aircraft skin as it exchanges heat with the coolant. Most information related to this idea is found in patents as little open literature was found on this novel idea. Vredenborg and Thielecke [9] refer to Patent WO 2012/130418 A1[3] which presents an invention of a cooling system within the tail section of the aircraft. The patent is specifically stated for application with fuel cell systems. A heat exchanger is integrated into the aircraft's skin. A fan at the rear of the tail section pulls the ambient air through the skin integrated heat exchanger into the tail section of the aircraft. Such a system can be operated during all flight phases including during stationary operation. If more cooling is required the fan speed can be simply increased. Additional ribs may be installed on the outer surface to guide airflow into the heat exchanger enhancing cooling performance[3]. The reader is referred to the patent[3] for more information on the invention. Such a system can lead to a large heat exchanger frontal area [9] without the drag associated with a ram air cooling system. Disadvantages of this system include damage to the heat exchanger [9] due to ingested FOD. Such a system requires parasitic power to operate the fan.

A similar invention with different integration is presented in Patent US 8,794,571 B2[4]. This invention proposes a skin heat exchanger system integrated into the belly and tail section of the aircraft as shown in figures 7 and 8 in the patent[4]. Another implementation of this idea taking inspiration from a ram air cooling system and a boundary layer ingestion propulsion system is shown in Figure II.4.3[4]. Here the ambient air enters a duct located at the root of the vertical tail. The air is pulled in by a fan and then passes through the skin integrated heat exchanger as it exits the aircraft. This is different from the invention in Patent WO 2012/130418 A1[3] where the ambient air enters the tail section through the skin heat exchanger. This implementation will have similar cooling drag penalties as those associated with a ram air cooling system.

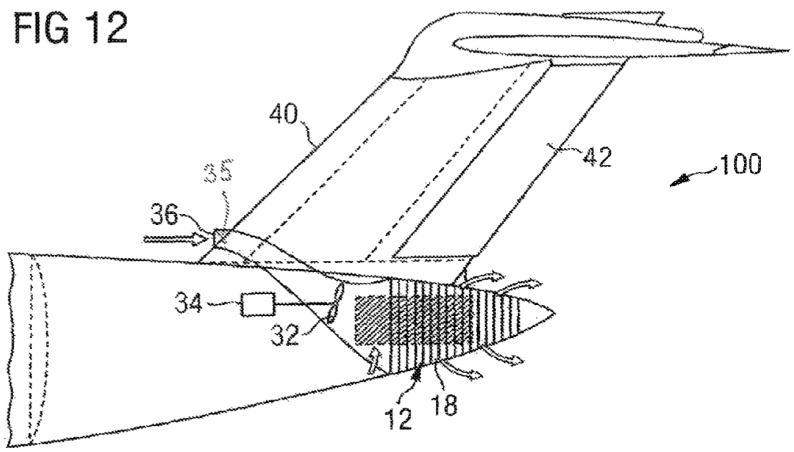

Figure II.4.3: Tail cone heat exchanger from Patent US 8,794,571 B2

II.4.1.4 Other

The invention presented in Patent US 10,618,636 B2[5] integrates a heat exchanger into a laminar flow control system. This invention is shown in Figure II.4.4[5]. The aim of a laminar flow control system is to reduce drag by maintaining a laminar boundary layer over as much of the aircraft surface as possible. Laminar boundary layers have a lower skin friction drag than turbulent boundary layers. The laminar boundary layer is maintained by sucking the laminar boundary layer into the aircraft surface preventing transition hence this system is also known as a boundary layer suction system. For more information on

[3]Aircraft tail region with a cooling system installed in aircraft tail region. WO 2012/130418 A1. URL: https://patents.google.com/patent/WO2012130418A1

[4]Cooler for an aircraft cooling system, aircraft cooling system and method for operating an aircraft cooling system. US 8,794,571 B2. URL: https://patents.google.com/patent/US8794571B2

[5]Heat exchanger for laminar-flow aircraft. US 10,618,636 B2. URL: https://patents.google.com/patent/US10618636B2

laminar flow control systems also known as boundary layer suction the reader is referred to literature on the subject including [63]. The airflow passing into the aircraft skin is proposed to pass through a subsequent heat exchanger to provide cooling to onboard systems. The major advantage of this system is the reduced drag due to both the laminar flow control system and the absence of the cooling drag associated with a ram air cooling system.

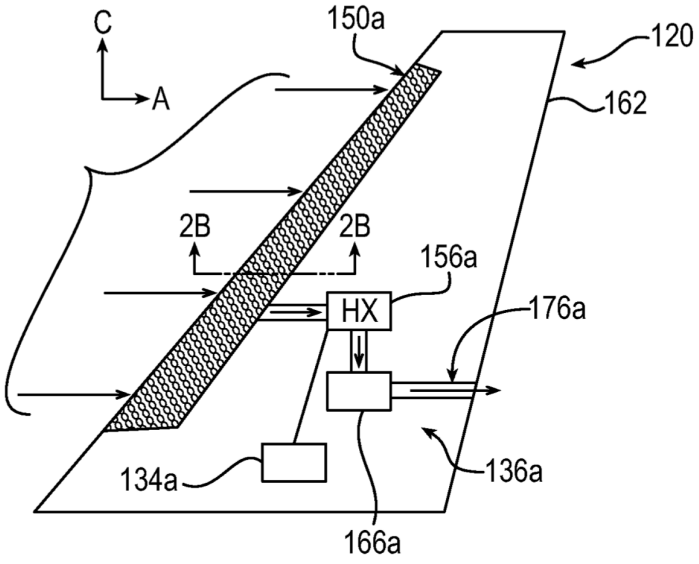

Figure II.4.4: Laminar flow control system with an integrated heat exchanger in vertical stabilizer from Patent US 10,618,636 B2

II.4.2 Fuel

Kellermann et al. [64] asses the use of kerosene fuel as a heat sink in HEA. The motivation for their assessment of this heat sink is *to avoid excessive drag from conventional cooling systems* i.e. ram air cooling systems which are discussed in Section II.4.1.1. In this assessment the fuel considered was kerosene. In a fuel cell powered aircraft the fuel will not be kerosene but hydrogen, likely stored in liquid form (cryogenic).

In a recent article by Nøland et al. [51] the use of liquid hydrogen for superconducting purposes in a PEMFC based propulsion system is analysed. The aircraft considered is similar to the ATR 72-600 [51]. The liquid hydrogen is primarily used to cool the electrical components of the powertrain to reduce electrical resistance. The liquid hydrogen is also used to cool the PEMFC. The hydrogen is heated by the PEMFC from 110 K to 358 K, the temperature it is required to be when it enters the PEMFC [51]. The article does not detail how the PEMFC is cooled by hydrogen. It is assumed that passing 110 K gaseous hydrogen through the PEMFC will lead to the water product freezing and inhibiting the flow of reactants and products. Nøland et al. [51] found that only a small amount of the heat generated by the PEMFC is able to be absorbed by the hydrogen due to the hydrogen not having *sufficient heat capacity to take out all the losses in the system* i.e. the hydrogen is heated to the PEMFC inlet temperature before all the heat from the components is removed. A ram air cooling system was required to cool the remaining heat losses, the major part being from the PEMFC. Based on the numbers in Nøland et al. [51] it is calculated that during cruise only 4% of the heat produced by the PEMFC is able to be absorbed by the hydrogen. The majority of the remaining heat is removed by the ram air cooling system.

Snyder et al. [7], Inacio et al. [8] and Pratt et al. [50] share similar findings. Snyder et al. [7] state that the heat *removed using the liquid- hydrogen fuel or put into the entrance air or exhaust streams [of the PEMFC]* can remove only about 15% of the heat generated by the PEMFC. It is however not clear if an optimized cooling system was designed for the liquid hydrogen or whether passive heat transfer was considered within the fuel cell stack. Snyder et al. [7] go on to design an additional thermal management system with heat exchangers mounted underneath the wings. Inacio et al. [8]

conceptually design a PEMFC propulsion system with liquid hydrogen storage for the Embraer EMB-203 Ipanema, a small crop dusting aircraft. It is intended that the heat from the PEMFC and electrical components evaporate and preheat the liquid hydrogen to temperatures allowable by the PEMFC. In their results they state that *there is constantly more heat within the system than it is required for the hydrogen conversion for propulsion* as shown in figure 7 in [8]. Adding additional liquid hydrogen to the aircraft for the sole purpose of cooling is proposed by considered not a viable option. An additional *11.6 to 36.5 times the LH2 utilized for propulsion* would be required [8]. A complementary cooling system is required to dissipate the remaining heat produced. A water cooling system with a heat exchanger is designed for the PEMFC and electrical systems as shown in Figure 5 in [8]. It is calculated that 93.6% of the additional cooling requirement is for the PEMFC alone [8]. Pratt et al. [50] consider the use of the heat from the thermal management system in heating the liquid hydrogen within the storage tank to maintain tank pressure. In their article a 20 kW PEMFC system for the inflight entertainment system onboard a Boeing 787 is designed and studied [50]. The heat required to maintain tank pressure and pre-heat the hydrogen is stated to be only 7% of the heat generated by the PEMFC system [50].

II.4.3 Other Heat Sinks

Another potential internal heat sink is the ice-protections systems [2] for the purpose of de-icing and anti-icing. These ice-protection systems required a large amount of heat to function [2] hence revealing a potential synergy with the thermal management system. The operation of this system is only required during icing conditions which depend on ambient conditions such as moisture levels and temperature. Hence the potential synergy between the ice-protection system and the thermal management system is not always able to be utilised. For these same reasons heat sinks related to passenger services are deemed as non optimal. These heat sinks can be used to reduce the heat removed from other heat sinks at certain points in aircraft operation. The three main uses of heat for passenger services are warm water for drinks, warm water for washing and heating of meals [50]. In the study by Pratt et al. [50] it was calculated that the warm water produced from the heat of an NPE PEMFC is *5- to 10-times that which is estimated to be reasonably used on board the airplane*, a Boeing 787 in their study. Even if these systems are used as heat sinks there will be operational cases when these heat sinks can not be utilised. Hence a different heat sink would be required to remove all of the heat from the thermal management system.

In their review on the challenge of aircraft thermal management van Heerden et al. [2] goes on to discuss novel heat sinks including *energy conversion using thermodynamic cycles*. Rankine cycles are proposed to generate additional shaft power which would further increase the efficiency of the fuel cell system. The authors state that high temperature heat sources are required in order to make the system feasible [2]. This cycle is hence incompatible with the low quality heat generated by the PEMFC. Another proposed cycle is the refrigeration cycle [2]. For both such cycles the additional system complexity, weight and reliability have to be considered against the advantages. The review goes on to discuss the use of thermal storage using phase change materials to absorb heat generation peaks [2]. The use of such phase change material would be in conjunction with other heat sinks for nominal heat generation. This would mean that the nominal heat sink does not have to deal with heat generation peaks. These phase change materials would then release the stored heat through the thermal management system during sub-nominal heat generation. Additional mass and volume as well as maintenance of these phase change materials should be considered [2]. In an article by Gkoutzamanis et al. [65] on thermal management system for HEA, phase change materials have also been presented. Shi et al. [66] propose the use of phase change materials as a solution to deal with peak thermal loads in a hybrid turboelectric regional jet. Two types of phase change materials were considered namely; magnesium chloride hexahydrate and Urea-KCl [66]. The study showed that these materials are *able to effectively manage the peak thermal load* but that there is a weight penalty. However this weight penalty was greater when adding additional coolant to the coolant loop than the addition of the phase change materials [66].

Other ideas proposed by van Heerden et al. [2] include the use of thermoelectric heat sinks to generate electricity from heat through the Seebeck effect or absorb heat through the Peltier effect. The use of thermoelectric generators (TEG) is also discussed by Abderezzak et al. [67] using the heat generated by PEMFC. They conclude that the resulting voltage is of value when considering a 1 kW PEMFC [67]. Other ideas include the use of caloric materials and thermoacoustic heat engines [2].

These ideas generally have low TRL levels [2] which may inhibit their immediate use.

A CO_2 air conditioning system has been proposed to provide additional cooling to the fuel cell stack during high power operation for fuel cell vehicles [44]. This system is used in conjunction with another heat sink in a thermal management system. An advantage of the addition of such a system in the thermal management system is that the other heat sink can be sized for nominal operation (e.g. cruise) and this air conditioning system could be used for high power operation (e.g. take off). A disadvantage of this system is the large amount of parasitic power required for the conditioning system.

II.5

Current State of Fuel Cell Thermal Management Systems onboard Aircraft

A number of aircraft have flown using a fuel cell propulsion system and a number of aircraft concepts using fuel cell propulsion systems have been proposed. These aircraft are presented and discussed in this chapter with specific attention given to the thermal management system on these aircraft. Section II.5.1 presents the Boeing Fuel Cell Demonstrator, Antares DLR-H2 and ENFICA-FC Rapid 200-FC fuel cell demonstrator aircraft. Section II.5.2 presents the concept aircraft from the CHEETA and UNIFIER19 projects.

II.5.1 Demonstrator Aircraft

A number of aircraft powered by fuel cell systems have flown demonstrating the use of propulsive fuel cell systems in aviation. These demonstrator aircraft are presented and analysed in this section with specific attention to the thermal management system. These three aircraft are shown in Figure II.5.1. Other fuel cell demonstrator aircraft exist, such as the H2FLY HY4 and ZeroAvia's retrofitted Piper M-class aircraft but have not been included in this section due to lack of open literature.

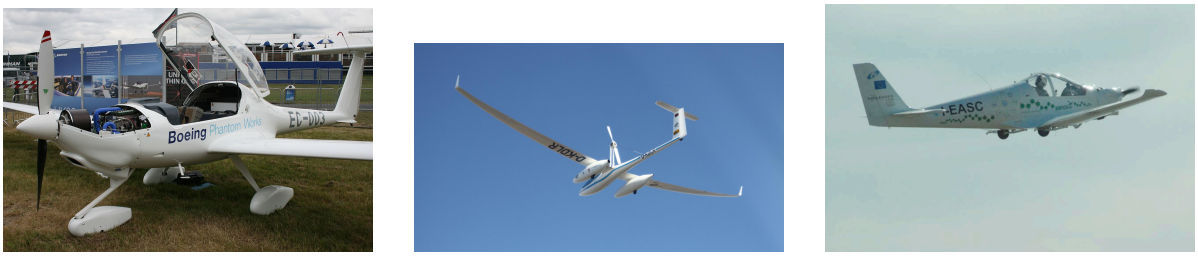

(a) Boeing Fuel Cell Demonstrator[1] **(b)** Antares DLR-H2[2] **(c)** ENFICA-FC Rapid 200-FC[3]

Figure II.5.1: Images of flown fuel cell demonstrator aircraft

The Boeing Fuel Cell Demonstrator was the first manned aircraft to fly using a hydrogen fuel cell propulsion system. A Diamond HK36 Super Dimona was modified by Boeing Research & Technology - Europe and first flew in February of 2008 at an airfield in Spain[4]. Lapeña-Rey et al. [69] identified thermal management as one of the main challenges in the design and development of aircraft. They go on to state *that the cooling requirements of a fuel cell powered aircraft are much higher than those of a conventional aircraft, which [...] poses a big challenge towards the use of this technology in aerospace systems* [69]. The propulsion system consisted of a compressed hydrogen tank and a PEMFC with

[1] Adambro, CC BY-SA 3.0 https://creativecommons.org/licenses/by-sa/3.0, via Wikimedia Commons
[2] DLR, CC BY-NC-ND 3.0 http://creativecommons.org/licenses/by-nc-nd/3.0, via www.dlr.de
[3] Image taken from Romeo et al. [68]
[4] T.J. Koehler *A green machine. Boeing makes history with flights of Fuel Cell Demonstrator Airplane*. In: *Boeing Frontiers*. (May, 2008) URL: https://www.boeing.com/news/frontiers/archive/2008/may/ts_sf04.pdf

an additional lithium-ion battery to supply sufficient power for take off and climb [69]. The thermal management system of the fuel cell systems consists of a water cooling loop [70]. Liquid water is first extracted from the cathode outlet and passed through two cyclones to separate any liquid water from the cathode outlet mixture [70]. A subsequent condenser condenses as much of the remaining water vapour in the remaining cathode outlet mixture [70]. It is inferred from these statements and the schematic in Figure 1 in [70] that the cooling water is directly added to the cathode inlet flow. The scavenged water is used for both cooling and humidification of the fuel cell stack. The cooling loop includes two tanks in which the water is stored after being scavenged from the cathode outlet. The cooling water is pumped from the storage tanks via two water solenoid valves into the fuel cell stack [70]. Another pump is used to pump the scavenged water into the storage tanks after the condenser [70]. It was observed during ground tests of the aircraft that the flow through the heat exchangers induced by the propeller *was enough to keep all system temperatures below their limits* [71]. Four test flights were performed with the aircraft in 2008 [71].

The Antares DLR-H2 was the first manned aircraft to fly exclusively with a fuel cell propulsion system during all flight phases[5]. The aircraft first flew in July of 2009 using an HT-PEMFC and has since also flown with an LT-PEMFC [72]. The aircraft is a modified Lange Aviation GmbH Antares 20E motor glider. Two additional pods were installed underneath the wings to house the fuel cell system and hydrogen tank [72]. The LT-PEMFC system uses liquid cooling and a *two-pass cross flow plate-and-bar heat exchanger* supported by a coolant pump and fan respectively [72]. It is claimed by Rathke et al. [72] that the proposed cooling system is able to reject up to 30 kW of heat. The coolant used, as presented in a different article on the Antares DLR-H2, is water [73]. Kallo et al. [73] present a detailed air flow diagram of the cooling system in Figure 8 in [73]. Figures presenting fuel cell data from Antares DLR-H2 test flights are shown in [73, 74] including fuel cell temperature and fuel cell system parasitic power data.

The Environmentally Friendly Inter-City Aircraft Powered by Fuel Cells (ENFICA-FC) is a European Commission (EC) funded project which aimed to develop and validate a fuel cell propulsion system in an aircraft [68]. A Jihlavan Aircraft (now Sky Leader) Rapid 200 was retrofitted with a PEMFC [68] and compressed hydrogen propulsion system and first flew in May of 2010[6]. Thermal management was identified as one of the most critical aspects of the demonstrator aircraft [68]. The thermal management system consists of a water cooling loop and a liquid-air heat exchanger located at the front of the aircraft [75]. The cathode outlet is cooled through a heat exchanger located at the nose of the aircraft. The cooled cathode outlet then passes through a cyclone (referred to as liquid separator in Figure II.5.2) which separates the air and water [68]. The water is pumped from the cyclone into the water storage tank. The water is pumped from the water storage tanks into the fuel cell stack for cooling as shown in Figure II.5.2. The water cooling loop includes a filter and a flow meter [76]. As for the Boeing Fuel Cell Demonstrator presented above, it is inferred from the literature that the cooling water is directly added to the cathode flow. A thermodynamic model is made to *predict the system temperature and the stack voltage as a function of the air cooling inlet conditions and the electrical power demand* [68]. Another model is made to model the heat exchanger and its air inlet [68]. Both models are implemented using Simulink[7] and are described in considerable detail in Romeo et al. [68]. A *computational fluid dynamics (CFD) engineering model* was developed using VSAERO[8] to support the aerodynamic design of the cooling air inlet and outlet [75]. The effect of the propeller on the air inlet was also taken into account. Correa et al. state that during flight tests the *temperatures were kept under their respective limits and the cooling system showed better performances than those recorded during the ground tests* [77]. It is proposed in a number of articles on the ENFICA-FC Rapid 200-FC aircraft that the models and methods developed could be used in the aircraft design of similar sized aircraft [68, 77].

[5]DLR *Antares DLR-H2*. URL: https://www.dlr.de/content/en/articles/aeronautics/research-fleet-infrastructure/dlr-research-aircraft/antares-dlr-h2-out-of-operation.html

[6]ENFICA-FC *The first European Commission funded Aircraft powered by a Hydrogen Fuel Cell took its first flight* (May, 2010) URL: http://www.enfica-fc.polito.it/content/download/246/1105/version/1/file/Press%20New%201st%20Flight%20Test_v4/index.pdf

[7]MathWorks Simulink https://www.mathworks.com/products/simulink.html

[8]Analytical Methods, Inc. VSAERO https://www.am-inc.com/VSAERO.html

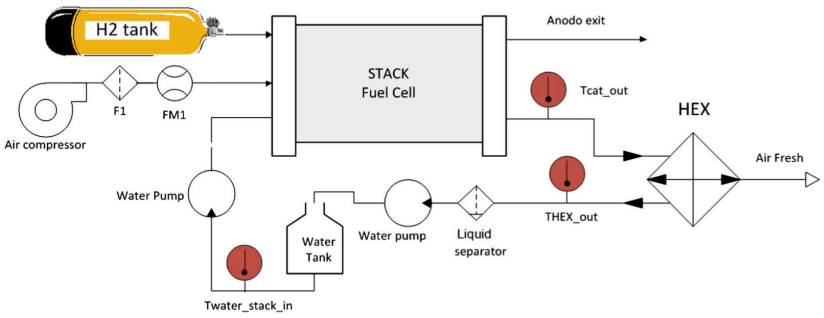

Figure II.5.2: Schematic of the fuel cell thermal management, air delivery and hydrogen delivery systems on the ENFICA-FC Rapid 200FC by Romeo et al. [68]

II.5.2 Conceptual Commercial Aircraft

Two concept aircraft from open literature are presented in this section with specific attention given to the thermal management system. Other concept aircraft and aircraft in development exist but are not presented due to a lack of open literature on these projects. These aircraft include the concept aircraft from the Airbus ZEROe project[9], the FZR-1E from the ATI FlyZero project[10] and those using the ZeroAvia powertrain including a retrofitted Dornier 228[11].

Waddington et al. [16] conceptually develop a liquid hydrogen and fuel cell propulsion system for an aircraft with capabilities similar to the Boeing 737-800. The thermal management of the fuel cell system is identified as one of the major challenges in the design of such an aircraft. Both PEMFC and SOFC architectures are considered for the 1 MW propulsion system on the Center for High-Efficiency Electrical Technologies for Aircraft (CHEETA) aircraft concept [16]. The CHEETA project is run by a multi-disciplinary US-based consortium[12] lead by the University of Illinois. In the modelling of the aircraft the additional weight, drag penalty and potential thrust of the thermal management system were taken into account including the pumps and heat exchangers [16]. The paper presents values for the weight and parasitic drag/ thrust of the thermal management system for both the HT-PEMFC and SOFC configurations. The weight of the thermal management system of the HT-PEMFC configuration is stated to be 803.66 lb (364.53 kg) [16]. The thermal management system of the HT-PEMFC configuration is stated to have a net axial force of -121.1 lb (-54.9 kg) at sea level with a Mach number of 0.25 and -139.9 lb (-63.5 kg) at FL370 with a Mach number of 0.77 [16]. This drag force is due to the heat exchanger. It is also noted that the net power generated by the HT-PEMFC system is stated to be 883.1 kW, below the 1 MW requirement. Waddington et al. [16] state that this difference is due to *parasitic losses used to drive the inlet compression system and balance of plant* [16]. Nothing else is mentioned with regard to the thermal management system of the fuel cell system in Waddington et al. [16]. Another paper on the CHEETA concept aircraft states that the fuel cell system is cooled by hydrogen after cryogenically cooling electrical components including the electric motors (at 20 K) and converters (at 115 K) [78]. A schematic of the cooling system is shown in Figure 4 in [78] and suggests that the hydrogen entering the fuel cell stack for cooling is at around 115 K (-158.15°C). The modelling presented in [78] is done using the Modelica modelling language[13]. Figure 1 in Stautner et al. [79] contradicts Podlaski et al. [78] and suggests that the fuel cell system on the CHEETA concept aircraft is cooled by a coolant at 216 K which passes through a ducted heat exchanger without mentioning which fuel cell configuration is considered.

UNIFIER19 is an EU funded project aimed at developing *a conceptual design for a 19-passenger commuter with multiple cargo and passenger-seating cabin layouts powered by a modular hybrid-electric powertrain*[14]. The project partners are Pipistrel Vertical Solutions, Politecnico di Milano and

[9] Airbus ZEROe `https://www.airbus.com/en/innovation/zero-emission/hydrogen/zeroe`

[10] FlyZero FZO-AIN-REP-0007 `https://www.ati.org.uk/wp-content/uploads/2022/03/FZO-AIN-REP-0007-FlyZero-Zero-Carbon-Emission-Aircraft-Concepts.pdf`

[11] ZeroAvia *ZeroAvia Expands its Hydrogen-Electric Aviation program to 19-Seat Aircraft and Raises Additional $13 Million in Funding for Large Engine Development.* (June, 2021) URL: `https://www.zeroavia.com/19-seater-release`

[12] Center for High-Efficiency Electrical Technologies for Aircraft (CHEETA) `https://cheeta.illinois.edu/`

[13] Modelica Language `https://modelica.org/modelicalanguage.html`

[14] UNIFIER19 Motivation & Goals `https://www.unifier19.eu/?page_id=35`

the TU Delft [53]. In the project's final concurrent design report [53] four concept aircraft are presented named C2, C3, C7A and PVS1. For each configuration the total heat exchanger frontal area, fuel cell heat exchanger frontal area, total cooling drag for both climb and cruise are given. These values are summarised in Table II.5.1. All configurations use a 50/50 mixture of mono ethylene glycol and water as the coolant in the liquid cooling system.

Configuration	Total HEX area [m^2]	FC HEX area [m^2]	FC HEX area / total HEX area [-]	Total cooling drag (climb) [N]	Total cooling drag (cruise) [N]
C3	2.07	1.6	0.77	1269.5	753.4
C7A	2.3918	1.7	0.71	1366.2	853.9
C2	2.3198	1.64	0.71	1459.2	829.0
PVS1	2.5589	1.936	0.76	1637.6	901.3

Table II.5.1: Thermal management system data for the UNIFIER19 concept aircraft configurations from Eržen et al. [53]

Only for configuration PVS1 is the fuel cell thermal management system presented in some detail. A schematic of the thermal management system system is shown in Figure II.5.3. The schematic shows a ducted air-liquid heat exchanger along with an electric pump to pump the coolant through the fuel cell stack. An expansion tank is also included in the coolant loop [53]. The heat exchanger was sized at sea level at International Standard Atmosphere (ISA) temperature with an offset of 24 K [53]. The intake efficiency of the diffuser was taken to be 1.0 [53].

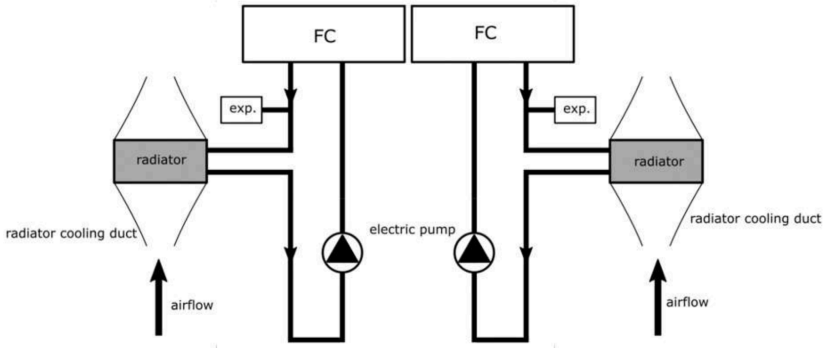

Figure II.5.3: Schematic of the fuel cell thermal management system proposed for the UNIFIER19 PVS1 concept aircraft by Eržen et al. [53]

II.6

Effects of Fuel Cell Thermal Management Systems on Aircraft Performance

This chapter deals with the effect of the thermal management system of fuel cell on overall aircraft performance. The thermal management system has a direct effect on aircraft aerodynamics (predominantly drag), aircraft weight and fuel cell power requirement. These all affect aircraft performance and hence should be taken into account during the preliminary and conceptual design phases. Section II.6.1 presents fuel cell aircraft sizing models from open literature. These are discussed with respect to the fuel cell thermal management system and what is considered in terms of cooling drag, weight and parasitic power. The paper by Kožulović is the only open literature found where the fuel cell thermal management system of a commercial fuel cell aircraft is specifically addressed and modelled. The remaining papers model a complete fuel cell aircraft or a fuel cell system for an aircraft subsystem whilst considering the fuel cell thermal management system. Cooling drag due to the fuel cell thermal management system is discussed in more detail in Section II.6.2. Calculations and estimations methods are also discussed. The thermal management system weight is discussed in more detail in Section II.6.3 and parasitic power is discussed in Section II.6.4.

II.6.1 Modelling of Fuel Cell Thermal Management Systems for Aircraft

This section presents the modelling of fuel cell thermal management systems on aircraft as found in literature. These models aim to take into account the parasitic drag, additional weight and parasitic power of the thermal management system into the overall aircraft design during the preliminary and conceptual design phases. This is not a complete overview of fuel cell thermal management system modelling from open literature but an overview of the most important and relevant modelling studies.

Kožulović [4] performs a preliminary sizing of a thermal management system for a fuel cell powered aircraft with similar size, weight and capacity as the Airbus A320neo and Boeing 737 MAX. Specific attention is given to calculating the parasitic drag of the thermal management system. In this preliminary design a water cooling system with a wing mounted ducted counter-flow liquid-air heat exchanger is used and sized for cruise condition [4]. The heat transfer rate $\dot{Q}_{all}$ is equated to the power required by the fuel cell P_{all} which is the sum of the power required by the aircraft P_{AC} and the additional power required due to the thermal management system P_{heat}. This additional power P_{heat} is attributed to the core drag of the ducted heat exchanger, the external drag of the ducted heat exchanger and the drag associated with the additional mass of the heat exchanger. The parasitic power required for the coolant pump is neglected due to its low power consumption compared to the other power demands. P_{heat} depends on the size of the heat exchanger which depends on $\dot{Q}_{all}$. As such $\dot{Q}_{all}$ is solved in an iterative manner. The core drag is calculated using the momentum theorem and the ramjet effect is taken into account. The external drag of the ducted heat exchanger takes into account the nacelle

surrounding the heat exchanger. This is estimated based on a C_D value from Hoerner [5] for a wing-mounted nacelle close to the wing trailing edge as shown in Equation II.6.1. The author acknowledges that *the estimation of the external drag is very difficult on this preliminary level, since suitable and synergetic integrations may considerably reduce the drag* [4]. Commenting further the author states *that the external drag estimation was the element with the largest uncertainty in the current study, an issue which has to be addressed much more intensely in the future* [4]. In the drag associated with the additional mass of the heat exchanger both the mass of the heat exchanger and coolant mass is considered. This mass is multiplied by a sizing factor of 1.2 to take into account the mass of the coolant pipes and pumps. The heat exchanger is sized to provide adequate cooling to the fuel cell. From this the required heat exchanger cross section is determined which is an input into the external drag calculations.

$$C_{D_{ext}} = \frac{D_{ext}}{\frac{1}{2}\rho {V_0}^2 A_{front}} = 0.06 \tag{II.6.1}$$

It is found that the propulsive power requirement of the aircraft is increased by 23.7% and the frontal area of the heat exchanger is 84% of the fuselage cross section [4]. The author comments that an improved heat exchanger integration is required in future work. A sensitivity analysis is performed and it is found that the Reynolds number of the tube flow Re_d, velocity ratio V_1/V_0, the temperature splitting factor $F_{T,split}$ and Mach number M_0 all have an effect on the thermal management system power demand. In future work the author recommends focusing on *aircraft-level integration of the large heat exchanger system, together with heat transfer enhancement methods* [4]. The paper does not mention which software or programming language, if any, was used.

Guida and Minutillo [6] analyze the use of a PEMFC as an APU in a more electric aircraft. A design methodology is proposed using an optimization procedure to maximize efficiency and minimize weight aiming for the highest specific energy. The methodology is implemented into a simulation tool using MATHCAD15[1], a commercial code. This methodology is applied to the design of a 24 kW APU for an AERMACCHI SF 260 (a 2 person light aircraft) with a number of high level requirements [6]. Here the hydrogen is stored in compressed gaseous form. The heat generated by the fuel cell stack Q is determined as a function of the stack efficiency η. The mass of the heat exchanger is taken into account by multiplying the heat transferred by the specific thermal power of the off-the-shelf Titan AIR H-1-20A-600 heat exchanger [6]. This heat exchanger is chosen due to its high thermal power to weight ratio of 30 kW/30 kg [6]. It is inferred from the article, specifically figure 8 in [6], that the fuel cells are air cooled in a closed loop cooling system. The heated air is inferred to be cooled by ambient air in an air-air heat exchanger. It is inferred that the parasitic power and parasitic drag of the thermal management system are not considered in this design methodology.

Snyder et al. [7] investigate the use of fuel cells in aircraft propulsion systems with the aim to further the understanding of these systems and guiding future research and analysis. A 100-passenger tube-and-wing aircraft with liquid hydrogen storage is considered in their study. The aircraft used PEMFC propulsion system with a water cooling system and a multiple-finned tube heat exchanger conceptually mounted underneath the wing. The thermal management system was sized for cruise conditions. Parametric studies were completed to determine the heat exchanger size, shape, weight and volume. For this the overall heat transfer coefficient and area-to-volume ratio were kept fixed. The weight of the heat exchanger was found to be 16.3% of the complete hydrogen fuel cell propulsion system [7]. In the investigation parasitic drag of the thermal management system was not considered as *drag reduction and optimization were beyond the scope of this study* [7]. Commenting on this topic the authors state that preliminary analyses yielded designs that reduce parasitic drag to a *less than a 10 per cent increase in total drag* [7]. It is inferred that the parasitic power and weight of the rest of the thermal management system are not considered. The effect of the cooling water exit temperatures on the heat exchanger size was studied. It was found that a higher exit temperature leads to a decrease in the volume and weight of the heat exchanger. Aircraft performance and sizing were done using the publicly available Flight Optimization System (FLOPS)[2] and the NASA developed open source Vehicle Sketch Pad (VSP)[3] was used to visualize the aircraft. The non-publicly available Numerical Propulsion System

[1] PTC MATHCAD `https://www.mathcad.com/en`

[2] Flight Optimization System (FLOPS) Software v.9 `https://software.nasa.gov/software/LAR-18934-1`

[3] Vehicle Sketch Pad (VSP) `https://software.nasa.gov/software/LAR-17491-1`

Simulation (NPSS) software[4] was used to develop the thermodynamic model of the fuel cell system.

Inacio et al. [8] study the use of liquid hydrogen storage and a PEMFC plus battery propulsion system in aircraft by conceptually retrofitting an Embraer EMB-203 Ipanema, a crop dusting aircraft. The PEMFC is the sole source of electricity during the cruise phase and nominal operation. As the liquid hydrogen required for propulsion is not able to absorb all of the heat from the PEMFC system, an electrical motor and inverter a complementary cooling system is designed. The complementary cooling system consists of a water cooling system and a heat exchanger. A flow schematic of the complementary cooling system is shown in Figure 5 in [8]. Note that the electrical motor and inverter are included in addition to the PEMFC system in this complementary cooling system. A clear list of assumptions made in the calculation of the complementary cooling system is also given. In calculating the mass of the total cooling system a cooling system gravimetric index is taken from a single commercial PEMFC fuel cell datasheet. The commercial PEMFC fuel cell system has a cooling subsystem gravimetric index of 2.27 kW/kg and is manufactured by Ballard Power Systems [8]. It is unclear whether the drag of the heat exchanger is considered in the aerodynamic modelling. The drag associated with the wing mounted hydrogen tanks is however specifically included in the aerodynamic modelling. The power of the cooling pump is included in the modelling [8] however how it is calculated is not shown in the article. For the modelling and simulation in the study the Stanford University Aerospace Vehicle Environment (SUAVE)[5] is used. The resulting parameters of the thermal management system sizing are shown in Table 7 in [8]. The total waste heat Q_{waste} is found to be 118.67 kW at a certain point during the cruise phase and the total *required for the hydrogen conversion for propulsion* $Q_{required}$ is 6.51 kW. The difference is Q_{extra} is the heat required to be dissipated by the cooling system and is found to be 112.16 kW as stated in Table 8 in [8]. However table 8 in [8] states that the *complementary cooling capacity* is 106.5 kW, which is below the waste heat requirement. A reason for this is not specified. The total weight of the aircraft is increased by 6% compared to the aircraft without the complementary cooling system [8]. Considering the cooling system gravimetric index of 2.27 kW/kg and the complementary cooling capacity of 106.5 kW, the mass of the complementary cooling system is calculated to be 46.9 kg. This is 60.9% of the difference in total weight between the aircraft with and without a complementary cooling system. The fuel cell power is stated to increase by 5.9% [8]. This increase can be primarily attributed to the complementary cooling system parasitic power. It is stated that 93.6% of the required complementary cooling is attributed to the PEMFC. Figure 9 in [8] shows the waster heat contributions of the converter, battery, motor and fuel cell.

Vredenborg and Thielecke [9] investigate the thermal management implications in the use of a PEMFC as an APU on a commercial aircraft. A model is built using the free Modelica modelling language[6] and the commercial Dymola[7] is used as the simulation environment. The system mass, parasitic power and parasitic drag are considered in the model however which specific components are considered are not entirely clear from the article. The model considers both the cooling heat transfer rate $\dot{Q}_{cool}$ as well as the heat transfer if the product water is condensed within the cathode $\dot{Q}_{cond}$. The cooling heat transfer rate $\dot{Q}_{cool}$ is equated to the product of the coolant mass flow rate, coolant specific heat coefficient and change in temperature from inlet to outlet. This formula is shown in Equation II.6.2 [9].

$$\dot{Q}_{cool} = \dot{m}_{coolant} c_{p,coolant} (T_{coolant,out} - T_{coolant,in}) \tag{II.6.2}$$

The pressure drop of the fluid through the piping is determined in order to determine the power consumption of additional pumps. A liquid cooling system is used in their modelling and three types of heat exchanger systems are proposed, all of which use ambient air as the heat sink. These are the ram air cooling system, tail cone cooling heat exchanger and liquid skin heat exchanger. The coolant used is this model is propylene glycol (PGW) [9]. In the modelling of the heat exchangers the epsilon-NTU method is used and a heat exchanger effectiveness ϵ is considered [9]. For the liquid skin heat exchanger a specific model is detailed which is based on the cell model approach and is validated with wind tunnel data. The weight of the pumps, pipes and fittings are also said to be considered in the model however which specific components are considered is not clear from the article. The article

[4]NPSS Numerical Propulsion System Simulation `https://software.nasa.gov/software/LEW-17051-1`

[5]Stanford Aerospace Design Lab SUAVE `https://suave.stanford.edu/`

[6]Modelica Language `https://modelica.org/modelicalanguage.html`

[7]Dassault Systemes DYMOLA Systems Engineering `https://www.3ds.com/products-services/catia/products/dymola/`

talks about an aerodynamic drag due to ram air flow, referred to as *ram air force* [9]. It is inferred that this doesn't refer to the PEMFC cooling system but rather to the ram air cooling system of the electrical environmental control system. This is backed up but the reasoning in the article that as the fuel cell is *cooled with a skin heat exchanger and [it] has [...] no aerodynamic drag due to ram air* [9]. Towards the end of the article a specific example of a PEMFC APU system is presented which is used in a global sensitivity analysis. The thermal management system in the example configuration includes both a tail cone heat exchanger and a liquid skin heat exchanger as shown in Figure 10 in [9]. For cooling on the ground the tail cone heat exchanger is exclusively used and for cruise and holding the liquid skin heat exchanger is exclusively used. For takeoff and landing both heat exchanger systems are used. In the global sensitivity analysis only the tail cone heat exchanger is considered. The schematic in Figure 10 in [9] also includes the liquid hydrogen tank in the coolant loop. Commenting on this in the article Vredenborg and Thielecke state that *the liquid hydrogen tank can be used as a heat sink for this cooling loop or to condense water* [9]. These low temperatures are beneficial for the DC-DC converter which is the first component in the cooling loop after the liquid hydrogen tank.

In his master thesis, Juschus [14] presents a preliminary sizing methodology for a PEMFC propulsion system on a fuel cell aircraft. The model is implemented into the Initiator[8], an in-house MATLAB tool. With respect to the thermal management system only the mass of an air-liquid plate heat exchanger and the liquid coolant is taken into account in the model [14]. The sizing of the heat exchanger was based on the methodology proposed by Kožulović [4]. The parasitic power consumption and parasitic drag of the thermal management system are not considered in this thesis [14]. The drag of the complete fuel cell engine is also not considered in the thesis. In Comincini's master thesis [11] a design methodology for the use of fuel cells in propulsion systems for aircraft is developed and analysed. This methodology is implemented into a MATLAB based software called Flycell. No fuel cell thermal management system is defined in the thesis. Commenting on the temperature of the fuel cell stack Comincini states that it *is supposed stable, but the way how this characteristic is achieved it is not defined* [11]. In subsequent articles by Comincini on the topic and the Flycell software, including [80] and [81], there is no mention of fuel cell thermal management.

Thirkell [10] in his PhD thesis models a fuel cell propulsion system in order to explore the use of fuel cells in aircraft. Though the topic of thermal management system is discussed in some detail, what of the thermal management system is modelled is not discussed beyond stating that *simplified modelling strategies have been developed*, *that the fuel cell stack [was] treated as a single control volume* and that *average stack thermal properties* were used [10]. It can be inferred from the fact that the topics of parasitic drag and heat exchanger sizing are not discussed that these are not modelled in the fuel cell propulsion system model. The variation in the properties of ambient air with regard to geographical location, altitude and time is discussed in some detail in the thesis and is specifically included in the model. The atmospheric models used are the common International Standard Atmosphere (ISA) as well as the hot, cold and extremes models from MIL-HDBK-310 [10]. These models are shown in Figure II.4.1 and also discussed by van Heerden et al. [2].

In Vonhoff's master thesis on the *Conceptual Design of Hydrogen Fuel Cell Aircraft* [12] the thermal management system is considered in some detail. The thermal management system design methodology is based on the methodology proposed by Chapman et al. [13]. This work presents the thermal design of a turboelectric 15-passenger VTOL aircraft with a liquid cooling system and a ducted heat exchanger [13]. Vonhoff implements his design methodology into a software tool called HAPPIE which uses SUAVE[5] to carry out aerodynamic analyses [12]. The parasitic drag is neglected as it is reasoned that *due to the action of the cooling fan pulling the air through the* heat exchanger there is a net zero thrust/ drag. Later on in the thesis, Vonhoff discusses the idea of 'cooling thrust' as predicted by Chapman et al. [13]. An equation is derived based on correlations in [13] to calculate $\frac{T_{cooling}}{W}$. Due to interdependencies an iterative loop is required to converge to determine $\frac{P_{shaft}}{W}$ and then $\frac{P_{FC}}{W}$. For the complete derivation and flowchart of the iteration loop, the reader is directed to section 3.7 in [12]. The cooling thrust calculations are not included in the full design loop but rather included for a side analysis. The power of the cooling fan and coolant pump are determined through Equations II.6.3 and II.6.4 [12] which are adapted from correlations in [13]. The stack efficiency η_{FC} is considered in calculating $P_{heat,rejected}$.

[8] TU Delft Initiator `https://fppwiki.lr.tudelft.nl/index.php/Synthesis/Initiator`

$$P_{cooling\,system} = (0.371 P_{heat,rejected} + 1.33) f(dT) \tag{II.6.3}$$

where

$$f(dT) = 0.0038 \left(\frac{T_{air}}{dT} \right)^2 + 0.0352 \frac{T_{air}}{dT} + 0.1817 \tag{II.6.4}$$

The mass of the cooling system is determined through Equation II.6.5 [12] which is adapted from correlation in [13]. The mass of the coolant line, cooling fan, coolant pump and 'wet' heat exchanger are specified to be included in the calculations performed in [13]. In Vonhoff's powertrain mass calculation a factor of 1.2 is included to *take into account auxiliary components, mounting and cables*.

$$m_{cooling\,system} = (0.194 P_{heat,rejected} + 1.39) f(dT) \tag{II.6.5}$$

It is found that the inclusion of cooling thrust reduces the power requirements of the fuel cell by *around 30%*. In the discussion Vonhoff states that the *mass and aerodynamic penalty [of the cooling system] were not very significant compared to the other powertrain performance parameters. This is unexpected and should be validated using a more detailed cooling system mode* [12]. He goes on to state that *the assumption of zero drag for the cooling system must be verified, as well as the cooling thrust contribution* [12].

II.6.1.1 Summary

Table II.6.1 provides a qualitative summary of the models in relation to the consideration of cooling drag, system weight and parasitic power. It includes the models presented in this section and those presented in Chapter II.5. A cell coloured red signifies that the model in the study didn't consider the respective column on aircraft performance. Orange signifies that it was considered to a certain extent but not completely and green signifies that it was fully considered. The components of the thermal management system included in the consideration of the respective column are included in the cell. In white cells with a question mark, it was unclear from the paper whether it was considered or not. In the red cells with a question it is inferred from the paper that the model didn't consider the respective column. The modelling software used in the respective studies is listed in the far right column.

Study	Parasitic Drag	Consideration of System Weight	Parasitic Power	Modelling Software
Kožulović [4]	Core & external drag	HEX, coolant & factor for coolant pipes and pumps		?
Guida and Minutillo [6]	?	HEX (empirical)	?	MATHCAD15
Snyder et al. [7]		HEX	?	FLOPS, VSP & NPSS
Inacio et al. [8]	?	Complete system (empirical)	Pump	SUAVE
Vredenborg and Thielecke [9]	Said to be considered	Said to be considered (pipes & fittings)	Said to be considered (pump)	Modelica & Dymola
Juschus [14]		Wet HEX, coolant pump & piping		MATLAB
Comincini [11]		Thermal management not considered		MATLAB
Thirkell [10]	?	?	?	?
Vonhoff [12] based on Chapman et al. [13]	Cooling thrust analysed	Wet HEX, pump, fan, pipes & factor for misc.	Pump & fan	Python & SUAVE
Scholz et al. [1]		Thermal management not considered		MATLAB & AVL
Waddington et al. [16]	HEX	Said to be considered	?	?
Eržen et al. [53]	Internal & external drag	?	?	Python, OpenVSP & pConcept
Pratt et al. [50]	Complete system (empirical)	HEX, Pump	?	?

Table II.6.1: Summary of fuel cell thermal management system modelling considering parasitic power, parasitic drag and system weight

It is clear from Table II.6.1 that parasitic drag and power are generally not considered in the modelling of fuel cell thermal management system in fuel cell aircraft. Thermal management system weight is often considered in the modelling of fuel cell thermal management system but incompletely. There is a wide variety of modelling software used in these models with MATLAB being the most common.

II.6.2 Parasitic Drag

The lift-to-drag ratio $\frac{L}{D}$ of an aircraft is one of the most important aircraft performance parameters. Maximising the lift-to-drag ratio maximises the range per the Breguet range equation[9] shown in Equation II.6.6 for a jet aircraft. Maximising the lift-to-drag ratio requires minimising the total aircraft drag.

[9] Z. S. Spakovszky et al. *13.3 Aircraft Range: the Breguet Range Equation*. MIT. https://web.mit.edu/16.unified/www/SPRING/propulsion/notes/node98.html

$$R = \frac{V}{g}\frac{1}{SFC}\frac{L}{D}\ln\left(\frac{W_{initial}}{W_{final}}\right) \tag{II.6.6}$$

Drag also has a direct effect on the power required by the aircraft to maintain steady level flight. During steady level flight, the required power is equal to the product of the drag (equal to thrust required) and the aircraft velocity as shown in Equation II.6.7. Minimising drag minimises the power required. For a fuel cell aircraft, a lower power requirement is beneficial as the size and weight of the fuel cell system decrease. It also reduces the amount of liquid hydrogen required to be stored on the aircraft.

$$P_{req} = DV \tag{II.6.7}$$

Because drag has a direct effect on aircraft performance it is important to accurately considered aircraft drag during the preliminary and conceptual design phases. Many components contribute to aircraft drag including the drag associated with the fuel cell thermal management system. It is also important to consider drag associated with the fuel cell thermal management system in the development of aircraft digital twins[10]. As presented in Section II.4.1 the drag associated with ambient air based cooling systems depends heavily on which system is used. Hence it is important to accurately model the drag associated with the different systems. Certain specially design air based cooling systems may offset this drag penalty (see Meredith effect discussed in Section II.4.1.1 and turbulent boundary layer heating in Section II.4.1.2). It is also important to model these contributions. Many drag models and calculation methods exist in open literature. A few will be presented and discussed in the rest of this section.

Hoerner [5] is his book on *Fluid Dynamic Drag* devotes a complete section (chapter IX, section B) to the drag of heat exchanger installations including drag associated with the internal and external flow. Section D of chapter IX discusses the effects of cooling heat on drag. Section E of chapter IX discusses drag associated with inlets and outlets. Drela [82] refers to previous literature, including Hoerner [5], in his article on the drag associated with airfoil integrated heat exchangers. A *viscous/inviscid numerical simulation method* is presented for calculating drag. Three components of cooling drag are presented by Drela [82]. Core drag is the drag associated with the change in flow momentum through the heat exchanger. The drag associated with the nacelle/ cowling is referred to as cowling drag. The drag associated with the installation and integration of the cooling system on the aircraft is referred to as interference drag. There are many more papers and books in open literature on the topic of drag of ram air cooling systems. Due to the similarity of ram air cooling systems and gas turbines, methods and models for calculating the cowling and interference drag of gas turbines can be considered. This is done by Chapman et al. [13] in their thermal management system modelling.

Kellermann et al. [64] in their *Assessment of Aircraft Surface Heat Exchanger Potential* qualitatively discuss the drag associated with surface heat exchangers. Quantification of the drag is left for future work.

II.6.3 Additional Weight

Like drag, aircraft weight has a direct effect on aircraft performance. Increased weight reduces aircraft range, increases take off and landing distance and reduces the rate of climb. An increased aircraft weight also results in an increased power requirement. Hence it is important to accurately model the weight of various components within the aircraft including the thermal management system.

The specific components and weight of a fuel cell thermal management system vary widely depending on the thermal management technique and ambient air cooling system used. Components in a thermal management system may include heat exchangers, coolants, piping, fans, control systems and pumps. Either physics/theoretically based models or empirical based models of these components can be developed and implemented into fuel cell thermal management system models. Both types of models have been implemented in the models discussed in Section II.6.1.

[10] The Alan Turing Institute *Digital twins in aeronautics* `https://www.turing.ac.uk/research/research-projects/digital-twins-aeronautics`

II.6.4 Parasitic Power

The various pumps, fans and control systems of the thermal management system all require electrical power to operate. This power is taken from the aircraft's electrical power source which in the case of fuel cell aircraft is a fuel cell. This may be the main (propulsive) fuel cell system or the auxiliary fuel cell system depending on the aircraft architecture. As the thermal management system is operated almost constantly the baseline power required from the fuel cell system increases. This in turn increases the size and weight of the fuel cell system. An increased fuel cell power requirement also increases the heat output of the fuel cell system which will increase the size of the thermal management system.

II.7

Formulation of Research Objective and Research Questions

Based on the analysis of literature related to thermal management systems for fuel cell systems on commercial aircraft a research gap has been identified. The identified gap is the complete consideration of the effects of the parasitic drag, additional weight and parasitic power of fuel cell thermal management systems on overall aircraft performance in the preliminary and conceptual design phases of aircraft. The objective of the subsequent master thesis is hence to **model the parasitic drag, additional weight and parasitic power associated with air-based fuel cell thermal management systems on commercial fuel cell aircraft and determine their effects on aircraft performance**. In caring out this objective the identified research gap will be covered and contributions made to the field of fuel cell thermal management system modelling for commercial fuel cell aircraft. The master thesis will set out to answer the following research questions.

Q1. How can the parasitic drag, additional weight and parasitic power of air-based fuel cell thermal management systems be taken into account during the preliminary and conceptual design phases of aircraft?

- Q1.1. Which air-based fuel cell thermal management system is seen as the conventional system for near-future commercial fuel cell aircraft?
- Q1.2. Which air-based fuel cell thermal management system is seen as an unconventional system for commercial fuel cell aircraft?
- Q1.3. How can the parasitic drag associated with the air-based fuel cell thermal management systems be modelled?
- Q1.4. How can the additional weight associated with the air-based fuel cell thermal management systems be modelled?
- Q1.5. How can the parasitic power associated with the air-based fuel cell thermal management systems be modelled?
- Q1.6. How can these models be integrated into the Initiator aircraft sizing environment?
- Q1.7. How can these models themselves and their integration within the Initiator aircraft sizing environment be validated?

Q2. How do the parasitic drag, additional weight and parasitic power associated with the air-based fuel cell thermal management systems affect the performance of commercial fuel cell aircraft?

- Q2.1. How does the parasitic drag of the air-based fuel cell thermal management systems contribute to the total drag of an aircraft?
- Q2.2. How does the additional weight of the air-based fuel cell thermal management systems contribute to the weight of an aircraft?
- Q2.3. How does the parasitic power of the air-based fuel cell thermal management systems contribute to the total power required from an aircraft's fuel cell system?

Q2.4. In how far can air-based fuel cell thermal management systems be used in commercial fuel cell aircraft?

The master thesis will begin on the 5th of September 2022. The first step is to create a plan for this nine-month project. As outlined in the research objective, the project will focus on developing and integrating fuel cell thermal management system models for drag, weight and power into the Initiator aircraft sizing environment. The models will be used to analyse the effect of air-based fuel cell thermal management systems on aircraft performance. The work in the Initiator will be a continuation of the work completed by D. Juschus during his master thesis [14]. The focus of the forthcoming master thesis will be first on regional aircraft before potentially expanding the scope to larger aircraft.

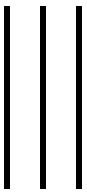

Scientific Paper

Aircraft Integration of Air-Based Thermal Management Systems for Propulsive Fuel Cell Systems

T. Hoogerdijk*
Delft University of Technology, 2628 CD Delft, the Netherlands

Hydrogen fuel cells are a promising technology pathway for aircraft with a considerably lower climate impact than current kerosene-powered aircraft. In addition to producing useful electrical power, fuel cell systems produce a considerable amount of heat which must be removed to ensure the continued and efficient operation of the fuel cell stack. This paper presents a thermal management system sizing methodology for propulsive fuel cell systems onboard 19-passenger commuter aircraft. The developed methodology is implemented into an aircraft sizing environment to study the characteristics of thermal management systems and their effects on aircraft design and aircraft performance. The results show that the thermal management system, through its additional mass, parasitic drag and parasitic power, has both a direct and indirect effect on aircraft performance. In addition to the conventional thermal management system, an unconventional system using nanofluids is studied. The use of nanofluids showed no considerable improvement in both system and aircraft level performance when compared to the base fluid. This paper shows the importance of considering the design of thermal management systems during the conceptual design of fuel cell aircraft.

I. Nomenclature

A	=	Area, m^2
A_0	=	Free flow area, m^2
C	=	Heat capacity rate, W/K
$C_{D,0}$	=	Zero lift drag coefficient, -
c_p	=	Specific heat capacity, J/kgK
C_r	=	Ratio of heat capacity rates, -
D_h	=	Hydraulic diameter, m
e_0	=	Oswald efficiency factor, -
f	=	Fanning friction factor, -
f_{Darcy}	=	Darcy friction factor, -
G	=	Mass velocity, kg/m^2s
h	=	Heat transfer coefficient, W/m^2K
h	=	Height, m
j	=	Colburn factor, -
k	=	Thermal conductivity, W/mK
K_c	=	Entrance loss coefficient, -
K_e	=	Exit loss coefficient, -
L	=	Length, m
$^L/_D$	=	Lift to drag ratio, -
M	=	Mach number, -
m	=	Mass, kg
$\dot{m}$	=	mass flow rate, kg/s
N_p	=	Number of passages, -
NTU	=	Number of transfer units, -
p	=	Power, W
P	=	Pressure, Pa

*MSc Candidate, Faculty of Aerospace Engineering, Kluyverweg 1, the Netherlands

Pr	=	Prandtl number, -
$\dot{Q}$	=	Heat transfer rate, W
$\dot{Q}/_m$	=	Heat rejection parameter, kW/kg
R	=	Thermal resistance, K/W
$R_{specific}$	=	Specific gas constant, J/kgK
r_h	=	Hydraulic radius, m
S	=	Surface area, m^2
T	=	Temperature, K
U	=	Overall heat transfer coefficient, W/m^2K
v	=	Velocity, m/s
V	=	Volume, m^3
w	=	Width, m
α	=	Surface area density w.r.t. V_{tot}, m^2/m^3
γ	=	Heat capacity ratio, -
γ	=	Installation angle, rad
ϵ	=	Heat exchanger effectiveness, -
η	=	Efficiency, -
θ	=	Fin angle, rad
μ	=	Dynamic viscosity, Pas
ρ	=	Density, kg/m^3
σ	=	Ratio of free flow area to frontal area, -
σ	=	Stefan-Boltzmann constant, W/m^2K^4
ϕ	=	Volume concentration, -
Ω_{mass}	=	Mass fraction, -
Ω_{vol}	=	Volume fraction, -
$_\infty$	=	Freestream
$_0$	=	Free flow
$_{bf}$	=	Basefluid
$_{CP}$	=	Coolant pump
$_{cr}$	=	Cruise
$_{EM}$	=	Electric motor
$_{FC}$	=	Fuel cell
$_{FCS}$	=	Fuel cell system
$_{HEX}$	=	Heat exchanger
$_{LH_2}$	=	Liquid hydrogen
$_{nf}$	=	Nanofluid
$_{np}$	=	Nanoparticle
$_{to}$	=	Take-off
$_{TMS}$	=	Thermal management system

II. Introduction

HYDROGEN is seen as one of the more promising energy carriers for the next generation of aircraft that will be more climate-friendly than the previous generation of kerosene powered aircraft*†‡. Two types of hydrogen-based propulsion systems are currently foreseen for such aircraft: hydrogen combustion and hydrogen fuel cell. Hydrogen fuel cells have been found to have a greater *climate impact reduction potential* than hydrogen combustion*. This is mainly due to the low-temperature electrochemical reaction in which no CO_2 or NO_x is emitted during operation. In addition to

* *Hydrogen-powered aviation. A fact-based study of hydrogen technology, economics, and climate impact by 2050.* McKinsey & Company, May 2020. URL: https://www.fch.europa.eu/sites/default/files/FCH%20Docs/20200507_Hydrogen%20Powered%20Aviation%20report_FINAL%20web%20%28ID%208706035%29.pdf Date accessed: 7 Mar. 2023.

† *Airbus reveals new zero-emission concept aircraft.* Airbus, September 2020. URL: https://www.airbus.com/en/newsroom/press-releases/2020-09-airbus-reveals-new-zero-emission-concept-aircraft Date accessed: 7 Mar. 2023.

‡ *Hydrogen | A future fuel for aviation?.* Roland Berger, March 2020. URL: https://www.rolandberger.com/publications/publication_pdf/roland_berger_hydrogen_the_future_fuel_for_aviation.pdf Date accessed: 7 Mar. 2023.

producing useful power, fuel cells produce a considerable amount of heat. For proton-exchange membrane fuel cells (PEMFC) the heat produced is of the same order of magnitude as the electrical power produced [1]. This heat must be removed from the fuel cell stack to ensure its continued and efficient operation. Due to the low operating temperature of PEMFC (around 80°C), the heat to be removed is considered 'low quality' or 'low grade' [2]. This makes the heat transfer more challenging and limits the number of possible heat sinks [2]. The thermal management system is the sub-system tasked with removing heat from the fuel cell stack and dissipating it to a heat sink. The topic of thermal management is not only an important design challenge for fuel cell systems onboard aircraft but also for electrical systems (including battery systems) on more electric aircraft (including the Boeing 787), hybrid-electric aircraft and full-electric aircraft. In their review paper on the topic, van Heerden et al. state these *thermal management challenges are so severe that they are becoming one of the major impediments to improving aircraft performance and efficiency* [2]. Similarly, Schiltgen et al. state that *the heat rejection capability of an aircraft is an often understated limiting factor on performance which can have a significant impact on the design of the* aircraft [3]. The United Kingdom's Aerospace Technology Institute has specified developing *lightweight thermal management systems for hybrid- and all-electric aircraft as a priority activity* [2]. Due to the identified impact on aircraft design and aircraft performance, the design of thermal management systems (TMS) should be adequately considered during the conceptual design of such aircraft.

Literature was studied on the thermal management of fuel cell systems, aircraft thermal management and conceptual design methods of thermal management systems for propulsive fuel cell systems onboard aircraft. These conceptual design methods model the additional mass, parasitic power and parasitic drag attributed to the thermal management system and study their effects on aircraft performance. The additional mass directly affects the operating empty mass (OEM) and maximum take-off mass (MTOM). An increase in aircraft mass increases the amount of lift required which in turn increases the lift-induced drag. This increases the power requirement from the fuel cell system requiring larger fuel cell systems. Increased aircraft mass also increases take-off and landing distances and decreases the rate of climb. The parasitic power of the thermal management systems increases the power required from the fuel cell system increasing system size and weight. The parasitic drag directly affects the zero-lift drag further affecting the power requirement of the fuel cell system. As presented in the following paragraphs the modelling of these contributions in literature has been performed to various levels of detail.

Kožulović [4], in his preliminary design of a thermal management system for a fuel cell aircraft, considered a water cooling system with a wing-mounted ducted counter-flow liquid-air heat exchanger sized for cruise [4]. The additional required power due to the thermal management system was attributed to the additional mass of the heat exchanger and the drag of the ducted heat exchanger. A simplified model to size the heat exchanger was developed. The model used a counter flow configuration which is unlikely to be used in commercial aircraft because the coolant outlet nozzles and header tanks will clutter and disrupt the flow of airflow through the ducting around the heat exchanger core. The mass of the heat exchanger core was multiplied by a sizing factor of 1.2 to take into account the mass of the coolant pipes and pumps. The parasitic power associated with the coolant pump was neglected due to its low power consumption in comparison to the required propulsive power. The core drag was calculated using the momentum theorem and the ramjet effect was taken into account. The external drag of the ducted heat exchanger was estimated based on a drag coefficient value from Hoerner [5] for a wing-mounted nacelle close to the wing trailing edge. The author states *that the external drag estimation was the element with the largest uncertainty in the current study, an issue which has to be addressed much more intensely in the future* [4]. Furthermore, the author recommends focusing on *aircraft-level integration of the large heat exchanger system, together with heat transfer enhancement methods* [4].

Snyder et al. [6] investigate the use of fuel cells in aircraft propulsion systems to further understand these systems and guide future research and analysis. They considered a PEMFC propulsion system with a water cooling system and a multiple-finned tube heat exchanger conceptually mounted underneath the wing sized for cruise. Parametric studies were completed to determine the heat exchanger's size, shape, mass and volume. The overall heat transfer coefficient and area-to-volume ratio were fixed in their modelling. The heat exchanger mass was found to be 16.3% of the complete fuel cell system [6]. Parasitic drag was not considered because *drag reduction and optimization were beyond the scope of this study* [6]. Commenting on this the authors state that preliminary analyses performed yielded designs that reduce parasitic drag to a *less than a 10 per cent increase in total drag* [6]. It was inferred that the parasitic power and mass of the rest of the thermal management system were not considered.

Inacio et al. [7] study the use of liquid hydrogen storage on a PEMFC hybrid-electric aircraft by conceptually retrofitting the Embraer EMB-203 Ipanema crop dusting aircraft. The PEMFC was the single source of power during cruise and nominal operation. As the liquid hydrogen required for propulsion was not able to take on all of the heat originating from the PEMFC powertrain a supplementary thermal management system was designed. The thermal management system consisted of a water cooling loop and a heat exchanger. The mass of the total cooling system was

determined using the specific power of a single off-the-shelf PEMFC fuel cell developed by Ballard Power Systems [7]. The cooling subsystem specific power, the net power output of the fuel cell divided by the mass of the cooling subsystem was 2.27 kW/kg [7]. It was unclear whether the drag of the heat exchanger was considered in the aerodynamic modelling of the aircraft. The power of the cooling pump was included in the modelling [7] however the calculation method was not presented in the paper. The total aircraft mass was increased by 6% compared to the aircraft without the thermal management system [7]. Considering the cooling system specific power of 2.27 kW/kg and the required cooling capacity of 106.5 kW, the mass of the thermal management system was calculated to be 46.9 kg. This is 60.9% of the difference in total mass between the aircraft with and without the thermal management system. The fuel cell power is stated to increase by 5.9% which was primarily attributed to the thermal management system's parasitic power [7].

Vredenborg and Thielecke [8] investigated the thermal management implications of a PEMFC auxiliary power unit (APU) on a commercial aircraft. The system mass, parasitic power and parasitic drag were all said to be considered. However, which specific components were considered was unclear from the paper. The pressure drop of the fluid was determined to calculate the required power for the coolant pumps. A liquid cooling system was used in their modelling and three types of ambient air-liquid heat exchanger systems were proposed. These were a ram air cooling system, tail cone cooling heat exchanger and liquid skin heat exchanger. In the modelling of the heat exchangers, the ϵ-NTU method [8] was implemented and propylene glycol (PGW) was used as the coolant [8]. The mass of the pumps, pipes and fittings are also said to be considered in the model however which specific components are considered was not clear from the paper.

In Comincini's master thesis [9] a design methodology for propulsive PEMFC systems onboard aircraft was developed and analysed. No fuel cell thermal management system was defined in the design methodology. Commenting on the temperature of the fuel cell stack Comincini states that it *is supposed stable, but the way how this characteristic is achieved [...] is not defined* [9]. In Vonhoff's master thesis on the *Conceptual Design of Hydrogen Fuel Cell Aircraft* [10] the thermal management system was considered in some detail. The design methodology was based on a methodology proposed by Chapman et al. [11]. This work presented the thermal design of a turboelectric 15-passenger vertical take-off and landing (VTOL) aircraft with a liquid cooling system and a ducted heat exchanger [11]. In Vonhoff's model, cooling fan and coolant pump power were considered using equations adapted from correlations in Chapman et al. [11]. The mass of the cooling system was determined through Eq. 1 [10] which was adapted from Chapman et al. [11]. The mass of the coolant line, cooling fan, coolant pump and 'wet' heat exchanger were included in the calculations performed by Chapman et al. [11]. A factor of 1.2 was included by Vonhoff on the powertrain mass calculation to *take into account auxiliary components, mounting and cables*.

$$m_{TMS} = (0.194 \cdot p_{heat,rejected} + 1.39) \cdot f(dT) \tag{1}$$

The parasitic drag was neglected as it was reasoned that *due to the action of the cooling fan pulling the air through the* heat exchanger there is a net zero thrust/ drag. Later on in the thesis Vonhoff however discusses the idea of 'cooling thrust' predicted by Chapman et al. [11]. An equation was derived based on correlations proposed by Chapman et al. [11] to calculate the cooling thrust. The cooling thrust calculations were not included in the full design loop but rather included for a side analysis. It was found that the inclusion of cooling thrust reduces the power requirements of the fuel cell by *around 30%*. In the discussion, Vonhoff stated that the *mass and aerodynamic penalty [of the cooling system] were not very significant compared to the other powertrain performance parameters. This is unexpected and should be validated using a more detailed cooling system mode* [10]. Vonhoff goes on to state that *the assumption of zero drag for the cooling system must be verified, as well as the cooling thrust contribution* [10].

Thirkell [12] modelled a propulsive fuel cell system to explore the use of fuel cells onboard aircraft. Though the topic of thermal management system was discussed which thermal management system components were modelled was not discussed beyond stating that *simplified modelling strategies have been developed*, *that the fuel cell stack [was] treated as a single control volume* and *average stack thermal properties* were used [12]. It is inferred that because the topics of parasitic drag and heat exchanger sizing were not discussed in detail that these were not modelled. The variation in ambient air properties with regards to geographical location, altitude and time was discussed in some detail and specifically included in the model. The atmospheric models used were the common International Standard Atmosphere (ISA) and the hot, cold and extremes models from MIL-HDBK-310 [12]. These atmospheric models were also discussed by van Heerden et al. [2] in their paper on aircraft thermal management.

A lot of research has been done into the modelling of fuel cell thermal management systems onboard aircraft and understanding the effects on aircraft design and aircraft performance. No model as found in open literature adequately considers all the effects of parasitic drag, additional weight and parasitic power on aircraft performance during the conceptual design phase. The studied literature does agree on the primary importance of considering the effects of

the fuel cell thermal management system on aircraft performance. The objective of the current study is to continue the development of these fuel cell thermal management models by modelling the parasitic drag, additional weight and parasitic power associated with air-based fuel cell thermal management systems. The focus is on commuter aircraft governed by the Certification Specifications for Normal-Category Aeroplanes (CS-23). This developed model will be implemented into an aircraft sizing environment to understand the characteristics of fuel cell thermal management systems and determine their effects on aircraft performance. The model will go further than previous literature by developing and implementing an unconventional thermal management system which uses nanofluids as the liquid coolant. This objective is formulated into the following research question:

"How can the parasitic drag, additional weight and parasitic power of air-based fuel cell thermal management systems be modelled during the conceptual design of CS-23 commuter aircraft and how do these contributions affect the performance of these fuel cell aircraft?"

The following section in this paper presents the problem background, the fuel cell thermal management systems considered in this study and the working principle of aircraft sizing environments. The developed fuel cell thermal management system sizing methodology is presented in section IV. Specific attention is given to the fuel cell heat model, heat exchanger model, coolant pump model, drag model and nanofluid model. The validation and verification of these models and the complete sizing methodology are detailed in section V. The next section presents and discusses the results of the developed thermal management system for many different configurations. The last section of this paper includes recommendations for future work.

III. Background and Research Objective

The schematic of the fuel cell system considered in the current study is shown in Fig. 1. The electrochemical reactions taking place on the anode and cathode of a PEMFC are shown in Eqs. (2) and (3) respectively. The air loop shown in orange delivers the oxygen to the cathode. The air is first compressed and humidified before entering the fuel cell stack. The hydrogen loop is shown in green and delivers the hydrogen to the anode.

$$\mathrm{H_2} \longrightarrow 2\,\mathrm{H^+} + 2\,\mathrm{e^-} \tag{2}$$

$$\frac{1}{2}\,\mathrm{O_2} + 2\,\mathrm{H^+} + 2\,\mathrm{e^-} \longrightarrow \mathrm{H_2O} \tag{3}$$

The coolant loop of the thermal management system is shown in blue in Fig. 1. The thermal management system consists of three main components: the cooling plates within the fuel cell stack, the ducted heat exchanger and the coolant pump. The cooling plate removes the heat produced by the thermochemical reactions presented above by transferring the heat to the liquid coolant. These cooling plates are integrated within the bipolar plates to reduce the mass and size of the fuel cell stack. The bipolar plates are multi functional as they also deliver the reactants to the cathode and anode and conduct the electrical current through the stack. The air-liquid heat exchanger transfers the heat from the hot liquid coolant to the cool ambient air. This air is directed into the heat exchanger core through a diffuser to *reduce cooling air speed and thereby [reducing] the cold-side pressure loss* through the heat exchanger [13] and minimizing parasitic drag [14]. A higher pressure drop is contradictorily beneficial for the heat transfer performance which leads to a reduced mass flow rate of air and a smaller heat exchanger. There is hence a direct trade-off between minimizing the pressure drop to reduce parasitic drag and maximising the heat transfer to reduce heat exchanger size. The heated ambient air is released back into the atmosphere through a nozzle. A schematic of the ducted heat exchanger with fairing is given in Fig. 2. The subsequent component pumps the coolant through the coolant loop overcoming the pressure drops in the cooling plates, heat exchanger and piping.

This system was based on literature in the field of fuel cell thermal management systems [2, 17–20], the systems implemented on demonstrator fuel cell aircraft [21–24] and the literature presented in section II. Similar thermal management systems have been proposed for the concept aircraft of the UNIFIER19 project [25]. It was inferred that a similar system has been installed on the Dash 8-300 aircraft retrofitted with a single fuel cell engine by Universal Hydrogen[§].

[§]M. Cousin, *Flight Testing an Integrated 1 MW Hydrogen Fuel Cell Powertrain*, Universal Hydrogen, November 2022. URL: `https://www.youtube.com/watch?v=8vZERmQF2I4`. Date accessed: 7 Mar. 2023.

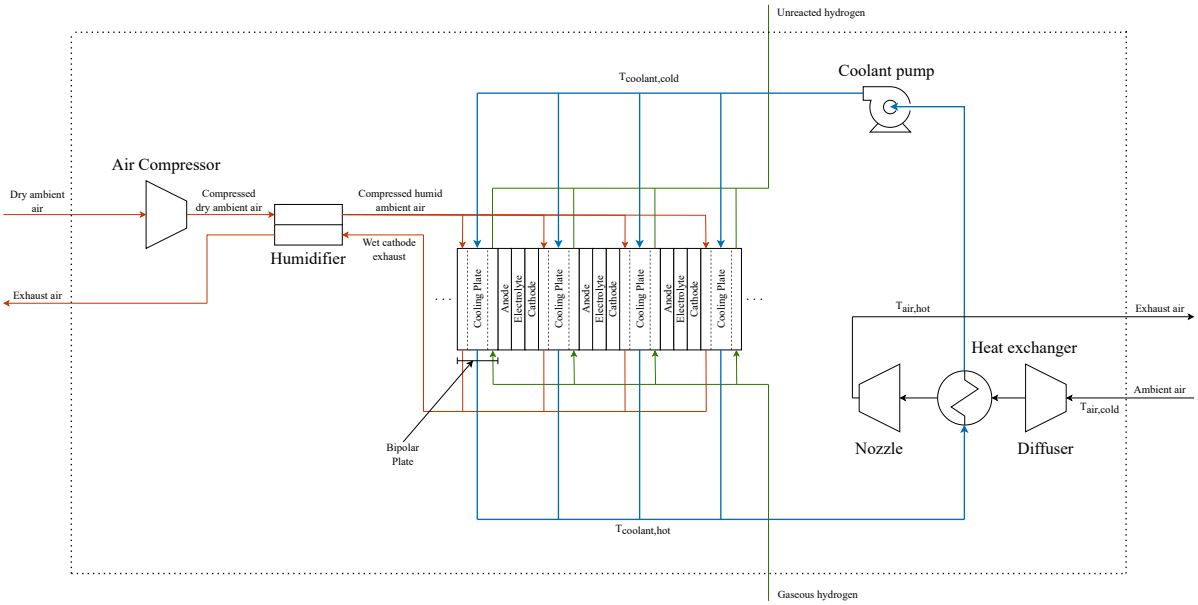

Fig. 1 Fuel cell system schematic (own work based on figure 2.1 in [15]).

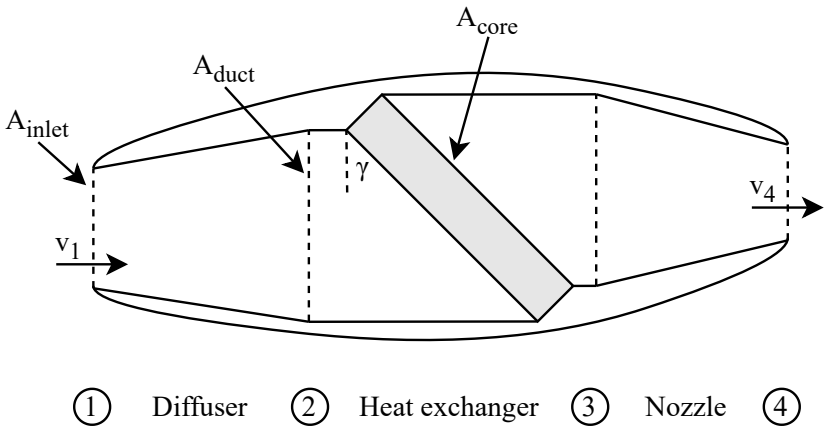

Fig. 2 Ducted heat exchanger schematic (own work based on figure 6 in [16]).

An unconventional thermal management system is proposed aiming to improve thermal management system performance. This system is the same as the conventional system except that nanofluids are used. The conventional system uses water or aqueous ethylene glycol solutions, also known as antifreeze as the liquid coolant [17, 20, 26]. The latter is required in operating environments where the ambient temperature dips below the freezing point of water. Both the Antares DLR-H2 [22] and ENFICA-FC Rapid 200-FC [27] demonstrator aircraft used water as the coolant. Islam et al. [28] propose the use of nanofluids in PEMFC due to their superior heat transfer properties in comparison with the aqueous ethylene glycol base fluid. The main advantages of nanofluids are stated to be an improvement in heat transfer performance, the self-de-ionizing mechanism of the coolant, and a lower freezing point [20, 28, 29]. The two former points mentioned are claimed to result in a smaller and lighter overall system with a lower parasitic power for the same cooing performance [28]. In a later article, Islam et al. [30] model the use of nanofluids in PEMFC and show that *by adding only 0.05 vol% of nanoparticles with 50/50 water/[ethylene glycol] mixture, the frontal area of the [heat exchanger] can be reduced by ~21% compared with the base fluid for [the] same coolant mass flow rate*. Bargal et al. [18] and Huang et al. [20] in their reviews on fuel cell thermal management state that with the use of nanofluids the frontal area of heat exchangers can be reduced by up to around 30%. Islam et al. [28] also mention several challenges in

the use of nanofluids. These include ensuring long-term stability and electrical conductivity. Possible solutions to these challenges include adding inhibitors to the nanofluids to increase stability and decrease electrical conductivity [28]. Zakaria et al. [31] propose the use of Al_2O_3 in water ethylene glycol (aq. EG) mixtures to improve the convective heat transfer coefficient of the coolant. They found that a 0.5% volume concentration improved the heat transfer by 21% for a 50:50% of aq. EG. In their experimental work, they noticed an increase in required pumping power due to a higher pressure drop through the cooling channels [31].

The developed sizing methodology will be implemented into an aircraft sizing environment to study the impact of the thermal management system on aircraft performance. An aircraft sizing environment takes in a considerable number of user-defined inputs and requirements such as the aircraft's design mission and powertrain architecture. Numerous sizing methods are then run in a nested loop sequence. These methods include empirical and physics-based models of varying fidelity in the fields of aircraft aerodynamics, system sizing and weight estimation. Once convergence has been reached the program stops and a conceptual aircraft design is presented. The Aircraft Design Initiator is one such aircraft sizing environment and is developed in-house at the Faculty of Aerospace Engineering at the Delft University of Technology. The software program, simply known as the Initiator was chosen because of its current capabilities in sizing fuel cell aircraft and its development support within the faculty. The Initiator's ability to size both conventional and unconventional aircraft was explained by La Rocca et al. [32] and Elmendorp et al. [33]. Since its inception in 2011 [33] the capabilities of the Initiator have been continuously developed and improved. It currently has two branches: a conventional branch and a hybrid branch. The hybrid branch was first developed by Hoogreef et al. to study *the effect of distributed hybrid-electric propulsion on aircraft performance and characteristics* [34]. Onorato [35] has since implemented physics-based design models to size liquid hydrogen tanks. Juschus [15] expanded the hybrid branch by implementing preliminary sizing models for PEMFC systems. Up until recently, the Initiator was able and validated to size CS-25 category aircraft. Zupanič [36] implemented the ability for CS-23 category commuter aircraft to be conceptually designed within the Initiator.

The fuel cell system is sized in the Initiator through the `FuelCellUnitSizing` function originally developed by Juschus [15]. This function is run within the class 2 weight estimation module and sizes a single fuel cell unit which consists of one or more fuel cell stacks, a compressor, a humidifier and a heat exchanger. Inputs into the function include the required propulsive power, cruise conditions, cell oversizing factor and cell temperature. The fuel cell system is sized for cruise through a while loop about the required fuel cell electrical power. The function determines, among others, the system mass, system dimensions and fuel cell unit efficiency. For a more detailed explanation of the fuel cell system sizing methods used in the Initiator, the reader is referred to work published by Juschus [15] and Zupanič [36].

The current study continues the development of the Initiator's fuel cell system sizing methodology by developing and implementing a new and improved fuel cell thermal management system sizing methodology. The fuel cell system sizing methodology developed by Juschus [15] inadequately considers the thermal management system. Only the effects of the heat exchanger mass were considered. The heat exchanger model used was based on a simplified model developed by Kožulović for a counter-flow configuration with triangular fins on the air side and tubes on the coolant side [4]. This flow configuration is unlikely to be implemented in any fuel cell aircraft because the coolant outlet nozzles and header tanks will disrupt the airflow through the ducting around the heat exchanger core which will have a negative effect on drag. Furthermore, the thermal management system was sized for cruise whereas take-off is seen as more challenging for the thermal management system. This is due to the higher temperatures at ground level and lower aircraft velocity during the take-off run. The effects of parasitic drag, the mass of the coolant pump and the power required by the coolant pump on the sizing of the fuel cell system and aircraft performance were not considered. The latter two are expected to have a minimal impact on overall aircraft performance however the parasitic drag may have a large and detrimental effect on aircraft performance.

IV. Methodology

In developing the fuel cell thermal management system sizing methodology several simplifying assumptions were made, the most significant are listed below and explained thereafter.

- The fuel cell system is sized for cruise when the required power is solely supplied by the fuel cell system. The heat exchanger is sized for take-off.
- The heat exchanger is placed at an installation angle within the ducted heat exchanger fairing such that the cross-sectional area of the duct is equal to the free flow area on the air side of the heat exchanger.
- The ducted heat exchanger includes an active ducting system and is installed on either side of the wing-mounted fuel cell engine.

- All heat produced by the fuel cell stack is removed by the thermal management system.
- The hot coolant temperature is 5% lower than the cell temperature of 80°C.

The first assumption was taken directly from previous work completed by Juschus [15]. In their modelling, the fuel cell system provides all the power required during cruise as is done in Inacio et al. [7] and Snyder et al. [6]. During higher power flight phases, such as take-off and climb, batteries supply additional power to the electrical motor. The heat exchanger is sized for take-off as this will be the most challenging environment for the heat exchanger to dissipate heat from the coolant to the atmosphere. The specific design point during the takeoff phase is taken to be lift off under ISA conditions at sea level. The atmospheric temperature at this point will be higher than, and the velocity lower than during cruise. It was further assumed that the thermal inertia of the fuel cell system will maintain the fuel cell stack temperature below the maximum operating temperature of the stack up until the design point of the thermal management system. The ducted heat exchanger was assumed to have an active flow control system which alters the inlet area of the diffuser and the outlet area of the nozzle. These areas change depending on the required mass flow rate of air through the heat exchanger. The active flow control system was assumed to be completely open during take-off. The mounting of the heat exchanger was based on the installation of the heat exchanger on the Dash 8-300 aircraft retrofitted by Universal Hydrogen[§].

The three main components of the thermal management system are individually modelled. The fuel cell heat model addresses the heat transfer between the fuel cell stack and liquid coolant within the cooling plate. The model is detailed in section IV.A. The heat exchanger model sizes a heat exchanger for the heat transfer problem defined by the fuel cell heat model and atmospheric conditions. It determines the dimensions, 'wet' mass and pressure drop in both fluid streams. This model is detailed in section IV.B. The coolant pump model determines the pump mass and power. This model is detailed in section IV.C. In addition to these models, models have been developed to determine the drag attributed to the thermal management system and the thermophysical properties of nanofluids for the unconventional system.

The new and improved fuel cell thermal management system sizing methodology was implemented into the Initiator in two locations. The function `FuelCellUnitSizing` was expanded to include the new thermal management system sizing methodology. This function contains the fuel cell heat model, heat exchanger model, coolant pump model and nanofluid model. This function is called within the preexisting `getEngineWeight` function and run in the class two weight estimation module. The drag model is run at a later stage in the design loop. The drag model was implemented in a new function called `thermalManagementSystemDrag` and run within the parasite drag estimation module.

A. Fuel Cell Heat Model

The total amount of heat produced within the fuel cell stack was determined using Eq. (4) where cell efficiency is the ratio of the cell voltage and thermodynamic voltage [37]. Equation (4) was based on Guida and Minutillo [38] and Thirkell [12].

$$\dot{Q}_{stack} = p_{stack}\left(\frac{1}{\eta_{cell}} - 1\right) \tag{4}$$

The assumption was made that all the heat produced within the fuel cell system is taken away by the thermal management system. This is however not the case in practice as other heat sinks exist in the fuel cell stack including heat dissipated through natural convection [18, 20], heat used for internal water evaporation [18, 20] and heat removed by reactants [18, 20]. Hence the sizing thermal management system will be a conservative one.

A simple parallel channel cooling plate with rectangular passages was implemented. The geometry of the rectangular channels was taken directly from table 1 in Baek et al. [39]. The surface area of the cooling plate was assumed to be equal to the area of the individual cells. The temperature of the coolant exiting the cooling plate (the hot coolant temperature) was calculated based on the assumption of $0.95T_{stack}$. For the assumed stack temperature of 80°C the hot coolant temperature calculated is very similar to the hot coolant temperature claimed by Universal Hydrogen in normal operation of the system installed on their retrofitted Dash 8 aircraft[§]. The required temperature of the coolant entering the cooling plate (the cold coolant temperature) was then determined through Eq. (5) [40]. The cold coolant temperature was calculated such that the coolant temperature difference was in agreement with literature, specifically Datta who states that the difference should be below 15°C [41]. This was done by varying the number of cooling plates in the stack. The required coolant mass flow rate was then calculated through Eq. (6) [40, 42, 43].

$$\dot{Q} = \frac{hA(T_{coolant,cold} - T_{coolant,hot})}{\log\left(\frac{T_{cell}-T_{coolant,hot}}{T_{cell}-T_{coolant,cold}}\right)} \tag{5}$$

$$\dot{Q} = \dot{m}_{coolant} C_{p,coolant} (T_{coolant,hot} - T_{coolant,cold}) \tag{6}$$

B. Heat Exchanger Model

A cross-flow single pass unmixed-unmixed air-liquid plate-fin heat exchanger (PFHE) with triangular fins was chosen for the fuel cell thermal management system. The PFHE type was chosen as it is extensively used in the aerospace industry due to its *compactness and lightweight properties* [44]. The cross-flow configuration allows for minimal disruption of the airflow through the ducted heat exchanger. Both fluids flows pass through triangular fins in a rectangular passage. Due to the finned passage on both sides, these passages are said to be *unmixed* [45]. The triangular fin geometry was based on the plate-fin 12.00T type presented in Kays and London [46].

For the sizing of the heat exchanger the ϵ-NTU method was chosen based on the recommendation by Incropera et al. [43] and Carozza [47] to use this method if only the inlet temperatures are known, which was the case in the current study. Shah and Sekulić state that the ϵ-NTU method *is used most commonly in the industry for [plate-fin heat exchangers]* [45]. This method was also used by Khan and Li [48] in their design of a PFHE using multi-objective algorithms and by Brooks and Marvis [49] in their sizing of compact heat exchangers for use in aircraft environmental control systems. A simplified flow diagram of the method implemented is shown in Fig. 3. The most important parts of the heat exchanger sizing problem and ϵ-NTU method are presented and elaborated upon in the following paragraphs.

The inputs into the heat exchanger model included the fin geometry, material properties, allowable pressure drops, amount of heat to be transferred, coolant mass flow rate, inlet temperature and outlet temperature. The first step in the model was to calculate the atmospheric properties at the take-off sizing case. This was calculated using the pre-existing `Atmosphere` function within the Initiator and the CoolProp [50] open-source thermophysical property library. The total air inlet temperature and pressure were calculated using the ram air relations as presented by van Herden et al. [2]. The mass flow rate of air was calculated based on this inlet area using the ideal compressible mass flow equation shown in Eq. (7)[¶]. For the first iteration of the model the ducted heat exchanger inlet area was set to 1 m^2. In subsequent iterations and following the assumption that the ducted heat exchanger with active flow control is fully open during take-off, the inlet area was set equal to the duct area from the previous iteration. If the ducted heat exchanger is located in the propeller wake the Mach number was calculated based on the velocity at the propeller disk. If not, the free stream Mach number was used.

$$\dot{m}_{air} = \frac{A_1 P_{amb,0}}{\sqrt{T_{amb,0}}} \sqrt{\frac{\gamma_{air}}{R}} M \left(1 + \frac{\gamma_{air} - 1}{2} M^2\right)^{-\frac{\gamma_{air}+1}{2(\gamma_{air}-1)}} \tag{7}$$

The air outlet temperature was calculated in an iterative manner using Eq. (8).

$$\dot{Q} = \dot{m}_{air} C_{p,air} (T_{air,hot} - T_{air,cold}) \tag{8}$$

The mean temperatures were used to determine the thermophysical properties of the respective fluids using CoolProp. If a nanofluid was used as the coolant medium the nanofluid model to be described in section IV.E was used.

The core of the ϵ-NTU method is the calculation of three non-dimensional parameters: the ratio of heat capacity rates, heat exchanger effectiveness and the number of transfer units (NTU). The first is defined as the ratio of the minimum and maximum heat capacity rate. The heat capacity rate is the product of the mass flow rate and specific heat capacity of the fluid. The heat exchanger effectiveness is calculated through the two equivalent relations shown in Eq. (9) [43, 45].

$$\epsilon = \frac{C_{coolant}(T_{coolant,in} - T_{coolant,out})}{C_{min}(T_{coolant,in} - T_{air,in})} = \frac{C_{air}(T_{air,out} - T_{air,in})}{C_{min}(T_{coolant,in} - T_{air,in})} \tag{9}$$

The equations for NTU are shown in Eq. (10) and were obtained from reference tables in Shah and Sekulić [45] and Incropera et al. [43] for the cross-flow single pass unmixed-unmixed flow arrangement. The equation for the case when

[¶]T. Benson. (ed.), *Mass Flow Rate*, NASA Glenn Research Center, 2021. URL: `https://www.grc.nasa.gov/www/k-12/rocket/mflchk.html`. Date accessed: 21 Feb. 2023.

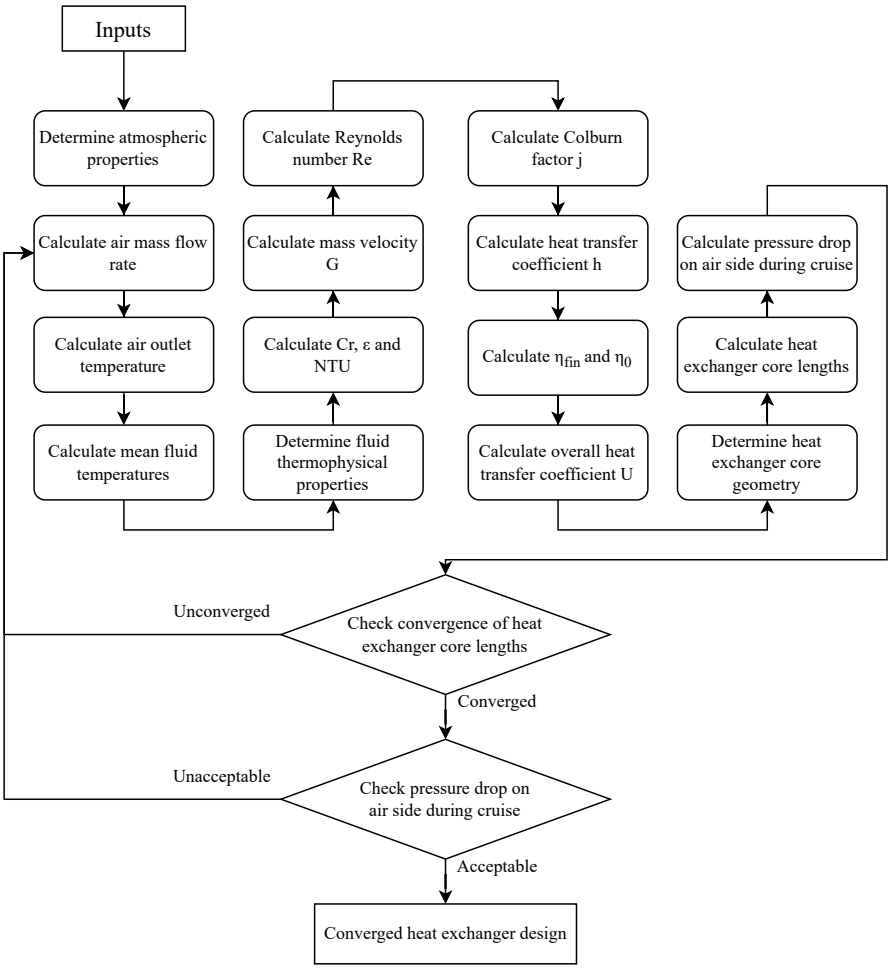

Fig. 3 Heat exchanger sizing methodology (own work based on ϵ-NTU method proposed in Shah and Sekulić [45]).

the ratio of heat capacity rates is zero was rearranged to solve for NTU directly. The equation for the other case was solved in an iterative manner using the `fzero` MATLAB function.

$$\epsilon = \begin{cases} 1 - \exp\left(-\mathrm{NTU}\right) & \text{if } C_r = 0 \\ 1 - \exp\left(\frac{1}{C_r}\mathrm{NTU}^{0.22}\left(\exp\left[-C_r\mathrm{NTU}^{0.78}\right] - 1\right)\right) & \text{if } C_r > 0 \end{cases} \tag{10}$$

The individual side ntu was then calculated based on the assumption proposed by Shah and Sekulić [45] for the case where there is a fluid on one side and a gas on the other. The specific assumption is shown in Eqs. (11) and (12) [45]. This assumption was checked as part of the verification of the model.

$$\mathrm{ntu}_{air} = 1.11\mathrm{NTU} \tag{11}$$

$$\mathrm{ntu}_{coolant} = 10C_r\mathrm{NTU} \tag{12}$$

In the first iteration, when the Reynolds number was unknown, the mass velocity of both fluid flows was calculated using Eq. (13) [45]. An approximation for the ratio of Colburn factor and Fanning friction factor was taken as the mean ratio over the complete Reynolds number range of available data for the plate-fin 12.00T geometry published by Kays and London [46] as suggested by Shah and Sekulić [45]. The Colburn factor relates the heat transfer with momentum and is defined as the product $\mathrm{St}\,\mathrm{Pr}^{2/3}$. The Fanning friction factor relates friction and pressure drop with flow velocity.

Both these factors are dependent on the fin geometry within the heat exchanger core and a function of the Reynolds number.

$$G = \sqrt{\frac{2}{\frac{1}{\rho_m}\mathrm{Pr}^{2/3}} \frac{\eta_0 \Delta P}{\mathrm{ntu}} \left(\frac{j}{f}\right)_{approx.}} \tag{13}$$

In subsequent iterations, Eq. (14) [45] was used to calculate the mass velocity of both fluids. The exact value of the Fanning friction factor was calculated based on data for the plate-fin 12.00T geometry. The entrance and exit loss coefficients were determined from figure 6.3 in Shah and Sekulić [45] for triangular core geometry with an abrupt entrance and exit.

$$G = \sqrt{\frac{2\rho_i \Delta P}{\left(1 - \sigma^2 + K_c\right) + 2\left(\frac{\rho_i}{\rho_o} - 1\right) + f\frac{L}{r_h}\rho_i \frac{1}{\rho_m} - \left(1 - \sigma^2 - K_e\right)\frac{\rho_i}{\rho_o}}} \tag{14}$$

Once the mass velocity was calculated for both fluid flows the Reynolds number was calculated through Eq. (15).

$$Re = \frac{GD_h}{\mu} \tag{15}$$

The exact Colburn factor was then calculated for the known Reynolds number of the flow using the data for the plate-fin 12.00T geometry from Kays and London [46]. The heat transfer coefficients on either fluid sides were calculated using Eq. (16) for the first iteration and Eq. (17) for subsequent iterations.

$$h = \frac{jG}{\mathrm{Pr}^{2/3}} \tag{16}$$

$$h = \frac{\mathrm{Nu}\, k}{D_h} \tag{17}$$

In the first iteration, Eq. (18) [45] was used to calculate the overall heat transfer coefficient on the air side. This equation neglects the convective thermal resistance of the wall as the wall area is unknown in the first iteration.

$$\frac{1}{U_{air}} = \frac{\alpha_{air}/\alpha_{coolant}}{(\eta_o h)_{coolant}} + \frac{\alpha_{air}/\alpha_{coolant}}{(\eta_0 h_f)_{coolant}} + \frac{1}{(\eta_0 h_f)_{air}} + \frac{1}{(\eta_0 h)_{air}} \tag{18}$$

In subsequent iterations, when the wall area is taken from from the previous iteration, Eq. (19) [45] was used to calculate the overall heat transfer coefficient on the air side.

$$\frac{1}{U_{air}} = \frac{A_{air}/A_{coolant}}{(\eta_o h)_{coolant}} + \frac{A_{air}/A_{coolant}}{(\eta_0 h_f)_{coolant}} + \frac{\delta_w A_{air}}{k_w A_w} + \frac{1}{(\eta_0 h_f)_{air}} + \frac{1}{(\eta_0 h)_{air}} \tag{19}$$

Once the overall heat transfer coefficient was calculated various geometric properties of the heat exchanger were calculated. These geometric properties included the heat transfer areas, free flow area to frontal area ratios, heat exchanger core lengths and the number of passages. The heat exchanger lengths are the coolant flow length, airflow length and no-flow length. The duct area was calculated based on the assumption that the heat exchanger is placed at an installation angle within the heat exchanger ducting such that the duct area is equal to the free flow area on the air side. The heat exchanger installation angle is defined in Fig. 1.

The pressure drop through the heat exchanger was calculated using Eq. (20) as used by Chapman et al. [11] in their thermal management system sizing methodology. This relation was similar to the equation presented in Shah and Sekulić's book on heat exchanger design [45] but with a number of simplifying assumptions. The entrance and exit loss coefficients were determined from figure 6.3 in Shah and Sekulić [45] for triangular core geometry with an abrupt entrance and exit.

$$\Delta P = \frac{G^2}{2\rho}\left((K_c + 1 - \sigma^2) + f\frac{L}{r_h} - (1 - \sigma^2 - K_e)\right) \tag{20}$$

In order to determine the pressure drop through the heat exchanger during cruise the required mass flow rate of air through the ducted heat exchanger during cruise was calculated. With the core heat exchanger geometry fixed the mass flow rate was determined through Eq. (8) in an iterative manner.

The previous steps were iterated upon until convergence was achieved on the heat exchanger core lengths and the pressure drop through the heat exchanger during cruise was deemed acceptable. An example of the convergence of the model is shown in Fig. 8 in Appendix A. In the instance of an unconverged or unacceptable heat exchanger design a subsequent iteration was initiated at the step in the method where the mass flow rate of air was calculated. In this subsequent iteration, the duct area from the previous iteration was used in calculating the mass flow rate of air at take-off in Eq. (7).

Once a converged heat exchanger design was achieved the mass of the wet heat exchanger was estimated. Aluminium was chosen as the heat exchanger material because of its low-density properties. Furthermore, Sunden and Fu state that *[i]n [the] aerospace industry, aluminum alloy PFHEs have been used for 50 years* [44]. Specifically 3003 series aluminium alloy was chosen due to its use in Linde's plate-fin heat exchangers[‖] and because of its higher thermal conductivity, specifically aluminium 3003-O was chosen. The material properties were taken from an online material property database based on supplier data[**]. The structural mass was estimated as the product of the internal volume of the fins and walls and the aluminium alloy density. The mass of the coolant within the heat exchanger was estimated as the product of the coolant passage volume and the density of the coolant. The calculated heat exchanger mass was multiplied by a factor of 1.2 to take into account inlet and outlet nozzles, headers tanks and support plates. This factor was taken from Brooks and Marvis [49] who used it in their sizing of compact heat exchangers for use in aircraft environmental control systems. A factor of 1.2 was also used by Vonhoff [10] for similar purposes.

C. Coolant Pump Model

Once the fuel cell stack and heat exchanger were sized the coolant pump was sized accordingly. The power required by the coolant pump was calculated using Eq. (21) [51, 52]. The total pressure drop of the coolant between the pump inlet and outlet was calculated as the sum of the pressure drop through the fuel cell stack, piping and heat exchanger. The hydraulic efficiency of the coolant pump was taken from Li et al. [52] to be 0.55. The efficiency of the electric motor was taken from Comincini [9] to be 0.95.

$$p_{CP} = \frac{\dot{m}_{coolant}\Delta P}{\rho_{coolant}\eta_{CP}\eta_{EM}} \tag{21}$$

The total pressure drop of the coolant between the pump inlet and outlet was calculated as the sum of the pressure drop through the fuel cell stack, piping and heat exchanger. The hydraulic efficiency of the coolant pump was taken from Li et al. [52] to be 0.55. The efficiency of the electric motor was assumed to be 0.95. The pressure drop of the coolant through the fuel cell stack was calculated using the equation shown in Eq. (22) [53, 54]. In the laminar flow regime, the relation $f_{Darcy}Re = 64$ was used to determine the Darcy friction factor. In the turbulent flow regime the Colebrook equation [55] was used.

$$\Delta P = f_{Darcy}\frac{L}{D_h}\frac{\rho {v_{avg}}^2}{2} \tag{22}$$

The pressure drop through the piping was calculated in a similar manner as for the fuel cell stack. In addition, the pressure drop through a number of open valves and 90-degree bends was also considered to determine the pressure drop for a representative piping system. The pressure drop of the coolant through the heat exchanger was detailed in section IV.B, specifically Eq. (20).

The mass of the coolant pump was empirically determined based on the performance curves of a number of off-the-shelf coolant pumps. These pumps, with the exception of the pump developed by Parker, are non-aerospace hence the calculated coolant pump mass was assumed to be a conservative estimate. The performance curves of the pumps are shown in Fig. 4. The coolant pump mass was determined as the average of the mass of one or more pumps of the same type where the coolant pump operating point lies within +0m and -16m of the respective pump performance curve. A maximum of five pumps were allowed to be connected in parallel to obtain the required volumetric mass flow rate.

[‖] Linde Engineering, *Aluminium plate-fin heat exchangers.*, The Linde Group. URL: `https://www.linde-engineering.com/en/images/30160_LE_Manufacturing_PFHE_brochure_update_RZ_VIEW_tcm19-406598.pdf`. Date accessed: 23 Feb. 2023.

[**] *Aluminum 3003-O*, MatWeb. URL: `https://www.matweb.com/search/DataSheet.aspx?MatGUID=fd4a40f87d3f4912925e5e6eab1fbc40`. Date accessed: 23 Feb. 2023.

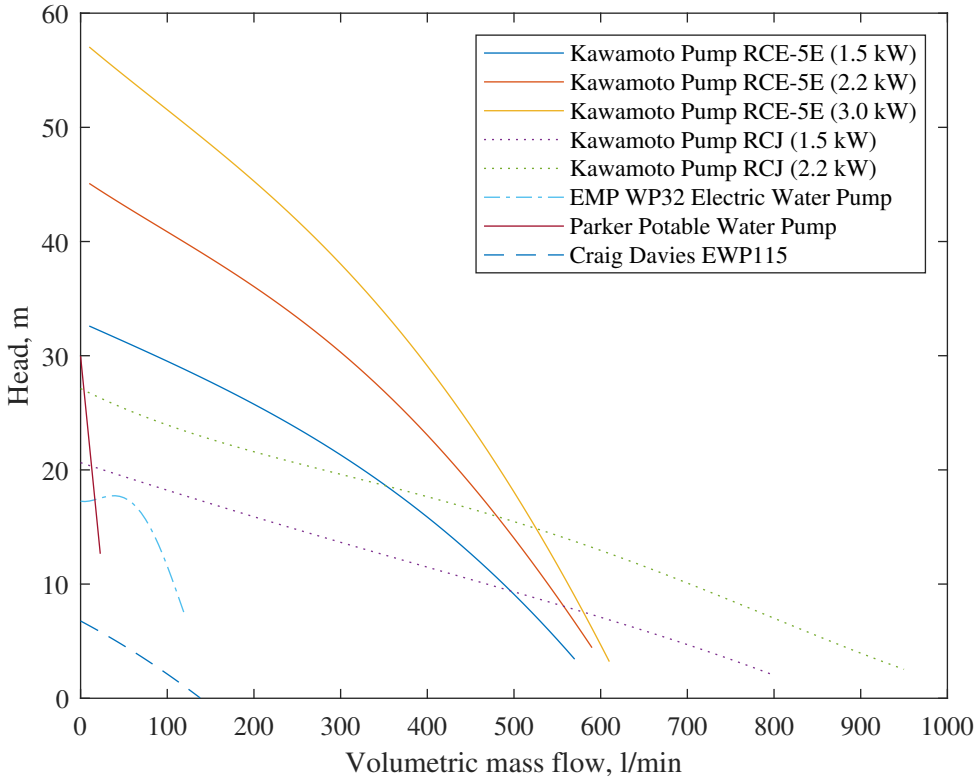

Fig. 4 Performance curves of coolant pumps used in coolant pump model.

D. Drag Model

The parasitic drag of the ducted heat exchanger comprises two components: core drag and external drag. The core drag was modelled by considering the momentum loss through the ducted heat exchanger. The core drag coefficient was determined through Eq. (23) which was based on the equation for momentum loss used by Drela [56] and the well-known drag equation. The exit velocity was calculated based on isentropic relations through the ducted heat exchanger. The diffuser isentropic efficiency was assumed to be 0.95 and the nozzle isentropic efficiency 0.98. The pressure drop of air through the heat exchanger and hot air temperature were taken from the heat exchanger model detailed in section IV.B.

$$C_{D_{0,TMS,core}} = \frac{\dot{m}_{air}(v_\infty - v_4)}{\frac{1}{2}\rho_{amb} {v_\infty}^2 S_{ref}} \tag{23}$$

The external drag of the ducted heat exchanger was modelled by increasing the diameter of the fuel cell engine nacelle to accommodate the ducted heat exchanger. This increase in diameter reduces the slenderness of the nacelle which in turn increases the form factor of the nacelle [57]. This leads to an increase in the zero-lift drag coefficient of the nacelle. This engine drag model was already present in the Initiator and was hence outside the scope of the current study. A modified engine drag model was used to obtain a zero-lift drag coefficient of the nacelle without accommodating for the ducted heat exchanger. The difference in the zero-lift drag coefficient with and without the installed heat exchanger was taken to be the external drag coefficient associated with the thermal management system. The components of external drag that are intended to be covered through this method include the skin friction drag of the heat exchanger ducting, spillage drag and interference drag between the heat exchanger ducting, fuel cell engine nacelle and the main wing.

E. Nanofluid Model

The nanofluid model was used to determine the specific heat, dynamic viscosity, thermal conductivity, Prandtl number and density of various nanofluids. The properties of the base fluids are obtained using CoolProp [50]. The

mixing ratio of solutions must be given in mass fraction into CoolProp. This is different to the industry standard where volume fraction is more common. To convert from volume fraction to mass fraction Eq. (24) was used.

$$\Omega_{mass,EG} = \frac{\rho_{EG}\Omega_{vol,EG}}{\rho_{EG}\Omega_{vol,EG} + \rho_{water}(1 - \Omega_{vol,EG})} \tag{24}$$

The effective dynamic viscosity was calculated using Einstein's model as shown in Eq. (25) [28, 58] and is a function of the volume concentration of the nanoparticle in the nanofluid. Maxwell's model was used to determine the effective thermal conductivity and is shown in Eq. (26) [28, 59]. Both models were used by Islam et al. [28] in their study on the use of nanofluids to reduce the size of PEMFC thermal management systems.

$$\mu_{nf} = (1 + 2.5\phi)\mu_{bf} \tag{25}$$

$$k_{nf} = \frac{k_{np} + 2k_{bf} + 2(k_{np} - k_{bf})\phi}{k_{np} + 2k_{bf} - (k_{np} - k_{bf})\phi} k_{bf} \tag{26}$$

The effective density and specific heat were determined through Eq. (27) and Eq. (28) respectively and were based on relations used by Zakaria et al. [31] in their analysis on the use of nanofluids for PEMFC thermal management. The Prandtl number was determined based on its definition shown in Eq. (29) [30].

$$\rho_{nf} = (1 - \phi)\rho_{bf} + \phi\rho_{np} \tag{27}$$

$$C_{p,nf} = \frac{(1 - \phi)C_{p,nf}\rho_{bf} + \phi\rho_{np}C_{p,nf}}{(1 - \phi)\rho_{bf} + \phi\rho_{np}} \tag{28}$$

$$\mathrm{Pr} = \frac{C_p\mu}{k} \tag{29}$$

V. Verification and Validation

A. Verification of the Fuel Cell Thermal Management Sizing Methodology

The verification of the development sizing methodology was done by checking the code and verifying model results with literature. A small number of examples are presented and discussed in this section. In the fuel cell heat model, the heat generated by the fuel cell stack was checked by calculating the value through two different methods and comparing the results. The baseline equation is shown in Eq. (4) and the second equation was taken from equation 6-18 from Spiegel [42]. It was shown that the difference in the values is less than 0.1%, if not a warning message was raised. A similar check is done on the amount of heat dissipated by the heat exchanger model by comparing the value calculated through Eq. 4 with the value calculated through Eq. (30) [45]. This verification step was done after the heat exchanger effectiveness and the minimum heat capacity ratio were calculated.

$$\dot{Q} = \epsilon C_{min}(T_{coolant,hot} - T_{coolant,cold}) \tag{30}$$

In the heat exchanger model, the assumption made when calculating the ntu value on either fluid side was checked with equation 9.22 in Shah and Sekulić [45]. If the temperature of the coolant leaving the fuel cell stack was not higher than the temperature of the coolant entering the stack an error message was raised within the fuel cell heat model. Other checks carried out include on the Reynolds number, surface area density, ratio of free flow area to frontal area and the speed of speed.

A parameter compared against literature is the ratio of the air velocity at the heat exchanger inlet and the freestream velocity. Hoerner [5] expects this ratio to be between greater than 0 and below 0.5. Kožulić [4] put forward an even narrower range for this value, stating it to be between 0.1 and 0.25. A warning message is raised for both ranges and an error message is raised if this ratio is greater than 1, which is impossible in the current system configuration. For the Metro 23 aircraft, to be discussed in section VI, this velocity ratio is shown to be at the very low end of the range put forward by Kožulić. The ratio of the heat removed from the fuel cell stack and the temperature difference between the atmospheric temperature and hot coolant temperature is also compared with literature. This ratio is compared with a target for automotive stacks, which is less than 1.45 kW/°C according to Datta [41]. The parameter was only verified for

the HY4 demonstrator aircraft, to be discussed in section V.D, as the system installed on this aircraft is similar in size to automotive stacks. The heat rejection parameter for the HY4 demonstrator aircraft was found to be 1.86 kW/°C. This value is 28.3% higher than the target put forward by Datta which is only beneficial.

The external drag coefficient is compared with data presented by Hoerner [5] in chapter IX section B of his book on *Fluid-Dynamic Drag*. For heat exchangers mounted underneath the engine nacelle, the external drag coefficient was stated to be between 0.1 and 0.2 [5]. For heat exchangers mounted in a ring configuration, the external drag coefficient was stated to be around 0.04 [5]. For heat exchangers mounted near or at the wing trailing edge, the external drag coefficient was stated to be around 0.06 [5]. These drag coefficients are defined with respect to the *protruding frontal area* of the ducted heat exchanger [5]. The external drag coefficient with respect to the ducted heat exchanger area was found to be 0.0187 for the Metro 23. This is quite a bit below the ranges given by Hoerner and most closely correlates to the ring mounted heat exchangers. This ring configuration is in line with the approximation made in the calculation of the ducted heat exchanger external drag coefficient presented in section IV.D. It is noted that Hoerner's values were based on World War Two era aircraft and wind tunnel investigations from the 1930s and 1940s. Aircraft aerodynamics has developed and improved tremendously since then hence these values are outdated and no longer completely representative of current technology. Nevertheless, the external ducted heat exchanger drag model should be developed further in future work.

B. Validation of the Heat Exchanger Model

The heat exchanger model was validated using EchTherm, a commercial heat exchanger sizing software tool developed by Neotherm Consulting[††]. The validation was carried out by running a validation case in the heat exchanger model developed in this study and comparing it with the results from EchTherm. The validation case was a cross-flow single pass unmixed-unmixed air-air plate fin heat exchanger with rectangular offset strip fins (OSF). There were two differences between the validation case and the heat exchanger used in this study: the coolant medium and fin type. The latter required additional relations for the Colburn factor and Fanning friction factor. The relations proposed by Manglik and Bergles [60] for rectangular OSF were implemented. The validation case in EchTherm was performed by a PhD student working on heat exchanger modelling. Selected results of the validation case are presented in Table 1. The average values for the figures of merit which vary through the fluid passages are given in Table 1. These figures of merit include the Reynolds number, heat transfer coefficient and Fanning friction factor.

Comparing the results it was shown that most of the figures of merit of the current model were within ±10% of the results obtained through EchTherm. The overall heat transfer coefficient was 8.3% lower and the core mass 3.1% higher than the values obtained through EchTherm. The heat exchanger core volume was considerably higher than the value obtained through EchTherm. This is linked back to the heat exchanger core lengths which were considerably different than the values obtained through EchTherm. This is believed to be related to the offset nature of the fins, something that was not fully modelled for the fins used in the heat exchanger used in the thermal management system. However, when comparing the frontal areas on the air and coolant side there is a better correlation between the current model and EchTherm. The heat transfer coefficients on both fluid sides are considerably higher than the values obtained through EchTherm. This is understood to be related, among other things, to the simplified modelling of the entrance and exit loss coefficients used in the calculation of the mass velocity. Both the fin efficiencies and overall heat transfer coefficient are a function of the heat transfer coefficients. These values were not largely affected by the heat transfer coefficients as these values were shown to be within ±10% of the values obtained through EchTherm.

The thermophysical properties of both fluids at the respective inlets and outlets were also validated against EchTherm. The properties at both inlets were found to be within ±0.0%. The properties at the outlets were also found to be within ±0.0% except for the density of the air and coolant and the Prandtl number of the coolant. These differences were -1.0%, -0.3% and -0.1% respectively.

In considering the results of the validation of the heat exchanger model the model was deemed sufficiently validated for the purposes of this study. It should however be considered when analysing the results that the core flow lengths and resulting volume are generally conservative.

C. Validation of the Nanofluid Model

The nanofluid model was validated against experimental measurements presented in literature. Unless stated otherwise the validation of the model was conducted with aqueous ethylene glycol containing Al_2O_3 nanoparticles at

[††]EchTherm v7.2.2. Neotherm Consulting, January 2023. URL: `https://greth.fr/telecharger-echtherm/`

Parameter	Unit	EchTherm	Current Model	Difference
Air outlet temperature	°C	63.73	63.74	0.0%
Heat exchanger efficiency	-	0.573	0.573	0.0%
Reynolds number (air side)	-	5721	5637	-1.5%
Reynolds number (coolant side)	-	6309	6302	-0.1%
Heat transfer coefficient (air side)	W/m^2K	268.2	328.6	+22.5%
Heat transfer coefficient (coolant side)	W/m^2K	305.9	387.9	+26.8%
Fin efficiency (air side)	-	0.749	0.760	+1.5%
Fin efficiency (coolant side)	-	0.719	0.740	+2.8%
Overall surface efficiency (air side)	-	0.786	0.777	-1.1%
Overall surface efficiency (coolant side)	-	0.760	0.768	+1.0%
Fanning friction factor (air side)	-	0.0417	0.0401	-3.9%
Fanning friction factor (coolant side)	-	0.0409	0.0388	-5.2%
Mass velocity (air side)	kg/m^2s	32.57	32.24	-1.0%
Mass velocity (coolant side)	kg/m^2s	39.55	39.60	+0.1%
Coolant flow length	m	0.25	0.29	+15.8%
Air flow length	m	0.25	0.29	+14.5%
No flow length	m	0.38	0.33	-12.2%
Frontal area (air side)	m^2	0.0954	0.0970	+1.6%
Frontal area (coolant side)	m^2	0.0954	0.0958	+0.5%
Volume	m^3	0.0238	0.0277	+16.4%
Core mass (wet)	kg	6.34	6.54	+3.1%
Overall heat transfer coefficient	W/m^2K	142.6	130.8	-8.3%

Table 1 Validation of the heat exchanger model against EchTherm.

20°C. The thermal conductivity of the current model was validated against measurements made by Zakaria et al. [31] and Syam Sundar et al. [61]. This validation is shown in Fig. 5a. The density was validated against measurements made by Vajjha et al. [62] and is shown in Fig. 5b. The dynamic viscosity was validated against measurements made by Yiamsawas et al. [63], Yu et al. [64] and Raja Sekhar and Sharma [65]. This validation is shown in Fig. 5c. The specific heat capacity of water containing Al_2O_3 nanoparticles was validated against measurements made by Barbes et al. [66] and O'Hanely et al. [67] as shown in Fig. 5d. The thermophysical properties of aqueous ethylene glycol obtained from CoolProp [50] were validated against reference data from the VDI Heat Atlas [68] and the 2021 ASHRAE Handbook [69].

A good correlation is shown between the current model and experimental measurements for the density and specific heat capacity over the entire range of volume concentration considered. As there was no good data for the specific heat capacity of aqueous ethylene glycol with Al_2O_3, not a lot can be said about the validation. It is however shown that there is a good correlation between the current model and experimental measurements for water with Al_2O_3 nanoparticles. A good correlation is shown for thermal conductivity when the composition of the aqueous ethylene glycol solution is around 50:50 for either mass fraction or volume fraction. For lower ratio ethylene glycol solutions (e.g. 20:80 mass%) the correlation worsens and the model underestimates the thermal conductivity. As the current study will only focus on an aqueous ethylene glycol solution of 50:50 vol% the use of the current model was deemed acceptable. As shown in Fig. 5c the current model for the dynamic viscosity differs substantially from the experimental measurements, especially for higher volume concentrations of Al_2O_3. The current model substantially underestimates the dynamic viscosity of the nanofluid. The dynamic viscosity model implemented is based on Einstein's model [58] which is applicable for the *effective viscosity of a suspension of spherical solids as a function of volume fraction (volume concentration lower than 5%) using the phenomenological hydrodynamic equations* [28]. Other dynamic viscosity models have been developed based on Einstein's model with the aim of improving its applicability [28]. These models were analysed,

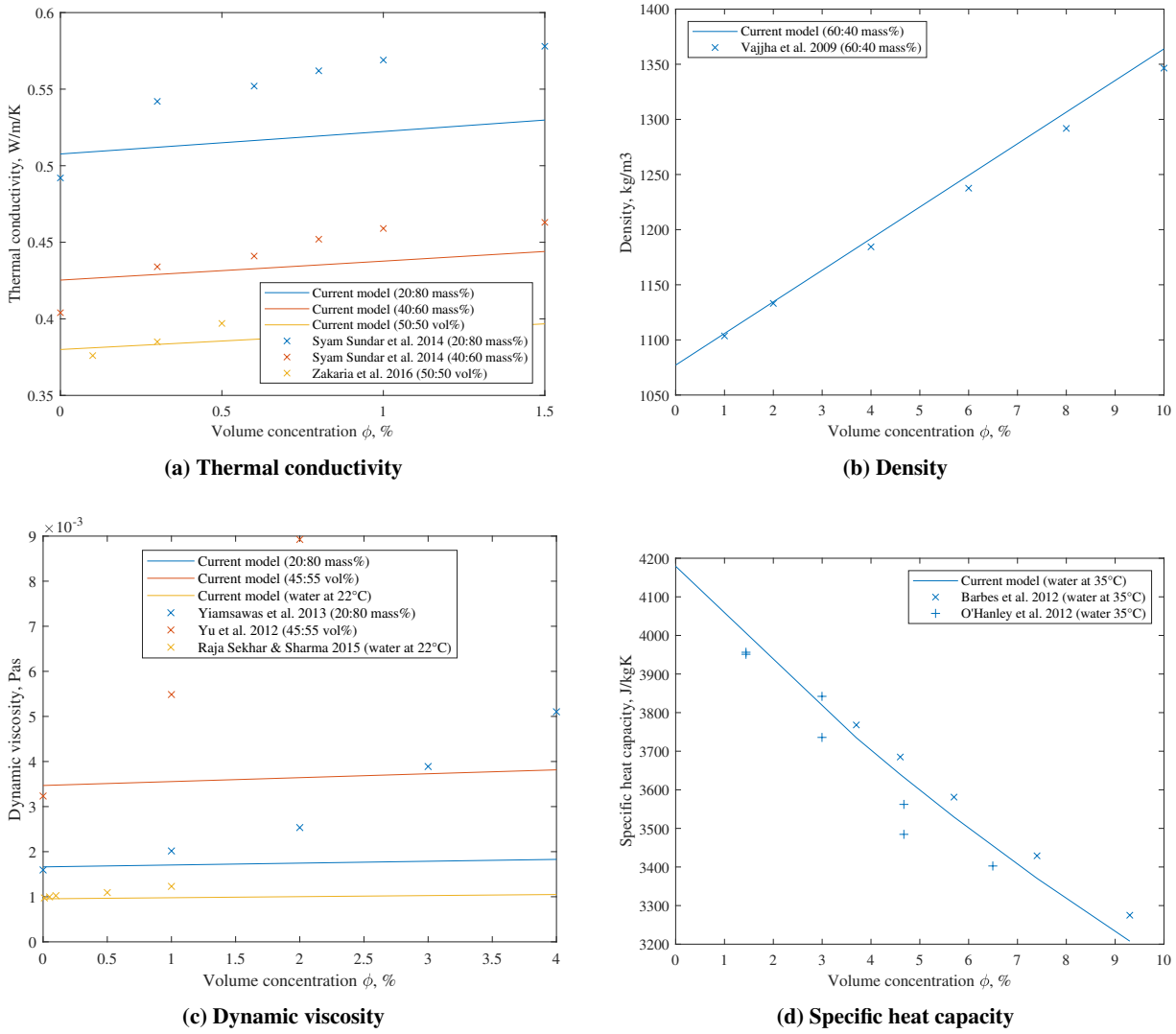

(a) Thermal conductivity **(b) Density**

(c) Dynamic viscosity **(d) Specific heat capacity**

Fig. 5 Properties of aqueous ethylene glycol as a function of volume concentration of Al_2O_3.

including models put forward by Brinkman [70], Batchelor [71] and Noni et al. [72] were validated against experimental measurements however none showed an improved correlation compared to Einstein's model for the specific nanofluid studied. Hence the implemented dynamic viscosity model was deemed unreliable for volume concentrations of greater than around 1%. The primary implications of the underestimation of the dynamic viscosity is on the Reynolds number and the pressure drop of the coolant through the system components. This has a direct impact on the coolant pump mass. This should be considered when analysing the results of the unconventional thermal management system. An improvement of the dynamic viscosity model should be addressed in future work.

D. Validation of the Fuel Cell Sizing Methodology

In order to validate the fuel cell thermal management system sizing methodology the sized system should be compared against a comparable commercial CS-23 commuter fuel cell aircraft. At the time of writing no such aircraft has flown. Therefore the fuel cell thermal management system sizing methodology together with the fuel cell system sizing methodology were validated against the HY4 fuel cell demonstrator aircraft. The HY4 is a four-seater hybrid-electric aircraft chosen due to the available data on the aircraft's powertrain and thermal management system. The aircraft's powertrain includes four low-temperature PEMFC modules connected in series [73] delivering a continuous power

output of 45 kW [23, 24] and a maximum of 52 kW [73]. The fuel cell system operates at a temperature of 60°C and ambient pressure [9]. The thermal management system includes a liquid cooling system [73]. A comparison of the fuel cell system sized by the current methodology and the fuel cell system installed on the HY4 is shown in Table 2. The coolant pump mass and pressure drop have been non-dimensionalized as the HY4 data was obtained from confidential MAHEPA reports. For the same reason, the mass flow rates are not disclosed and only the differences given. The validation of the fuel cell powertrain was performed at sea-level ISA conditions for take-off.

Parameter	Unit	Current Methodology	HY4	Source	Difference
Fuel cell system mass	kg	102	100	[9]	+2.0%
Fuel cell power density	W/kg	580	600	[9]	-3.3%
Coolant pump mass (non-dimensional)	-	0.0386	0.0590		-34.6%
Fuel cell efficiency	%	40.9	> 44	[24]	n/a
Mass flow rate of air (required during cruise)	kg/s				-76.1%
Mass flow rate of air (required on ground)	kg/s				-2.5%
Pressure drop air (cruise) (non-dimensional)	-	0.00598	0.00464		+29.0%

Table 2 Validation of fuel cell thermal management system sizing methodology against the fuel cell system installed on the HY4.

Table 2 shows that there is a general agreement between the fuel cell system sized through the Initiator and the system installed on the HY4 demonstrator aircraft. The fuel cell system mass, power density and mass flow rate at sizing conditions are all within ±5% of the HY4 demonstrator aircraft. The results differ however in the mass of the coolant pump and the mass flow rate of air during cruise. The coolant pump mass is underestimated in comparison to the mass of the coolant pump installed on the HY4 demonstrator aircraft. The pressure drop during cruise is overestimated but of the same order of magnitude. The calculated fuel cell efficiency is slightly lower than the efficiency during cruise as reported in *Jane's All the World's Aircraft* [24]. This was deemed acceptable and should be considered when analysing the results of the developed sizing methodology.

The temperature difference of the coolant was determined to be 7.35°C which is in line with the 'less than 15°C' expected by Datta [41] for this temperature difference. The temperature difference is also in line with the 10°C claimed by Universal Hydrogen in normal operation of the fuel cell stacks installed on their retrofitted Dash 8 aircraft[§]. The core drag coefficient of the ducted heat exchanger during cruise was calculated to be 0.000356. Though the external drag coefficient of the ducted heat exchanger is calculated within the developed sizing methodology it was not able to be calculated for this specific aircraft. This is because the HY4 demonstrator aircraft, specifically its double fuselage is currently unable to be modelled by the Initiator. No direct validation of this parameter was possible due to a lack of data in literature. Piccio and Porrini [73] reference an estimation made by Pipistrel Vertical Solutions' Flight Physics Department for the total cooling drag coefficient of the HY4 to be 0.00267. It was presumed based on section 5.2 and table 5.3 in Piccio and Porrini [73] that this drag coefficient was calculated for steady-level cruise flight. Based on this presumption it was determined that the core drag coefficient calculated within the sizing methodology is 13.4% of the total cooling drag coefficient presented in Piccio and Porrini [73]. In Kožulović's [4] preliminary sizing of a thermal management system for a fuel cell powered aircraft the core drag was calculated to be 24.4% of the drag attributed to the thermal management system[‡‡]. Based on the previous presumption, the core drag component of the thermal management system is slightly underestimated, but acceptable for the HY4 demonstrator aircraft. The specific power of the thermal management systems was calculated to be 0.21 kW/kg. This is slightly below the specific power range analysed by Inacio et al. (0.34 kW/kg - 2.27 kW/kg) [7]. In the case of the Metro 23, to be discussed in section VI, the calculated specific heat rejection is slightly above the range presented in Inacio et al. [7].

The mass of the heat exchanger was found to be 61.45 kg which is 60.3% of the fuel cell system mass. This is considerably larger than the 16% determined by Snyder et al. [6] in their preliminary sizing of a 100-person fuel cell aircraft and the 24% determined by Bradely et al. [74] in their development of a small fuel cell powered unmanned UAV. In the case of the Metro 23, the mass of the heat exchanger accounts for 41.6% of the fuel cell system mass. The mass of the heat exchanger is considerably overestimated for the HY4 demonstrator aircraft but more in line, though quite conservative with the literature for CS-23 aircraft. This overestimation of the heat exchanger mass was also seen in the

[‡‡]Excluding the drag component attributed to the additional mass of the thermal management system.

validation of the heat exchanger model presented in section V.B. This conservative value may merit reducing the factor of 1.2 applied to the heat exchanger mass to take into account inlet and outlet nozzles, headers tanks and support plates in future work.

The frontal area of the heat exchanger core (non-dimensionalized) was determined to be 0.0072. The frontal area of the heat exchanger core installed on the redesigned HY4 demonstrator aircraft is unknown. However, a value (non-dimensionalized) of 0.0187 is given in a confidential MAHEPA report detailing the development of the HY4 demonstrator aircraft. This value was calculated for a preliminary heat exchanger design that ended up not being manufactured and installed due to the intended supplier shutting down. Nevertheless, the difference between these two frontal areas is -61.6%. This significant difference could be due different sizing cases being used or the conservative sizing methodology used for the development of the HY4 demonstrator aircraft.

The validation of the fuel cell thermal management sizing methodology is by no means perfect but is the best that could've been done within the framework of the study. The sizing methodology developed for CS-23 commuter aircraft could not be validated against a comparable commercial aircraft as no such aircraft exists. The sizing methodology was hence validated against a four-seat fuel cell demonstrator aircraft. In order to improve the robustness of the sizing methodology it should be validated against comparable aircraft once they are flown in the future. In the mean time the sizing methodology should be validated at fuel cell engine level against those retrofitted onto fuel cell demonstrator aircraft developed and flown by ZeroAvia and Universal Hydrogen.

It was assumed that the rest of the functionality and models implemented within the Initiator have been verified and validated. The fuel cell system sizing methodology was specifically verified and validated by Juschus [15] and the capability to size CS-23 commuter aircraft by Zupanič [36].

VI. Results and Discussion

The developed fuel cell thermal management sizing methodology implemented into the Initiator was run and results obtained. The results for a hybrid-electric aircraft based on the Fairchild Aerospace Metro 23 are presented and discussed first before discussing the results of other CS-23 turboprop commuter aircraft. The baseline aircraft is conceptually sized with a conventional fuel cell thermal management system for sea-level ISA conditions at take-off using water as the liquid coolant. This aircraft is visualized in Fig. 6 with the heat exchangers shown in red located within the wing-mounted fuel cell engines. This configuration is referred to as configuration A in Table 4 in Appendix B.

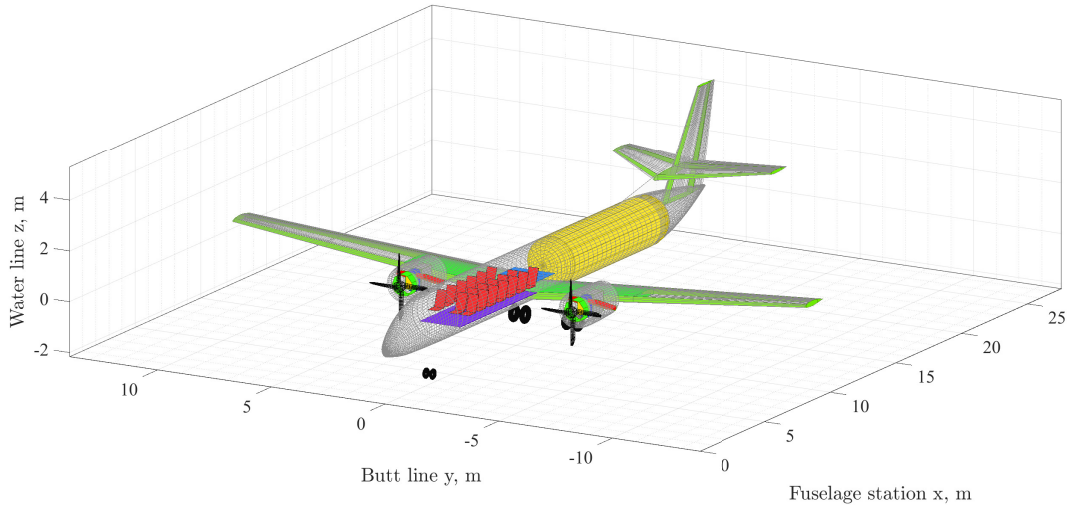

Fig. 6 Three-dimensional view of a hybrid-electric aircraft based on the Metro 23 conceptually sized by the Initiator.

Two additional aircraft configurations based on the Metro 23 were sized by the Initiator and the impact of the thermal management system on aircraft performance analyzed. Selected figures of merit of all three aircraft are shown in Table 3. The first configuration in Table 3 is a conventional kerosene aircraft. The second and third configurations are hybrid-electric aircraft sized without and with considering the fuel cell thermal management system.

The fuel cell efficiency given in Table 3 and subsequently Tables 4 and 5 is different to the fuel cell system efficiency. For the calculation of the fuel cell efficiency, the higher heating value (HHV) of hydrogen was used. The fuel cell system efficiency is the ratio of the electrical power used for propulsion and the total fuel power.

Parameter	Unit	Configuration					Comparison with and without TMS
		Conventional kerosene	Hybrid-electric without TMS		Hybrid-electric with TMS		
MTOM	kg	7781.46	12227.50	+57.1%	14962.29	+92.3%	+22.4%
OEM	kg	4602.80	10057.44	+118.5%	12673.17	+175.3%	+26.0%
S_{ref}	m^2	29.81	49.33	+65.5%	60.47	+102.8%	+22.6%
$C_{D,0}$	cts	203.25	192.47	-5.3%	193.91	-4.6%	+0.7%
$^L/_{D_{max}}$	-	18.78	19.62	+4.4%	19.93	+6.1%	+1.6%
V_{fuel}	m^3	2.78	8.25	+196.4%	10.12	+263.8%	+22.7%
m_{fuel}	kg	2254.44	585.74	-74.0%	718.89	-68.1%	+22.7%
p_{shaft} (cruise)	kW	394.45	659.45	+67.3%	818.30	+107.5%	+24.0%
η_{FC}	%		38.55		38.55		0.0%
m_{FCS}	kg		303.89		740.53		+143.7%
Specific power[§§]	W/kg		2222.33		1119.60		-49.6%

Table 3 Results of conceptually sized aircraft based on the Metro 23 sized by the Initiator.

Comparing the conventional aircraft with the hybrid-electric aircraft without the thermal management system a considerable increase in OEM and wing reference area can be seen. This is due to the installation of the liquid hydrogen storage and fuel cell systems and the redesigning of the aircraft to fulfil the mission requirements. There is a slight decrease in the zero-lift drag coefficient which leads to a slight increase in the lift-to-drag ratio, something that is beneficial for aircraft performance. As expected, the hydrogen-powered aircraft has a higher fuel volume (+196.4%) and a lower fuel mass (-74.0%) than the kerosene aircraft. The conventional aircraft converged after 7 iterations and the hybrid-electric aircraft without the thermal management system after 8 iterations.

Comparing the hybrid-electric aircraft with and without the thermal management system, the impact of the thermal management system on aircraft performance can be analyzed. Overall it can be seen that when considering the thermal management system the mass and size of the aircraft increase. The OEM is shown to increase by 26.0%. The mass of the thermal management system however only accounts for 14.1% of this increase directly. The remaining increase in OEM is due to the snowball effect of the additional mass, parasitic drag and parasitic power attributed to the thermal management system. The increased drag (+0.7%), though minimal requires more propulsive power and hence a larger propulsive fuel cell system and more fuel for the same mission requirements. The consideration of the parasitic power of the thermal management system, though very small, also requires a larger propulsive fuel cell system which requires more cooling.

The specific power of the fuel cell system without the thermal management system is considerably higher than the expected values in literature. Nicolay et al. [75] used a fixed specific power of 0.86 kW/kg [75] in their conceptual design of a four-person fuel cell aircraft. Juschus [15] states that the expected power density is *in the order of magnitude of 1 kW/kg*. This higher value was expected as the thermal management system and the snowball effect thereof were not considered in this configuration. When considering the thermal management system the specific power of the fuel cell system decreases to a value more in line with literature. The specific power is slightly above the values from literature. This is most likely due to the fact that not all mass components of the fuel cell system were modelled. Such mass components include the coolant mass outside the heat exchanger. That said, the major mass-contributing components were modelled. The aircraft without the thermal management system converged after 8 iterations and the aircraft after 16 iterations.

A number of additional aircraft configurations based on the Metro 23 were sized and their results are presented in Table 4 found in Appendix B. Configurations B and C challenge the assumption that all heat produced within the

[§§] System level specific power considering the fuel cell stack, compressor, humidifier, heat exchanger and coolant pump.

fuel cell stack must be removed by the thermal management system. Other heat sinks exist within the stack including heat dissipated through natural convection [18, 20], heat dissipated through radiation [41] and heat used for internal water evaporation [18, 20]. Configuration B models the former two heat sinks based on relations used by Datta [41] in their PEMFC sizing models for urban air mobility applications. Configuration C considers a constant value for the heat removed by the thermal management system. Huang et al. [20] and Bargal et al. [18] estimate this to be 80% whereas Tomažič [76] estimates it to be 90%. For configuration C an average of these two values was taken. Configuration D sizes the thermal management system for take-off at a hot and high airport. This sizing case is a much more challenging take-off condition for the thermal management system than the sea-level ISA conditions considered in the other configurations. Denver International Airport was used as a reference hot and high airport. The temperature and pressure were taken as the maximum average for the month of July for the period 1991 to 2020 and were found to be 32.2°C and 101210 Pa respectively[¶¶]. The airport lies at an altitude of 1656.22 m[***]. The Initiator didn't converge within the maximum number of iterations for a configuration considering only the hot and high take-off conditions due to the size of the heat exchangers being to large and heavy. The 85% considered in configuration C was then also considered and a converged design was reached for the hot and high take-off conditions after 18 iterations. All configurations in Table 4 used water as the coolant. The thermal management system level results refer to a single fuel cell unit, which is part of a single fuel cell engine. For configurations B, C and D the difference in parameters compared to configuration A are presented in the column adjacent to the values.

In configuration B the heat removed by the thermal management system was determined to be 98.2% of the total heat produced in the fuel cell stack. This is far above the 80% to 90% range given in literature [20, 76]. This was expected as the current methodology does not model all heat sinks within the fuel cell system. In order to better align with literature the heat removed by the thermal management system was set to 85% for configuration C. Nevertheless comparing configuration B with configuration A it was shown that the amount of heat to be removed by the thermal management system is decreased by 1.8% resulting in a slightly lighter fuel cell system (-1.2%) and a slightly lighter aircraft (-0.1%). This was expected as a reduction in the amount of heat removed by the thermal management system will reduce the system's size. The drag component during cruise was also reduced (-2.8%) however this had only a minute effect on the zero-lift drag coefficient at aircraft level, reducing it by only 0.1%. In general, it can be said that the slight decrease in the amount of heat to be removed by the fuel cell stack results in a slight decrease in system size and a very slight effect on aircraft performance. A greater impact on system-level performance and aircraft performance is anticipated in configurations where even less heat is to be removed by the thermal management system.

Reducing the heat removed by the thermal management system further down to 85% more pronounced differences are shown when compared to configuration B. The snowball effect is evident when considering the amount of heat removed by the thermal management system as this reduces by more than 15% as otherwise expected. The amount of heat removed by the thermal management system in configuration C is 17.9% less than the amount of heat removed in configuration A. By reducing the amount of heat removed the size of the thermal management system is reduced, leading to a further reduction in the size of the fuel cell system (mass reduction of -12.0%) leading to a further reduction in the size of the thermal management system. This snowball effect has a direct effect on aircraft performance. The OEM is reduced by 4.0% and the zero-lift drag coefficient at aircraft level by 0.2%. In order to further reduce the amount of heat removed by the thermal management system other heat sinks could be employed including heating the cryogenic liquid hydrogen to the acceptable inlet temperature for the fuel cell as proposed by Inacio et al. [7] and others.

Comparing configuration D with configuration A the aircraft is shown to be heavier, with an increased power requirement from the fuel cell and an increase in the zero-lift drag coefficient. Due to the more challenging take-off condition the size of the heat exchanger core is increased (+91.4% compared to configuration C) in order to transfer the heat over a smaller temperature difference between the coolant and ambient air. The ambient air temperature increased from 15°C at sea-level ISA to 32.2°C (+114.7%) whereas the stack temperature remained constant at 80°C. The larger heat exchanger core results in a heavier heat exchanger (+93.9%) which leads directly to a heavier aircraft (OEM +18.8%). Furthermore, the larger heat exchanger also increases the drag of the thermal management system during cruise (+187.2%) increasing the zero-lift drag coefficient of the aircraft (+4.2%). This leads to a higher required thrust and propulsive power requirement from the fuel cell system (+20.0%). This increase in required fuel cell system power further increases the amount of heat generated by the fuel cell stack hence requiring a larger thermal management system and so forth.

Comparing all configurations in Table 4 it can be seen that both the heat exchanger installation angle and fuel cell

[¶¶] *Denver International Airport*, Meteostat, 2023. URL: https://meteostat.net/en/station/72565. Date accessed: 10 Mar. 2023.

[***] *Denver, Colorado*, Federal Aviation Administration, 2022. URL: https://www.faa.gov/air_traffic/publications/atpubs/aip_html/part3_ad_2.0_colorado.html. Date accessed: 10 Mar. 2023.

efficiency remain constant. The heat exchanger installation angle is fixed at 68.04 deg. This angle is a function of σ_{air} which is directly related to the heat exchanger core geometry. Since the core geometry is the same for all configurations, the resulting installation angle is the same. The fuel cell efficiency is related to the operating voltage of the stack the thermodynamic voltage. Since the sizing case for the cell is the same for all configurations the fuel cell efficiency is the same. It is expected that the fuel cell system efficiency will differ for the configurations in Table 4 because of the change in compressor and coolant pump power requirements. Webber et al. [77] as part of the Aerospace Technology Institute's FlyZero project target the thermal management specific heat rejection to be 5 kW/kg by 2026 and 10 kW/kg by 2035. The results show that configurations A, B and C are in line with these targets considering a linear rate of technological development. Configuration D is slightly below this trend. In a similar study, Bhatti et al. [78] target the specific power of the fuel cell system[§§] to be between 1.5 kW/kg and 2.0 kW/kg by 2026 and between 2.5 kW/kg and 3.0 kW/kg by 2035. Unlike for the specific heat rejection, the specific power of the configurations presented in Table 4 is slightly below the targeted trend.

A. Unconventional Thermal Management System

In the unconventional thermal management system introduced in section III nanofluids are used as the liquid coolant. Several coolants were selected to study the effect of their thermophysical properties on system and aircraft level performance. The selected coolants were water, 50:50 vol% aqueous ethylene glycol (also known as antifreeze), 50:50 vol% aqueous ethylene glycol with 0.5% Al_2O_3 nanoparticles and 50:50 vol% aqueous ethylene glycol with 2% Al_2O_3 nanoparticles. Al_2O_3 was chosen for this study as it was used by Zakaria et al. [31] in their experimental study on the use of nanofluids in PMEFC cooling plates and shows promising thermophysical properties. The thermophysical properties of the coolants were determined using CoolProp [50] and the nanofluid model presented in section IV.E. The calculated properties are presented in the top section of Table 5 found in Appendix B. At the time of writing, there was a lack of adequate models than could determine the freezing temperature of nanofluids. Haiping and Walter have shown through experiments that adding nanoparticles to 50:50% aqueous ethylene glycol reduces the freezing temperature further compared to the base fluid [79]. It was hence presumed that the freezing temperature of the nanofluids containing Al_2O_3 is lower than the freezing temperature of the aqueous ethylene glycol base fluid. This is beneficial for operation in sub-zero temperatures. Table 5 also presents the system and aircraft-level performance of the hybrid-electric aircraft with different coolants. The percentage differences are given for the nanofluids with respect to the aqueous ethylene glycol base fluid in the adjacent column. All these aircraft were sized for sea-level ISA conditions at take-off with all heat produced by the fuel cell system taken away by the thermal management system.

The baseline aircraft used water as the coolant. Such an aircraft would not be able to operate in environments where the ambient temperature drops below the freezing point of water. To overcome this aqueous ethylene glycol is often used as the coolant in such systems [17, 20, 26]. Aqueous ethylene glycol however is however not a good coolant due to its reduced thermal conductivity compared to water [28]. Furthermore, the dynamic viscosity of aqueous ethylene glycol is 228.9% higher than that of water. This will have an effect on the pressure drop of the coolant through the cooling loop components requiring larger diameter piping and a larger coolant pump. This is however not shown in the results in table 5 because of the limitations in the implemented dynamic viscosity model as discussed in section V.C. What is shown in the results is the increased mass of the heat exchanger and increased size of the heat exchanger core due to the worsened thermodynamic properties of aqueous ethylene glycol. The mass of the heat exchanger increases by 93.8% and the frontal area by 88.1%. In order to improve the thermodynamic properties of the coolant nanoparticles are added to the coolant as discussed in section IV. Even with only a 2% volume concentration of Al_2O_3 the thermal conductivity is increased by 5.9% compared to the base fluid. A similar magnitude decrease is however not seen in the size and mass of the heat exchanger. The opposite is seen, the frontal area and mass of the heat exchanger increase with nanoparticle volume concentration. This is despite the improvement in the thermodynamic properties of the nanofluid. Any improvement is counteracted by the increase in the density of the coolant. The density of the nanofluid with 2% Al_2O_3 is 5.5% greater than the density of the base fluid. The use of nanofluids hence shows no overall performance improvement at both system and aircraft level when compared to the base fluid.

B. Additional CS-23 Commuter Aircraft

Three additional CS-23 commuter aircraft were conceptually sized in order to assess the applicability of the developed thermal management system sizing methodology on aircraft other than the Metro 23. These hybrid-electric aircraft were based on the British Aerospace Jetstream 31, Embraer EMB 110P2 Bandeirante and the Dornier 228-200. All aircraft were sized for sea-level ISA conditions at take-off with all heat produced by the fuel cell system taken away

by the thermal management system which used water as the coolant. These conceptually sized aircraft are shown in Fig. 7.

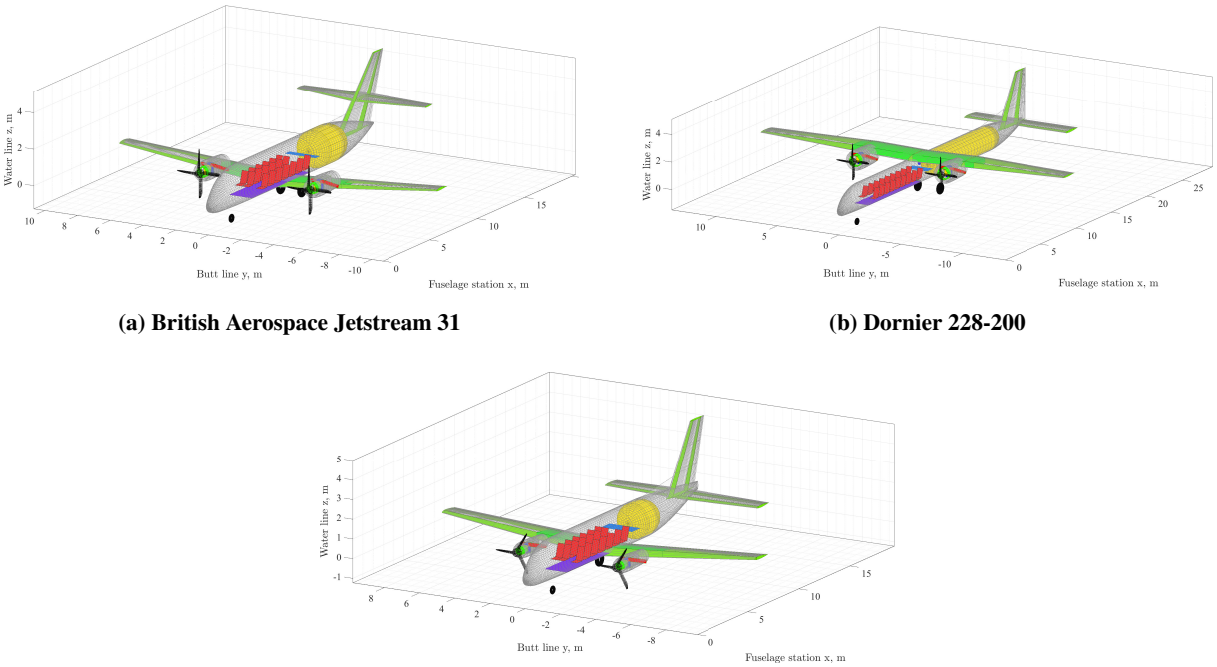

(a) British Aerospace Jetstream 31

(b) Dornier 228-200

(c) Embraer EMB 110P2 Bandeirante

Fig. 7 Three-dimensional view of three CS-23 commuter hybrid-electric aircraft conceptually sized by the Initiator.

The Initiator ran smoothly, was able to size a thermal management system and reached a converged design for all aircraft. The results were in agreement with each other and the Metro 23 when considering their inherent differences. The Do228, despite having the second-highest MTOM, had the largest and heaviest heat exchanger of all four aircraft. This was due to the Do228 having the lowest take-off velocity of all the aircraft. The EMB 110P2, the smallest of the four aircraft had the highest zero-lift drag coefficient. The conceptually sized hybrid-electric aircraft based on the Metro 23 converged within 16 steps whereas the Jetstream 31, EMB 110P2 and Do228 converged within 11, 16 and 21 iteration steps respectively.

C. CS-25 Aircraft

In order to assess the applicability of ambient air-based thermal management systems on larger commercial aircraft the developed sizing methodology was run for a hybrid-electric aircraft based on the ATR 72-600. The developed sizing methodology, in its current state, was unable to size the thermal management system required for the aircraft. Modifications had to be made to the sizing methodology in order to conceptually size the fuel cell thermal management system for this larger aircraft. The initial guess for the ducted heat exchanger inlet area was increased from 1 m^2 to 2.5 m^2. In order to determine the mass of the coolant pumps the maximum number of pumps connected in parallel was increased from 5 to infinity. In future versions of the coolant pump mass model, it is recommended to add the performance curves and masses of coolant pumps with a higher volumetric mass flow rate to accommodate the larger systems on these larger aircraft.

Once these changes were implemented the thermal management system sizing methodology was able to size a system and the Initiator reached a converged design after 42 iterations. The aircraft was sized for sea-level ISA conditions at take-off with all heat produced by the fuel cell system taken away by the thermal management system using water as the coolant. The resulting conceptual aircraft, though converged was an unrealistic aircraft design. Further modifications to the thermal management system sizing methodology are required in order to make the sizing methodology applicable to larger aircraft. Even with such modifications it is currently unknown whether a converged and realistic aircraft design

will be reached with the conventional air-based thermal management system considered in this study.

VII. Conclusion and Recommendations

The objective of the current study was to develop and implement a fuel cell thermal management system sizing methodology into the Initiator and analyze the impact of these systems on aircraft performance and aircraft design. This was done by developing several interlinked sizing models. A cross-flow single-pass unmixed-unmixed air-liquid plate-fin heat exchanger was modelled and the parasitic drag components of a ducted heat exchanger were calculated. A nanofluid model was developed to study the use of nanofluids in fuel cell thermal management systems onboard aircraft. These models were implemented into the Initiator and then verified and validated. As there are no commercial CS-23 commuter aircraft with a comparable powertrain architecture currently in service, the fuel cell thermal management system sizing methodology was validated against the four-person HY4 fuel cell demonstrator aircraft. The effect of the fuel cell thermal management system on aircraft performance was studied for hybrid-electric aircraft based on the Metro 23, Jetstream 31, Embraer EMB 110P2 Bandeirante and Dornier 228. The sizing methodology was able to size a thermal management system for all CS-23 commuter aircraft considered.

The results show that the fuel cell thermal management system has both a direct and indirect effect on aircraft performance. The mass of the thermal management system was found to contribute around 3% to the operating empty mass which increased by +26.0% compared to the same aircraft sized without a fuel cell thermal management system. The drag attributed to the thermal management system was found to contribute around 3% to the total zero-lift drag coefficient which increased by +0.7% compared to the same aircraft sized without a fuel cell thermal management system. The required power of the coolant pump was found to be negligible compared to the electrical gross power output of the fuel cell system. In all, the consideration of the thermal management system detrimentally affected the OEM, lift-to-drag ratio and the power requirement of the fuel cell system. This highlights the need to adequately consider the design of the thermal management systems during the conceptual design of fuel cell aircraft. This is in agreement with the literature studied. Of importance is modelling the mass of the system and its impact on aircraft performance and aircraft design.

The use of nanofluids showed no overall performance improvement at both system and aircraft level when compared to the aqueous ethylene glycol base fluid. This was shown despite the improved thermal conductivity of the coolant which was counteracted by the increase in coolant density. The developed fuel cell thermal management system sizing methodology was also used in the conceptual sizing of a larger, CS-25 fuel cell aircraft. The developed sizing methodology was able to size the thermal management system required for the aircraft but led to an unrealistic aircraft design. Further modifications of the developed thermal management system sizing methodology are required to make it applicable for larger aircraft. Even with these modifications, it is currently unknown whether a converged and realistic aircraft design will be reached with the conventional air-based thermal management system considered in this study. Other unconventional and novel fuel cell thermal management systems such as two-phase cooling or skin-integrated heat exchangers may need to be considered for this larger category of aircraft.

Though the fuel cell thermal management system sizing methodology presented in the current study is an improvement on the previous methodology implemented in the Initiator it has several limitations. Recommendations for further development of the sizing methodology include the development of an improved ducted heat exchanger external drag model. The current model, though physics-based is a loose estimation of the external drag. An improved external drag model should be based on empirical methods[†††] or (three-dimensional) simulation. It is furthermore recommended to develop a physics-based coolant pump mass model which considers aerospace-optimized coolant pumps for the specific application at hand. Such a physic-based coolant pump model should also determine the size of these coolant pumps such that it can be confirmed that these fit within the fuel cell engine nacelle.

It is recommended that the fuel cell heat model be improved to better consider and model the other heat sinks within the fuel cell stack. This will reduce the amount of heat that needs to be taken away by the thermal management system which will reduce the size of the system for a given aircraft configuration. This will however remove the conservative aspect of the sized thermal management system. In order to maintain a conservative system size a factor could be applied to the heat removed by the thermal management system. Different types of pumps should be studied and specific attention should be given to the net positive suction head (NPSH) of the pump. It is further recommended to study and trade-off maximising pressure drop through the heat exchanger to maximise heat transfer performance against minimising the pressure drop to minimize core drag. The heat exchanger model should be replaced with a

[†††] Such as ESDU 03006 on the *subsonic drag and pressure recovery of rectangular planform flush auxiliary inlets with ducts at angles up to 90 degrees* or ESDU 86002 on the *drag and pressure recovery characteristics of auxiliary air inlets at subsonic speeds*.

more advanced (commercial) heat exchanger sizing code. One good option for this is the heat exchanger sizing and optimization code developed by F. Beltrame specifically for aerospace applications.

Sensitivity studies should be performed on the stack operating temperature, cooling plate channel geometry and type of heat exchanger core. This will improve the understanding of the effect of these parameters on system and aircraft level performance. To adequately considered the effects of the cooling plate channel geometry, the fuel cell model should be improved to better consider the effect of operating conditions on fuel cell performance. Of importance is the fuel cell temperature uniformity. The type of heat exchanger core used will affect the heat transfer and the pressure drop through the heat exchanger. Carrying out these sensitivity studies will provide insight into and support the optimization of the fuel cell thermal management system. In addition, the ducting around the heat exchanger, the sizing of the heat exchanger core and the placement of the coolant pump in the cooling loop should all be considered in the optimization.

In the short term, the developed sizing methodology should be validated at the fuel cell engine level against CS-23 fuel cell demonstrator aircraft such as the Dornier 228 retrofitted by ZeroAvia and the Dash 8-300 retrofitted by Universal Hydrogen. In the longer term, once commercial CS-23 commuter fuel cell aircraft are developed and data becomes available, the sizing methodology should be validated against these aircraft. Once further validated the robustness and applicability of the sizing methodology developed in the current study will be improved. It is recommended to study the use of other heat sinks onboard aircraft such as the cryogenic hydrogen fuel. Novel thermal management systems such as two-phase cooling and skin integrated heat exchangers should also be studied. The aim should be to reduce the impact of the fuel cell thermal management system on aircraft performance and aircraft design.

Appendix A

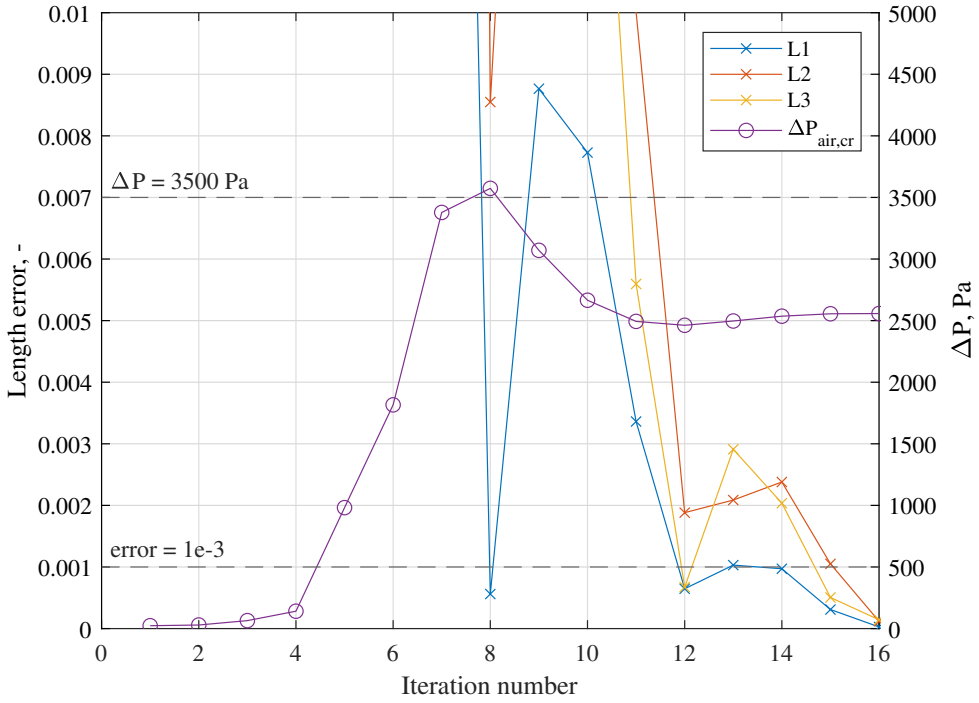

Fig. 8 Example convergence plot of the heat exchanger model.

Appendix B

	Parameter	Unit	Configuration						
			A	B		C		D	
Sizing case	Take-off		0m ISA	0m ISA		0m ISA		Hot & high	
	$\dot{Q}_{TMS}/\dot{Q}_{FC}$		100%	Eqs. in [41]		85%		85%	
Thermal management system level	$\dot{Q}_{TMS}$	kW	1214.15	1192.50	-1.8%	996.58	-17.9%	1196.07	-1.5%
	m_{HEX}	kg	308.03	298.97	-2.9%	232.02	-24.7%	449.86	+46.0%
	w_{HEX}	m	0.44	0.44	-0.1%	0.42	-4.2%	0.61	+36.7%
	h_{HEX}	m	3.01	2.93	-2.8%	2.38	-21.1%	3.19	+5.9%
	l_{HEX}	m	0.18	0.18	-0.1%	0.18	-0.5%	0.18	+1.4%
	γ_{HEX}	deg	68.04	68.04	0.0%	68.04	0.0%	68.04	0.0%
	m_{CP}	kg	60.5	60.5	0.0%	60.5	0.0%	78.0	+28.9%
	$C_{\text{D,0,TMS,core}}$	cts	2.92	2.73	-6.6%	1.67	-42.8%	8.90	+204.5%
	$C_{\text{D,0,TMS,external}}$	cts	1.63	1.70	+4.1%	1.79	+9.5%	1.03	-36.9%
	$C_{\text{D,0,TMS}}$	cts	4.56	4.43	-2.8%	3.46	-24.1%	9.93	+118.1%
	$\dot{m}_{air,to}$	kg/s	54.65	53.06	-2.9%	41.32	-24.4%	76.68	+40.3%
	$\dot{m}_{air,cr}$	kg/s	16.44	15.96	-2.9%	12.42	-24.5%	24.49	+48.9%
	$\dot{m}_{coolant}$	kg/s	13.32	13.54	+1.6%	14.77	+10.8%	18.00	+35.1%
	$\Delta T_{coolant}$	°C	21.76	21.02	-3.4%	16.12	-26.0%	15.86	-27.1%
	$\dot{Q}_{TMS}/m_{TMS}$	kW/kg	3.29	3.32	+0.7%	3.41	+3.4%	2.27	-31.2%
Aircraft level	MTOM	kg	14962.29	14946.84	-0.1%	14426.06	-3.6%	16840.08	+12.6%
	OEM	kg	12673.17	12656.29	-0.1%	12166.29	-4.0%	14447.54	+14.0%
	S_{ref}	m^2	60.47	60.55	+0.1%	58.47	-3.3%	67.99	+12.4%
	V_{LH_2}	m^3	10.13	10.13	0.0%	9.78	-3.4%	11.74	+16.0%
	$C_{\text{D,0}}$	cts	193.91	193.46	-0.2%	193.52	-0.2%	201.63	+4.0%
	L/D_{max}	-	19.93	19.72	-1.1%	19.73	-1.0%	19.48	-2.3%
	p_{FC} (gross)	kW	2150.79	2151.39	0.0%	2076.91	-3.4%	2492.66	+15.9%
	p_{FC} (elect. gross)	kW	829.10	829.33	0.0%	800.62	-3.4%	960.89	+15.9%
	η_{FC}	%	38.55	38.55	0.0%	38.55	0.0%	38.55	0.0%
	m_{FCS}	kg	740.53	731.58	-1.2%	651.91	-12.0%	958.25	+29.4%
	Specific power[§§]	W/kg	1119.60	1133.62	+1.3%	1228.13	+9.7%	1002.76	-10.4%

Table 4 Results of conceptually sized hybrid-electric aircraft based on the Metro 23 with a conventional fuel cell thermal management system.

	Parameter	Unit	Coolant					
			Water	aq. EG	aq. EG w/ 0.5% Al_2O_3		aq. EG w/ 2% Al_2O_3	
Coolant properties	ρ	kg/m^3	988.04	1050.14	1064.62	+1.4%	1108.04	+5.5%
	C_p	J/kgK	4181.34	3410.67	3362.71	-1.4%	3226.37	-5.4%
	μ	mPas	0.547	1.799	1.821	+1.2%	1.889	+5.0%
	k	W/mK	0.641	0.397	0.403	+1.5%	0.421	+5.9%
	T_{freeze}	°C	0	-39.82				
Thermal management system level	m_{HEX}	kg	308.03	587.09	603.67	+1.1%	636.86	+16.2%
	w_{HEX}	m	0.44	1.20	1.25	+3.8%	1.41	+17.1%
	h_{HEX}	m	3.01	2.08	2.02	-3.1%	1.86	-10.6%
	l_{HEX}	m	0.18	0.18	0.18	-0.1%	0.18	-0.1%
	$A_{frontal}$	m^2	1.33	2.51	2.53	+0.6%	2.63	+4.7%
	m_{CP}	kg	60.5	134.5	134.5	+0.0%	158.5	+17.8%
	$C_{\mathrm{D,0,TMS}}$	cts	4.56	-2.08	-1.59	-23.7%	0.12	-105.5%
	$\dot{m}_{air,to}$	kg/s	54.65	102.3	103.48	+0.6%	107.63	+4.7%
	$\dot{m}_{air,cr}$	kg/s	16.44	20.30	20.53	+1.1%	21.67	+6.7%
	$\dot{m}_{coolant}$	kg/s	13.33	32.37	34.59	+6.9%	42.14	+30.2%
	$\Delta T_{coolant}$	°C	21.76	14.37	13.89	-3.3%	12.78	-11.1%
	Q_{TMS}/m_{TMS}	kW/kg	3.29	2.22	2.43	+1.0%	2.24	+0.7%
Aircraft level	MTOM	kg	14962.29	19402.75	19648.92	+1.3%	20813.79	+17.2%
	OEM	kg	12673.17	16893.40	17105.55	+1.3%	18206.22	+7.8%
	$C_{D,0}$	cts	193.91	202.80	204.61	+0.9%	207.92	+2.5%
	L/D_{max}	-	19.93	19.43	19.39	-0.2%	19.19	-1.2%
	p_{FC} (gross)	kW	2150.79	2879.27	2933.64	+1.9%	3151.71	+9.5%
	p_{FC} (elect. gross)	kW	829.10	1109.92	1130.88	+1.9%	1214.94	+9.5%
	η_{FC}	%	38.5	38.5	38.5	0.0%	38.5	0.0%
	m_{FCS}	kg	740.53	1228.00	1243.86	+1.3%	1338.29	+9.0%
	Specific power[§§]	W/kg	1119.60	903.85	909.17	+0.6%	907.82	+0.4%

Table 5 Coolant properties and results of conceptually sized hybrid-electric aircraft based on the Metro 23 with an unconventional fuel cell thermal management system.

References

[1] Scholz, A., Michelmann, J., and Hornung, M., "Fuel Cell Hybrid-Electric Aircraft: Design, Operational, and Environmental Impact," *AIAA SciTech 2022 Forum*, Technical University of Munich, AIAA, San Diego, California, 2020. https://doi.org/10.2514/6.2022-2333.

[2] van Heerden, A., Judt, D., Jafari, S., Lawson, C., Nikolaidis, T., and Bosak, D., "Aircraft thermal management: Practices, technology, system architectures, future challenges, and opportunities," *Progress in Aerospace Sciences*, Vol. 128, 2022, p. 100767. https://doi.org/10.1016/j.paerosci.2021.100767.

[3] Schiltgen, B., Freeman, J., and Hall, D., "Aeropropulsive Interaction and Thermal System Integration within the ECO-150: A Turboelectric Distributed Propulsion Airliner with Conventional Electric Machines," *AIAA Aviation Forum*, AIAA, Washington, D.C., 2016. https://doi.org/10.2514/6.2016-4064.

[4] Kožulović, D., "Heat Release of Fuel Cell Powered Aircraft," *GPPS Chania20*, Hamburg University of Applied Sciences, 2020. https://doi.org/10.33737/gpps20-tc-99.

[5] Hoerner, S., *Fluid-Dynamic Drag*, 2nd ed., Hoerner Fluid Dynamics, Bakersfield, CA, 1965.

[6] Snyder, C., Geiselhart, K., Kascak, A., Berton, J., Brown, G., and Dolce, J., "Propulsion Investigation for Zero and Near-Zero Emissions Aircraft," Tech. rep., NASA TM—2009-215487, 2009. URL https://ntrs.nasa.gov/citations/20090023315.

[7] Inacio, G., Mourao, C., Castro, A., and Lacava, P., "Feasibility Study of Using Liquid Hydrogen Tanks as Energy Carriers and Cooling Agents for a Small Aircraft Powered by PEMFCs," *AeroTech® Digital Summit*, SAE International, 2022. https://doi.org/10.4271/2022-01-0009.

[8] Vredenborg, E., and Thielecke, F., "Thermal Management Investigations for Fuel Cell Systems On-Board Commercial Aircraft," *SAE 2013 AeroTech Congress & Exhibition*, Hamburg University of Technology, SAE International, 2013. https://doi.org/10.4271/2013-01-2274.

[9] Comincini, D., "Modular Approach to Hydrogen Hybrid-Electric Aircraft Design," Master's thesis, Politecnico di Milano, Milan, Italy, 2018. URL https://www.politesi.polimi.it/handle/10589/143966.

[10] Vonhoff, G., "Conceptual Design of Hydrogen Fuel Cell Aircraft," Master's thesis, Technische Universiteit Delft, Delft, the Netherlands, February 2021. URL http://resolver.tudelft.nl/uuid:8bd63dec-b67b-496b-92bc-3d5c07ff859f.

[11] Chapman, J., Schnulo, S., and Nitzsche, M., "Development of a Thermal Management System for Electrified Aircraft," *AIAA SciTech 2020 Forum*, NASA, Orlando, Florida, 2020. https://doi.org/10.2514/6.2020-0545.

[12] Thirkell, A., "Systems study for fuel cell powered more electric aircraft," Ph.D. thesis, Loughborough University, Loughborough, United Kingdom, 2021. https://doi.org/10.26174/thesis.lboro.14758005.v1.

[13] Kellermann, H., Lüdemann, M., Pohl, M., and Hornung, M., "Design and Optimization of Ram Air–Based Thermal Management Systems for Hybrid-Electric Aircraft," *Aerospace*, Vol. 8, No. 1, 2021. https://doi.org/10.3390/aerospace8010003.

[14] Piancastelli, L., Frizziero, L., and Donnici, G., "The Meredith Effect: an efficient way to recover the heat wasted in piston engine cooling," *Journal of Engineering and Applied Sciences*, Vol. 10, No. 2, 2015. URL https://www.arpnjournals.com/jeas/research_papers/rp_2015/jeas_0715_2249.pdf.

[15] Juschus, D., "Preliminary Propulsion System Sizing Methods for PEM Fuel Cell Aircraft," Master's thesis, Technische Universiteit Delft, the Netherlands, October 2021. URL http://resolver.tudelft.nl/uuid:fdc14875-175e-4a4b-8cde-f2f4b6028194.

[16] Nøland, J., Hartmann, C., Nilssen, R., and Mellerud, R., "Dual Use of Liquid Hydrogen in a Next-Generation PEMFC-Powered Regional Aircraft with Superconducting Propulsion," *IEEE Transaction on Transportation Electrification*, Vol. x, 2022, p. x. https://doi.org/10.1109/TTE.2022.3170827.

[17] Zhang, G., and Kandlikar, S., "A critical review of cooling techniques in proton exchange membrane fuel cell stacks," *International Journal of Hydrogen Energy*, Vol. 37, 2012, pp. 2412–2429. https://doi.org/10.1016/j.ijhydene.2011.11.010.

[18] Bargal, M., Abdelkareem, M., Tao, Q., Li, K., Shi, J., and Wang, Y., "Liquid cooling techniques in proton exchange membrane fuel cell stacks: A detailed survey," *Alexandria Engineering Journal*, Vol. 59, 2020, pp. 635–655. https://doi.org/10.1016/j.aej.2020.02.005.

[19] Kandlikar, S., and Lu, Z., "Thermal management issues in a PEMFC stack – A brief review of current status," *Applied Thermal Engineering*, Vol. 29, 2009, pp. 1276–1280. https://doi.org/10.1016/j.applthermaleng.2008.05.009.

[20] Huang, Y., Xiao, X., Kang, H., Lv, J., Zeng, R., and Shen, J., "Thermal management of polymer electrolyte membrane fuel cells: A critical review of heat transfer mechanisms, cooling approaches, and advanced cooling techniques analysis," *Energy Conversion and Management*, Vol. 254, 2022, p. 115221. https://doi.org/10.1016/j.enconman.2022.115221.

[21] Rathke, P., Kallo, J., Schirmer, J., Stephan, T., Waiblinger, W., and Weiss-Ungethüm, J., "Antares DLR-H2 – Flying Test Bed for Development of Aircraft Fuel Cell Systems," *ECS Transactions*, Vol. 51, No. 1, 2013, pp. 229–241. https://doi.org/10.1149/05101.0229ecst.

[22] Kallo, J., Rathke, P., Stephan, T., Thalau, O., Schirmer, J., and Teich, H., "Fuel Cell Systems for Aircraft Application & Antares DLR-H2 All-Electric Flying Testbed," *51st AIAA Aerospace Sciences Meeting including the New Horizons Forum and Aerospace Exposition*, DLR, AIAA, Grapevine, Texas, 2013. https://doi.org/10.2514/6.2013-936.

[23] "Hy4 - Zero-emission passenger flights," Online, November 2015. URL https://www.dlr.de/tt/en/desktopdefault.aspx/tabid-10743/, Date accessed: 16 Feb. 2023.

[24] *All the World's Aircraft: Development & Production*, Jane's Information Services, 2022, Chap. H2FLY HY4. Accessed through Janes Customer Portal online.

[25] Eržen, D., Trainelli, L., Riboldi, C., Rolando, A., Salucci, F., Oliviero, F., Pirnar, J., Koopman, T., Žnidar, A., Andrejašič, M., Lapuh, R., Soikkeli, J., and Čretnik, G., "UNIFIER19 D2.2: Final Concurrent Design Report," Tech. rep., Pipistrel Vertical Solutions, Politecnico di Milano and Technische Universiteit Delft, 7 2021. URL https://www.unifier19.eu/wp-content/uploads/2021/07/D2.2_Final_concurrent_design_report_Open.pdf.

[26] Wang, Y., and Chen, K. S., *PEM Fuel Cells: Thermal and Water Management Fundamentals*, Momentum Press, 2013.

[27] Romeo, G., Correa, G., Borello, F., Cestino, E., and Santarelli, M., "Air Cooling of a Two-Seater Fuel Cell-Powered Aircraft: Dynamic Modeling and Comparison with Experimental Data," *Journal of Aerospace Engineering*, Vol. 25, No. 3, 2012, pp. 356–368. https://doi.org/10.1061/(ASCE)AS.1943-5525.0000138.

[28] Islam, M., Shabani, B., Rosengarten, G., and Andrews, J., "The potential of using nanofluids in PEM fuel cell cooling systems: A review," *Renewable and Sustainable Energy Reviews*, Vol. 48, 2015, pp. 523–539. https://doi.org/10.1016/j.rser.2015.04.018.

[29] Baroutaij, A., Arjunan, A., Ramadan, M., Robinson, J., Alaswad, A., Abdelkareem, M. A., and Olabi, A.-G., "Advancements and prospects of thermal management and waste heat recovery of PEMFC," *International Journal of Thermofluids*, Vol. 9, 2021, p. 100064. https://doi.org/10.1016/j.ijft.2021.100064.

[30] Islam, M., Shabani, B., and Rosengarten, G., "Nanofluids to improve the performance of PEM fuel cell cooling systems: A theoretical approach," *Applied Energy*, Vol. 178, 2016, pp. 660–671. https://doi.org/10.1016/j.apenergy.2016.06.090.

[31] Zakaria, I., Azmi, W., Mamat, A., Mamat, R., Saidur, R., Abu Talib, S., and Mohamed, W., "Thermal analysis of Al_2O_3-water ethylene glycol mixture nanofluid for single PEM fuel cell cooling plate: An experimental study," *International Journal of Hydrogen Energy*, Vol. 41, No. 9, 2016, pp. 5096–5112. https://doi.org/10.1016/j.ijhydene.2016.01.041.

[32] La Rocca, G., Langen, T., and Brouwers, Y., "The design and engineering engine. Towards a modular system for collaborative aircraft design," *28th Congress of the International Council of the Aeronautical Sciences 2012, ICAS 2012*, Vol. 5, 2012. URL https://www.icas.org/ICAS_ARCHIVE/ICAS2012/PAPERS/603.pdf.

[33] Elmendorp, R., Vos, R., and La Rocca, G., "A conceptual design and analysis method for conventional and unconventional airplanes," *29th Congress of the International Council of the Aeronautical Sciences, ICAS 2014*, 2014. URL http://resolver.tudelft.nl/uuid:1dc55ce5-18c3-4986-b668-f70d9b24aac0.

[34] Hoogreef, M., Vos, R., de Vries, R., and Veldhuis, L. L., "Conceptual Assessment of Hybrid Electric Aircraft with Distributed Propulsion and Boosted Turbofans," *AIAA Scitech 2019 Forum*, 2019. https://doi.org/10.2514/6.2019-1807.

[35] Onorato, G., "Fuel Tank Integration for Hydrogen Airliners," Master's thesis, Technische Universiteit Delft, the Netherlands, August 2021. URL http://resolver.tudelft.nl/uuid:5700b748-82c6-49c9-b94a-ad97c798e119.

[36] Zupanič, M., "Conceptual Design of Fuel Cell Commuter Aircraft: A study into the performance and feasibility of CS-23 category transport aircraft utilising hydrogen fuel cell propulsion," Master's thesis, Technische Universiteit Delft, the Netherlands, 2023. URL http://resolver.tudelft.nl/uuid:d499f4bb-921a-4e3d-a676-614961104172.

[37] Dicks, A., and Rand, D., *Fuel Cell Systems Explained*, 3rd ed., John Wiley & Sons Inc, Chichester, England, 2018. https://doi.org/10.1002/9781118706992.

[38] Guida, D., and Minutillo, M., "Design methodology for a PEM fuel cell power system in a more electrical aircraft," *Applied Energy*, Vol. 192, 2017, pp. 446–456. https://doi.org/10.1016/j.apenergy.2016.10.090.

[39] Baek, S. M., Yu, S. H., Nam, J. H., and Kim, C.-J., "A numerical study on uniform cooling of large-scale PEMFCs with different coolant flow field designs," *Applied Thermal Engineering*, Vol. 31, No. 8, 2011, pp. 1427–1434. https://doi.org/10.1016/j.applthermaleng.2011.01.009.

[40] Al-Neama, A. F. M., "Serpentine Minichannel Liquid-Cooled Heat Sinks for Electronics Cooling Applications," Ph.D. thesis, The University of Leeds, Leeds, United Kingdom, January 2018. URL https://etheses.whiterose.ac.uk/20318/1/AL-Neama_A.%20F.%20M._Mechanical%20Engineering_PhD_2018.pdf.

[41] Datta, A., "PEM Fuel Cell MODEL for Conceptual Design of Hydrogen eVTOL Aircraft," Tech. rep., NASA CR-0284, January 2021. URL https://ntrs.nasa.gov/citations/20210000284.

[42] Spiegel, C., *PEM Fuel Cell Modeling and Simulation Using Matlab*, 1st ed., Academic Press, 2008. https://doi.org/10.1016/B978-0-12-374259-9.X5001-0.

[43] Incropera, F. P., DeWitt, D. P., Bergman, T. L., and Lavine, A. S., *Fundamentals of Heat and Mass Transfer*, 6th ed., John Wiley & Sons, 2007.

[44] Sunden, B., and Fu, J., *Heat Transfer in Aerospace Applications*, 1st ed., Academic Press, 2016.

[45] Shah, R. K., and Sekulić, D. P., *Fundamentals of Heat Exchanger Design*, John Wiley & Sons, 2003. https://doi.org/10.1002/9780470172605.

[46] Kays, W. M., and London, A. L., *Compact Heat Exchangers*, 3rd ed., McGraw-Hill, New York, 1984.

[47] Carozza, A., *Heat Exchangers in the Aviation Engineering*, IntechOpen, Rijeka, Croatia, 2017, Chap. 7, pp. 149–166. https://doi.org/10.5772/67486.

[48] Khan, T. A., and Li, W., "Optimal design of plate-fin heat exchanger by combining multi-objective algorithms," *International Journal of Heat and Mass Transfer*, Vol. 108, 2017, pp. 1560–1572. https://doi.org/https://doi.org/10.1016/j.ijheatmasstransfer.2017.01.031.

[49] Brooks, J., and Mavris, D. N., "Compact Heat Exchanger Sizing and Weight Estimation," *AIAA Propulsion and Energy 2021 Forum*, Virtual, 2021. https://doi.org/10.2514/6.2021-3711.

[50] Bell, I. H., Wronski, J., Quoilin, S., and Lemort, V., "Pure and Pseudo-pure Fluid Thermophysical Property Evaluation and the Open-Source Thermophysical Property Library CoolProp," *Industrial & Engineering Chemistry Research*, Vol. 53, No. 6, 2014, pp. 2498–2508. https://doi.org/10.1021/ie4033999, URL http://pubs.acs.org/doi/abs/10.1021/ie4033999.

[51] Hesselgreaves, J., Law, R., and Reay, D., *Compact Heat Exchangers*, Butterworth-Heinemann, Oxford, United Kingdom, 2016.

[52] Li, Y., Li, D., Ma, Z., Zheng, M., and Lu, Z., "Thermodynamic Modeling and Performance Analysis of Vehicular High-Temperature Proton Exchange Membrane Fuel Cell System," *Membranes*, Vol. 12, No. 1, 2022. https://doi.org/10.3390/membranes12010072.

[53] Cengel, Y. A., and Cimbala, J. M., *Fluid Mechanics*, McGraw-Hill, 2004, Chap. Flow in Pipes, pp. 321–398.

[54] Kandlikar, S. G., Li, D., King, M. R., Garimella, S., and Colin, S., *Heat Transfer and Fluid Flow in Minichannels and Microchannels*, 2nd ed., Butterworth-Heinemann, 2014. https://doi.org/10.1016/C2011-0-07521-X.

[55] Colebrook, C. F., "Turbulent Flow in Pipes, with Particular Reference to the Transition Region between the Smooth and Rough Pipe Laws," *Journal of the Institution of Civil Engineers*, Vol. 11, No. 4, 1939, pp. 133–156. https://doi.org/10.1680/ijoti.1939.13150.

[56] Drela, M., "Aerodynamics of Heat Exchangers for High-Altitude Aircraft," *Journal of Aircraft*, Vol. 33, No. 2, 1996, pp. 176–184. https://doi.org/10.2514/3.46919.

[57] Raymer, D. P., *Aircraft Design: A Conceptual Approach*, 2nd ed., American Institute of Aeronautics and Astronautics, Inc., Washington, DC, 1992.

[58] Einstein, A., "Eine neue Bestimmung der Moleküldimensionen," *Annalen der Physik*, Vol. 324, No. 2, 1906, pp. 289–306. https://doi.org/10.1002/andp.19063240204.

[59] Maxwell, J. C., *A Treatise on Electricity and Magnetism*, Oxford University Press, United Kingdom, 1873.

[60] Manglik, R. M., and Bergles, A. E., "Heat transfer and pressure drop correlations for the rectangular offset strip fin compact heat exchanger," *Experimental Thermal and Fluid Science*, Vol. 10, No. 2, 1995, pp. 171–180. https://doi.org/10.1016/0894-1777(94)00096-Q.

[61] Syam Sundar, L., Venkata Ramana, E., Singh, M. K., and Sousa, A. C., "Thermal conductivity and viscosity of stabilized ethylene glycol and water mixture Al2O3 nanofluids for heat transfer applications: An experimental study," *International Communications in Heat and Mass Transfer*, Vol. 56, 2014, pp. 86–95. https://doi.org/10.1016/j.icheatmasstransfer.2014.06.009.

[62] Vajjha, R., Das, D., and Mahagaonkar, B., "Density Measurement of Different Nanofluids and Their Comparison With Theory," *Petroleum Science and Technology*, Vol. 27, No. 6, 2009, pp. 612–624. https://doi.org/10.1080/10916460701857714, URL https://doi.org/10.1080/10916460701857714.

[63] Yiamsawas, T., Mahian, O., Dalkilic, A. S., Kaewnai, S., and Wongwises, S., "Experimental studies on the viscosity of TiO_2 and Al_2O_3 nanoparticles suspended in a mixture of ethylene glycol and water for high temperature applications," *Applied Energy*, Vol. 111, 2013, pp. 40–45. https://doi.org/10.1016/j.apenergy.2013.04.068.

[64] Yu, W., Xie, H., Li, Y., Chen, L., and Wang, Q., "Experimental investigation on the heat transfer properties of Al_2O_3 nanofluids using the mixture of ethylene glycol and water as base fluid," *Powder Technology*, Vol. 230, 2012, pp. 14–19. https://doi.org/10.1016/j.powtec.2012.06.016.

[65] Raja Sekhar, Y., and Sharma, K., "Study of viscosity and specific heat capacity characteristics of water-based Al_2O_3 nanofluids at low particle concentrations," *Journal of Experimental Nanoscience*, Vol. 10, No. 2, 2015, pp. 86–102. https://doi.org/10.1080/17458080.2013.796595.

[66] Barbés, B., Páramo, R., Blanco, E., Pastoriza-Gallego, M. J., Piñeiro, M. M., Legido, J. L., and Casanova, C., "Thermal conductivity and specific heat capacity measurements of Al2O3 nanofluids," *Journal of Thermal Analysis and Calorimetry*, Vol. 111, 2013, pp. 1615–1625. https://doi.org/10.1007/s10973-012-2534-9.

[67] O'Hanley, H., Buongiorno, J., McKrell, T., and Hu, L., "Measurement and Model Validation of Nanofluid Specific Heat Capacity with Differential Scanning Calorimetry," *Advances in Mechanical Engineering*, Vol. 4, 2012, p. 181079. https://doi.org/10.1155/2012/181079.

[68] VDI e. V. (ed.), *VDI Heat Atlas*, 2nd ed., Springer Berlin, Heidelberg, Germany, 2010. https://doi.org/10.1007/978-3-540-77877-6.

[69] American Society of Heating, Refrigerating and Air-Conditioning Engineers, Inc. (ASHRAE), *2021 ASHRAE® Handbook - Fundamentals (SI Edition)*, American Society of Heating, Refrigerating and Air-Conditioning Engineers, Inc. (ASHRAE), 2021.

[70] Brinkman, H. C., "The Viscosity of Concentrated Suspensions and Solutions," *The Journal of Chemical Physics*, Vol. 20, No. 4, 1952, pp. 571–571. https://doi.org/10.1063/1.1700493.

[71] Batchelor, G. K., "The effect of Brownian motion on the bulk stress in a suspension of spherical particles," *Journal of Fluid Mechanics*, Vol. 83, No. 1, 1977, p. 97–117. https://doi.org/10.1017/S0022112077001062.

[72] De Noni Jr, A., Garcia, D. E., and Hotza, D., "A modified model for the viscosity of ceramic suspensions," *Ceramics International*, Vol. 28, No. 7, 2002, pp. 731–735. https://doi.org/10.1016/S0272-8842(02)00035-4.

[73] Piccio, M., and Porrini, A., "Planning and simulation of the flight test campaign for a hydrogen hybrid-electric aircraft," Master's thesis, Politecnico di Milano, Milan, Italy, 2020. URL https://www.politesi.polimi.it/handle/10589/170188.

[74] Bradley, T., Moffitt, B., Mavris, D., and Parekh, D., "Development and experimental characterization of a fuel cell powered aircraft," *Journal of Power Sources*, Vol. 171, 2007, pp. 793–801. https://doi.org/10.1016/j.jpowsour.2007.06.215.

[75] Nicolay, S., Karpuk, S., Liu, Y., and Elham, A., "Conceptual design and optimization of a general aviation aircraft with fuel cells and hydrogen," *International Journal of Hydrogen Energy*, Vol. 46, No. 64, 2021, pp. 32676–32694. https://doi.org/https://doi.org/10.1016/j.ijhydene.2021.07.127.

[76] Tomažič, T., *Fuel Cell and Hydrogen Technologies in Aviation*, Springer International Publishing, Cham, Switzerland, 2022, Chaps. Fuel Cell–Powered Passenger Aircrafts, pp. 83–95. https://doi.org/10.1007/978-3-030-99018-3_4.

[77] Webber, H., Llambrich, J., and Davoudi, H., "Thermal Management Roadmap Report," Tech. Rep. FZO-PPN-MAP-0019, Aerospace Technology Institute, March 2022. URL https://www.ati.org.uk/wp-content/uploads/2022/03/FZO-PPN-COM-0019-Thermal-Management-Roadmap-Report.pdf.

[78] Bhatti, W., Wu, W., Doyle, F., Llambrich, J., Webber, H., and Town, N., "Fuel Cells Roadmap Report," Tech. Rep. FZO-PPN-COM-0033, Aerospace Technology Institute, March 2022. URL https://www.ati.org.uk/wp-content/uploads/2022/03/FZO-PPN-COM-0033-Fuel-Cells-Roadmap-Report.pdf.

[79] Hong, H., and Roy, W., "Nano materials for efficiently lowering the freezing point of heat transfer nanofluids," *Nanoengineering: Fabrication, Properties, Optics, and Devices IV*, Vol. 6645, edited by E. A. Dobisz and L. A. Eldada, International Society for Optics and Photonics, SPIE, 2007, p. 66451A. https://doi.org/10.1117/12.731660.

IV

Supporting Work

IV.1 Methodology

This chapter provides supplemental information about the fuel cell thermal management system sizing methodology developed in this thesis. This chapter supplements section III.IV. Sections IV.1.1 and IV.1.2 present the calculation of the Nusselt number, Colburn factor and Fanning friction factor. The calculation of the overall heat transfer coefficient is presented in section IV.1.3. The heat exchanger core geometry is detailed in section IV.1.4 and additional heat exchanger geometric relations are presented in section IV.1.5.

IV.1.1 Nusselt Number

The Nusselt number is a non-dimensional number defined as the ratio of the convective heat transfer to conductive heat transfer between a fluid and a surface. A function `getNusseltNumber` was developed to calculate the Nusselt number using empirical relations from literature. Different empirical relations exist for different passage geometry, flow conditions and boundary conditions. Not all cases have corresponding relations and hence assumptions are made for which relation should be used. Though the Nusselt number relations for numerous passage types and flow conditions were included in the `getNusseltNumber` function only those used in the current thermal management system are presented and discussed in this section. In the cooling plates of the fuel cell stack a rectangular passage is used for the heat transfer between the cooling plates and the coolant. The uniform wall temperature boundary condition and laminar flow conditions were assumed for this case. Equation (IV.1.1) from Bhatti and Shah [83] as obtained via Hesselgreaves et al. [84] was used for this case.

$$Nu_T = \begin{cases} 7.541\left(1 - 2.61AR^{-1} + 4.97AR^{-2} - 5.119AR^{-3} + 2.702AR^{-4} - 0.548AR^{-5}\right) & \text{if } AR \geq 1 \\ 7.541\left(1 - 2.61AR + 4.97AR^{2} - 5.119AR^{3} + 2.702AR^{4} - 0.548AR^{5}\right) & \text{if } AR < 1 \end{cases} \tag{IV.1.1}$$

Triangular passages are found in the heat exchanger core geometry. The H1 boundary condition, where there is an axially constant wall heat flux and peripherally constant wall temperature was assumed. This was based on Hesselgreaves et al. [84] and Vocale [85] who state that the H1 boundary condition is applied when the boundary material has a high thermal conductivity as is the case with the aluminium used in the core. For the laminar flow regime tabulated data from Shah and London [86] as a function of the angle between the two equal lengths of the isosceles triangle was used. A 5$^{\text{th}}$-order polynomial was fitted to the tabulated data and used to evaluate the Nusselt number. For the transitional flow regime, as no specific relations were found in literature and based on the recommendation of Hesselgreaves et al. [84], the relations proposed by Bhatti and Shah [83] are used. This relation is shown in Equation (IV.1.2) where Nu_l is 4.364 for the H boundary conditions and Nu_t is given in Equation (IV.1.3) where Nu_o is 6.3 for the H boundary conditions.

$${Nu_{H1}}^{10} = {Nu_l}^{10} + \left[\frac{\exp\left(2000 - Re\right)/365}{{Nu_l}^2} + \frac{1}{{Nu_t}^2}\right]^{-5} \tag{IV.1.2}$$

$$Nu_t = Nu_o + \frac{0.078(f/2)^2 RePr}{(1 + Pr^{4/5})^{5/6}} \tag{IV.1.3}$$

For the turbulent flow regime, Equation (IV.1.4) from Kays and Crawford [87] was used as it was also used by Kožulović [4].

$$Nu = 0.022\sqrt{Pr}Re^{0.8} \tag{IV.1.4}$$

IV.1.2 Colburn Factor and Fanning Friction Factor

The Colburn factor and Fanning friction factor are obtained from tabulated data for the specific heat exchanger core geometry from Kays and London [88]. For the Colburn factor an exponential fit of the form $y = a^{bx} + c^{dx}$ is applied to the data across the entire Reynolds number range. A power equation of the form $y = ax^b + c$ is used for the Fanning friction factor. The tabulated data from Kays and London [88] and corresponding fits are shown in Figure IV.1.1.

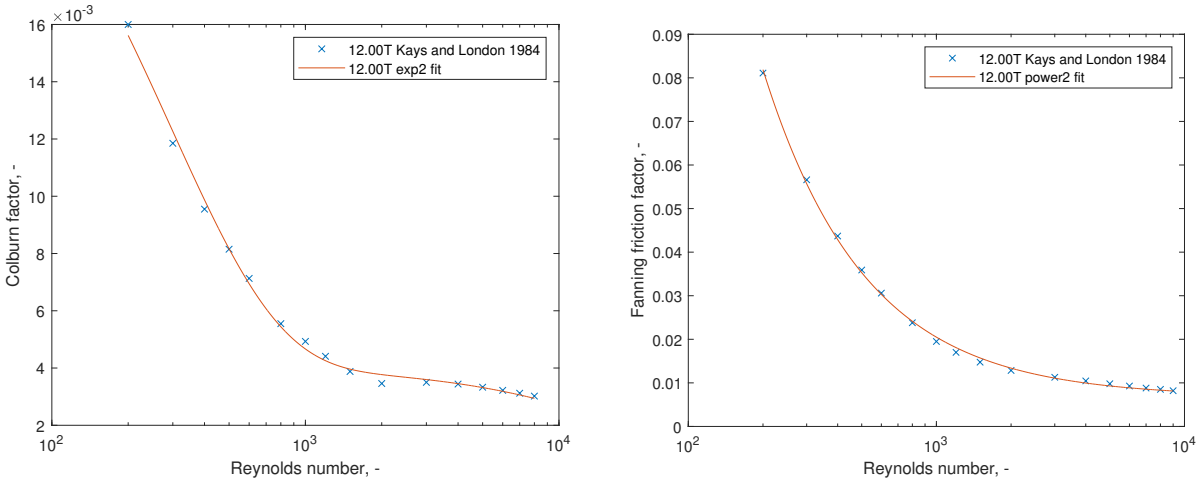

(a) Colburn factor

(b) Fanning friction factor

Figure IV.1.1: Colburn factor and Fanning friction factor as a function of Reynolds number for plate-fin type 12.00T from Kays and London [88]

IV.1.3 Overall Heat Transfer Coefficient

The overall heat transfer coefficient is calculated based on the thermal circuit analogy presented in literature including Incropera et al. [89] and Shah and Sekulić [90]. Figure IV.1.2 visualises this analogy for the heat exchanger considered in the thesis. Each resistor in the circuit represents a thermal resistance referring to either a convective thermal resistance (e.g. heat transfer through the cold fluid) or a conductive thermal resistance (e.g. heat transfer through the heat exchanger wall). The construction of the thermal circuit into series and parallel branches is directly related to the heat exchanger core geometry.

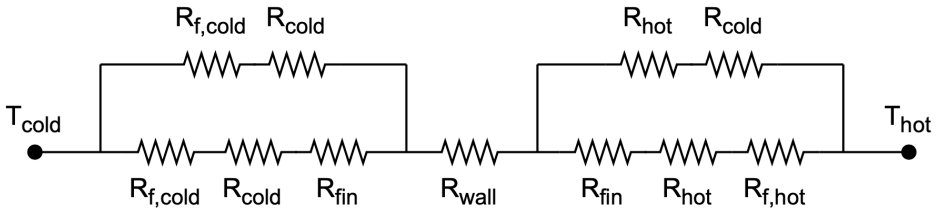

Figure IV.1.2: Thermal circuit (own work based on work by Shah and Sekulić [90])

The overall heat transfer coefficient is *defined in terms of the total thermal resistance to heat transfer between two fluids* [89]. The total thermal resistance is the sum of the thermal resistances as shown in Equation (IV.1.5). This equation includes the fouling layer thermal resistance and convective thermal resistance. It excludes the thermal contact resistance between the wall and fins as these were neglected. The equation is a simplification of the thermal circuit shown in Figure IV.1.2 whereby the two parallel branches on either fluid side were simplified into a single series branch. A more detailed version of Equation IV.1.5 showing the calculation of the individual thermal resistances can be found in Equation (III.19).

$$R_o = R_{hot} + R_{f,hot} + R_{wall} + R_{f,cold} + R_{cold} \tag{IV.1.5}$$

The convection resistance on both fluid sides as shown in Equation (IV.1.5) is the effective convection resistance which considers the presence of the fins through the overall surface efficiency which is calculated through Equation (IV.1.6) [89]. The fin efficiency is calculated through Equation (IV.1.7) [89]. An approximation for m is given in Equation (IV.1.8) [90] and l is defined as half the length of the equal sides of the isosceles triangle [90].

$$\eta_0 = 1 - \frac{A_{fin}}{A}(1 - \eta_{fin}) \tag{IV.1.6}$$

$$\eta_{fin} = \frac{\tanh ml}{ml} \tag{IV.1.7}$$

$$m = \sqrt{\frac{2h}{k_{fin} t_{fin}}} \tag{IV.1.8}$$

Once the total thermal resistance was determined the overall heat transfer coefficient was calculated through Equation (IV.1.9) [90]. The overall heat transfer coefficient on each heat exchanger side may differ. Regardless, the product of the overall heat transfer coefficient and heat transfer area UA is constant [89, 90]. Once the overall heat transfer coefficient on one side is calculated the overall heat transfer coefficient of the other side can be calculated through Equation (IV.1.9) or through the surface area density ratio α_1/α_2 [90].

$$U = \frac{1}{AR_o} \tag{IV.1.9}$$

IV.1.4 Heat Exchanger Core Geometry

The heat exchanger core geometry based on the triangular plate-fin type 12.00T from Kays and London [88] is shown in Figure IV.1.3 and the dimensions in Table IV.1.1. The lengths labelled as L_1, L_2 and L_3 in Figure IV.1.3 are referred to as the coolant flow length, air flow length and no flow length respectively.

Parameter	Symbol	Unit	Value	Source
Plate spacing	b	m	$6.35 \cdot 10^{-3}$	[88]
Fin density	ρ_{fin}	$^1/_{\text{inch}}$	12.00	[88]
Fin pitch	f	m	2.118	[1]
Hydraulic diameter	D_h	m	$2.87 \cdot 10^{-3}$	[88]
Fin thickness	t_{fin}	m	$0.152 \cdot 10^{-3}$	[88]
Surface area density	β	m^2/m^3	1288.4	[88]
Fin area to total area ratio	$\frac{A_{fin}}{A}$	-	0.773	[88]
Wall thickness	t_{wall}	m	$1.5 \cdot 10^{-3}$	Guess

Table IV.1.1: Dimensions of heat exchanger core based on plate-fin type 12.00T from Kays and London [88]

[1] F-Chart Software *PF_plain_fin_1200T* Engineering Equation Solver. URL: https://fchartsoftware.com/ees/heat_transfer_library/compact_hx/plain_fins/hs1087.htm. Date accessed: 6 Apr. 2023

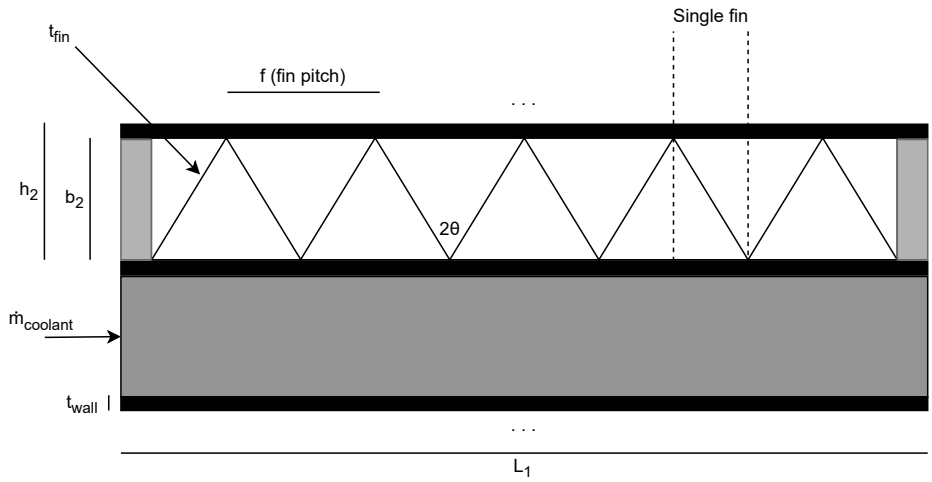

(a) Front view of the heat exchanger core towards the air side passage inlet

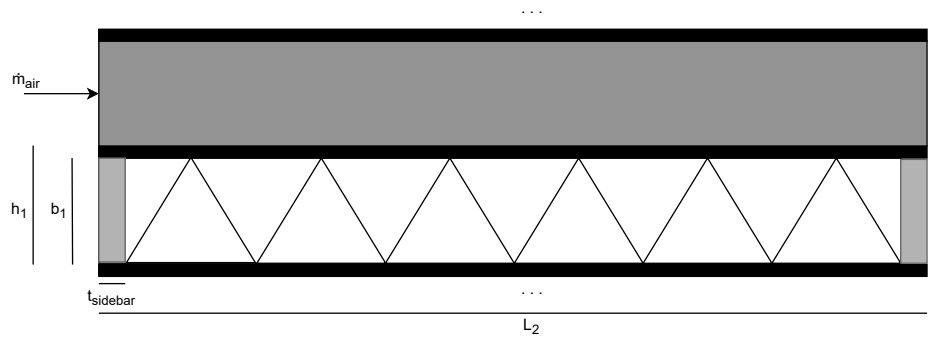

(b) Side view of the heat exchanger core towards the coolant side passage inlet

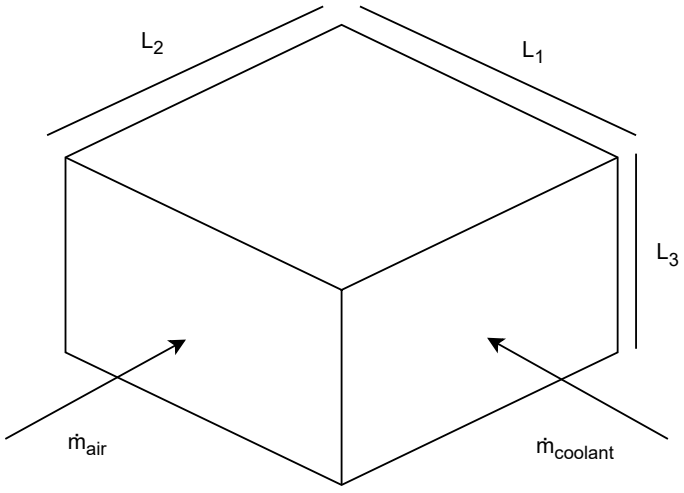

(c) Isometric view of the heat exchanger core

Figure IV.1.3: Schematics of the heat exchanger core [88]

IV.1.5 Heat Exchanger Geometric Relations

Relations for the geometric properties of the heat exchanger core omitted in section IV.B for conciseness are presented in this section. The angle between two fins in the triangular fin geometry, shown in Figure IV.1.3a is calculated through Equation (IV.1.10).

$$\theta = \arctan \frac{\frac{1}{2}f}{b} \tag{IV.1.10}$$

The adiabatic length of the fin, as defined in figure 4.15 in Shah and Sekulić [90] is calculated through Equation (IV.1.11). This length is shown in Figure IV.1.3b.

$$l = \frac{1}{2}\frac{b_2 - h_{tc}}{\cos\theta} \tag{IV.1.11}$$

The surface area density with respect to the total volume of the heat exchanger core is calculated through Equation (IV.1.12) [89].

$$\alpha = \frac{b\beta}{b_1 + b_2 + 2t_{wall}} \tag{IV.1.12}$$

For both fluid sides the total heat transfer area is calculated through Equation (IV.1.13) [89] and the free flow area through Equation (IV.1.14) [90].

$$A_{tot} = \frac{C_{min}NTU}{U} \tag{IV.1.13}$$

$$A_0 = \frac{\dot{m}}{G} \tag{IV.1.14}$$

The ratio of the free flow area to the frontal area can be rearranged into Equation IV.1.15 [90] as a function of the surface area density.

$$\sigma = \frac{1}{4}\alpha D_h \tag{IV.1.15}$$

The frontal areas of both fluid sides are then calculated through Equation (IV.1.16). The frontal area of the air side is also referred to as the frontal area of the heat exchanger core due to its placement within the fairing.

$$A_{fr} = \frac{A_0}{\sigma} \tag{IV.1.16}$$

The coolant flow length is calculated through Equation (IV.1.17) [90] and the airflow length through Equation (IV.1.18) [90, 84].

$$L_1 = \frac{D_{h,hot}A_{tot,hot}}{4A_{0,hot}} \tag{IV.1.17}$$

$$L_2 = \frac{D_{h,cold}A_{tot,cold}}{4A_{0,cold}} \tag{IV.1.18}$$

The no-flow length is then calculated through the two, in theory, equivalent relations shown in Equation (IV.1.19) based on the frontal area of the two fluid sides. In practice, the no-flow lengths are slightly different and the mean is taken.

$$L_3 = \frac{A_{fr,cold}}{L_1} = \frac{A_{fr,hot}}{L_2} \tag{IV.1.19}$$

The installation angle of the heat exchanger core is calculated through Equation (IV.1.20) based on the assumption that the cross-sectional area of the duct is equal to the free flow area on the air side.

$$\gamma = \arccos \frac{A_{0,cold}}{A_{fr,cold}} \tag{IV.1.20}$$

The number of passages on the air and coolant sides is calculated through Equations (IV.1.21) and (IV.1.22) respectively.

$$N_{p,air} = \frac{L_3 - b_2 - 2t_{wall}}{b1 + b2 + 2t_{wall}} \tag{IV.1.21}$$

$$N_{p,coolant} = N_{p,air} + 1 \tag{IV.1.22}$$

IV.2

Verification and Validation

Additional verification and validation of the developed fuel cell thermal management system sizing methodology is presented in this chapter. This chapter supplements section III.V. The first section presents the validation of the thermophysical properties of aqueous ethylene glycol as obtained from CoolProp [91]. Section IV.2.2 visually compares the heat exchanger sized by the developed fuel cell thermal management system sizing methodology and the heat exchanger installed on a fuel cell engine retrofitted onto a Dash 8 aircraft. Though not a direct validation of the sizing methodology it supports the credibility of the methodology and its results with a real-world thermal management system.

IV.2.1 Validation of Thermophysical Properties of Water Ethylene Glycol Mixtures

The thermophysical properties of the aqueous ethylene glycol base fluid were determined using CoolProp [91]. These properties were validated against data from literature including the VDI Heat Atlas [92] and the 2021 ASHRAE handbook [93]. The validation was carried out at 20°C and is shown in Figure IV.2.1.

The dynamic viscosity, specific heat capacity and freezing temperature determined through CoolProp show good agreement with literature. There is a considerable spread in thermal conductivity data from the VDI Heat Atlas [92] and the 2021 ASHRAE handbook [93]. The current model is shown to take the average of these two data sets. CoolProp underestimates the density in comparison to literature for the entire range of mass fractions considered. This underestimation becomes larger at higher mass fractions. Based on these figures it was deemed that the thermophysical properties of the aqueous ethylene glycol as determined through CoolProp are in sufficient agreement with literature for the purposes of this thesis.

IV.2.2 Visual Comparison with Universal Hydrogen Dash 8

As mentioned in section III.V.D it was not possible to validate the developed fuel cell thermal management sizing methodology against a comparable system on a comparable aircraft. At the time of writing no commercial CS-23 commuter fuel cell aircraft had flown. However, during the thesis two larger demonstrator fuel cell aircraft were flown for the first time. ZeroAvia flew a Do228 retrofitted with a single fuel cell engine in January of 2023[1]. In March of 2023, Universal Hydrogen flew a Dash 8 retrofitted with a single fuel cell engine[2]. Little to no technical data was made publicly available on the fuel cell thermal management system of either aircraft. However numerous images were published of the fuel cell engine retrofitted on the Dash 8 showing the heat exchanger in considerable detail. This made a visual comparison possible. A visual comparison between systems is shown in Figure IV.2.2.

[1] *ZeroAvia Makes Aviation History, Flying World's Largest Aircraft Powered with a Hydrogen-Electric Engine*. ZeroAvia, January 2023. URL: https://www.zeroavia.com/do228-first-flight. Date accessed: 17 Mar 2023

[2] D. Gates, *Pioneering Moses Lake flight uses hydrogen to power regional airplane*, The Seattle Times, March 2023. URL: https://www.seattletimes.com/business/boeing-aerospace/pioneering-moses-lake-flight-uses-hydrogen-to-power-regional-airplane/. Date accessed: 8 Mar. 2023

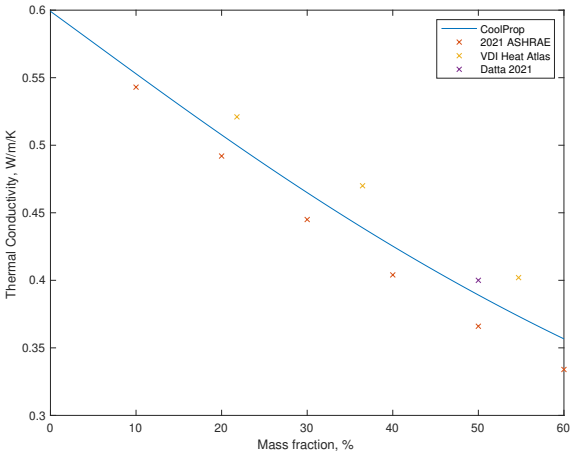

(a) Thermal conductivity

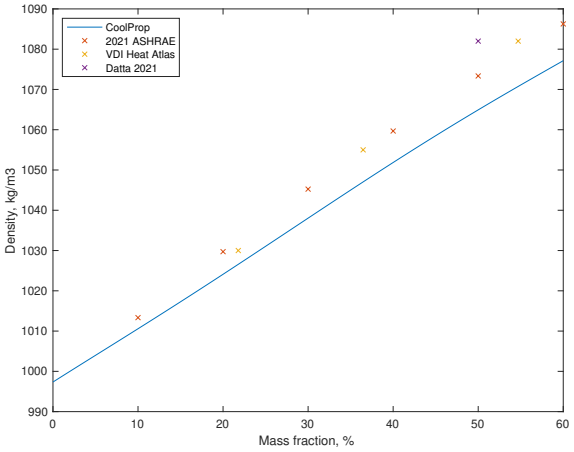

(b) Density

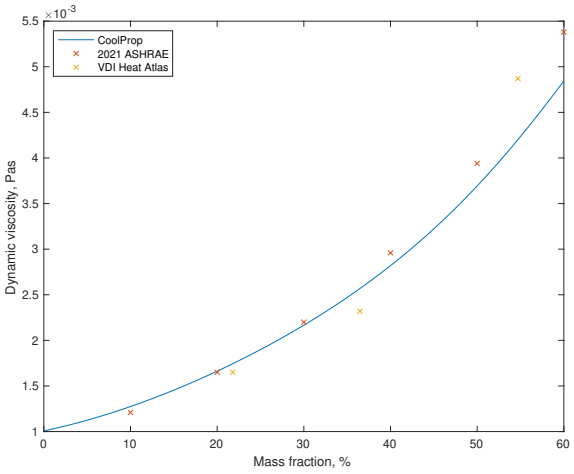

(c) Dynamic viscosity

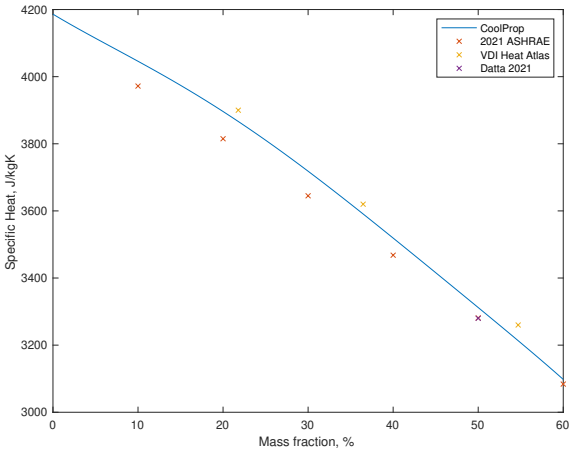

(d) Specific heat capacity

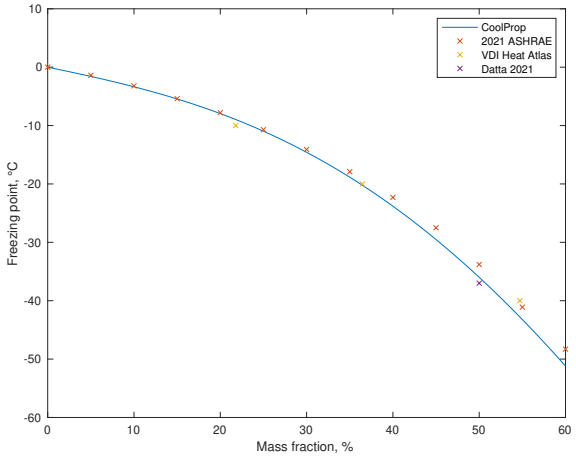

(e) Freezing temperature

Figure IV.2.1: Thermophysical properties of aqueous ethylene glycol as a function of mass fraction of ethylene glycol in water

In Figure IV.2.2a the heat exchangers sized by the developed sizing methodology are shown in red mounted on either side of the fuel cell stack, compressor and humidifier within the fuel cell engine. This thermal management system corresponds to configuration A from section III.VI. Figure IV.2.2b shows a single heat exchanger mounted on the outboard side of the fuel cell engine. Other images published by

Universal Hydrogen show that a similarly sized, presumed identical, heat exchanger is mounted on the inboard side of the fuel cell engine. It is unknown what the dimensions, orientation of the fluid streams, design point and type of coolant used are hence a direct and proper validation was not possible. It is however publicly known that the heat exchanger is of a *microtube* type[3]. Both thermal management systems are sized to dissipate around 1 MW of heat.

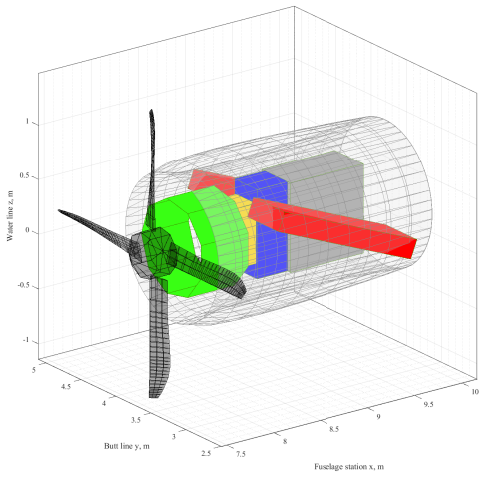

(a) Heat exchanger mounted on fuel cell engine conceptually sized by the Initiator for an hybrid-electric aircraft based on the Metro 23

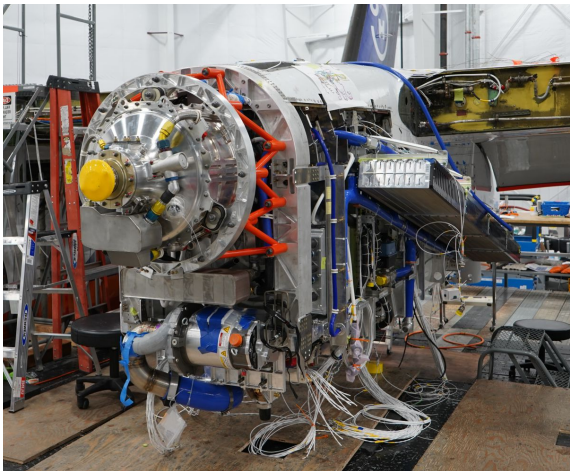

(b) Heat exchanger mounted on the fuel cell engine retrofitted onto a Dash 8. Photo tweeted by P. Eremenko[3]

Figure IV.2.2: Comparison of the heat exchanger sized by the Initiator through the developed thermal management sizing methodology and the heat exchanger mounted on a fuel cell engine

Visually comparing the two heat exchangers it is clear to see there are similarities in the external dimensions of the heat exchangers in relation to the size of the fuel cell engine. It is clear to see from Figure IV.2.2b what the airflow length is. Comparing this with the airflow length in Figure IV.2.2a it is shown that these are very similar. This visual comparison, though not a complete validation, adds to the robustness and credibility of the developed and implemented fuel cell thermal management system sizing methodology. In future work, once more data becomes available or accessible a proper validation at fuel cell engine level can be carried out.

[3]P. Eremenko, November 2022. `https://twitter.com/PaulEremenko/status/1595083565611745281`. Date accessed: 6 Apr. 2023

IV.3

Results and Discussion

This chapter provides additional results of the developed fuel cell thermal management system sizing methodology and the analysis thereof. This chapter supplements section III.VI. Section IV.3.1 presents and compares the results of all the CS-23 commuter aircraft considered in this thesis. Two sensitivity studies were performed and the results thereof are presented in section IV.3.2. The second to last section presents a number of additional views of the conceptually sized hybrid-electric aircraft based on the Metro 23 as sized by the Initiator. The last section of this chapter answers the thesis research questions.

IV.3.1 Comparison of CS-23 Commuter Aircraft

In supplement to section III.VI.B, selected results for all the CS-23 commuter aircraft studied in this thesis are presented in Figure IV.3.1. The hybrid-electric aircraft considered were based on the Fairchild Swearingen Metro 23, British Aerospace Jetstream 31, Embraer EMB 110P2 Bandeirante and the Dornier 228-200.

Considering Figures IV.3.1a-IV.3.1c a general trend can be seen between the operating empty mass (OEM) and respective parameters. With increasing OEM the fuel cell power, fuel cell system mass and frontal area increase linearly. The Do228 is an outlier to this linear trend being placed slightly above the linear trend. This is linked to the sizing case of the thermal management system for this aircraft, specifically the take-off velocity. The take-off velocity of the Do228 is slightly lower than the other three CS-23 commuter aircraft. This more challenging sizing case leads to a considerably larger frontal area as shown in Figure IV.3.1c and a heavier overall fuel cell system as shown in Figure IV.3.1c. The fuel cell system mass is also affected by the snowball effect of the increase in thermal management system mass. This heavier system leads to an increase in fuel cell power to propel the aircraft. The zero-lift drag coefficients are all within the same range (max: 219 cts, min: 178 cts). This range was slightly higher but comparable to the range of the conventional aircraft these are based on (max: 232 cts, min: 188 cts).

IV.3.2 Sensitivity Studies

Two sensitivity studies were carried out to further analyze and understand the characteristic of the thermal management system. The first study analysed the effect of the ratio of the heat removed by the thermal management system to the total heat produced within the fuel cell stack on system and aircraft level performance. The second focused on the inputs into the heat exchanger model and the effects on the sizing of the heat exchanger.

IV.3.2.1 Heat removed by the thermal management system

In the development of the thermal management system sizing methodology, it was assumed that all heat produced within the fuel cell stack must be taken away by the thermal management system. This is however not the case as heat sinks exist including heat dissipated through natural convection [27, 26], heat dissipated through radiation [94] and heat used for internal water evaporation [27, 26]. This

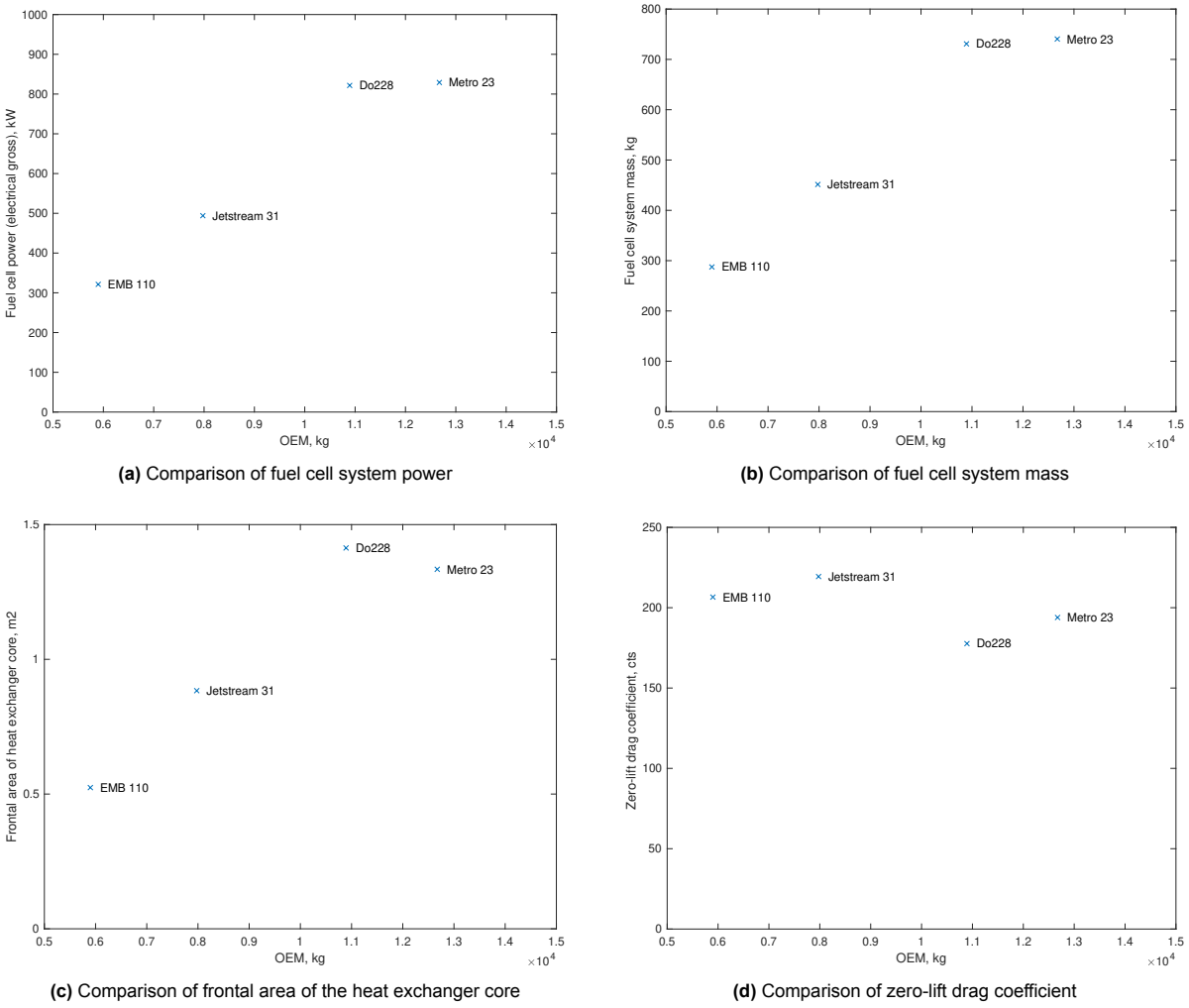

(a) Comparison of fuel cell system power

(b) Comparison of fuel cell system mass

(c) Comparison of frontal area of the heat exchanger core

(d) Comparison of zero-lift drag coefficient

Figure IV.3.1: Comparison of thermal management system and aircraft level performance of four CS-23 commuter aircraft

sensitivity study analysed six different configurations with varying ratios of $\dot{Q}_{TMS}/\dot{Q}_{stack}$. Huang et al. [26] and Bargal et al. [27] estimate the ratio to be 80% whereas Tomažič [95] estimates it to be 90%. These ratios along with 85%, 95%, the ratio resulting from configuration B from Table III.4 and the assumption of 100% were considered. Configuration B used equations presented by Datta [94] to model the heat dissipated through natural convection and radiation. The ratio $\dot{Q}_{TMS}/\dot{Q}_{stack}$ for this configuration was found to be 98.2%, far above the ratios given in literature. Selected results of the sensitivity study are visualized in the subsequent figures. The sensitivity study was performed for hybrid-electric aircraft based on the Metro 23 sized at sea-level ISA conditions for take-off with water as the coolant. The fits shown in Figures IV.3.2b-IV.3.2f are all 2nd-order polynomial fits.

Considering all the figures it is clear to see a general trend that with decreasing Q_{TMS}/Q_{stack} the mass of the thermal management system, OEM, fuel cell power and zero-lift drag coefficient of the thermal management system decrease. This was excepted as reducing the amount of heat removed by the thermal management system reduces the system size which will have a snowball effect on both system and aircraft level performance. This snowball effect is clearly shown in Figure IV.3.2a. The actual amount of heat removed by the thermal management system (blue data points) considers the snowball effect of the reduction in heat removed by the thermal management system. The expected amount of heat removed by the thermal management system (orange line) is given as the percentage of the heat removed by the thermal management system for the assumed 100%. The calculation of this linear relation is shown in Equation (IV.3.1) where $\dot{Q}_{TMS,all}$ is the heat removed by the thermal management system for configuration A in Table III.4.

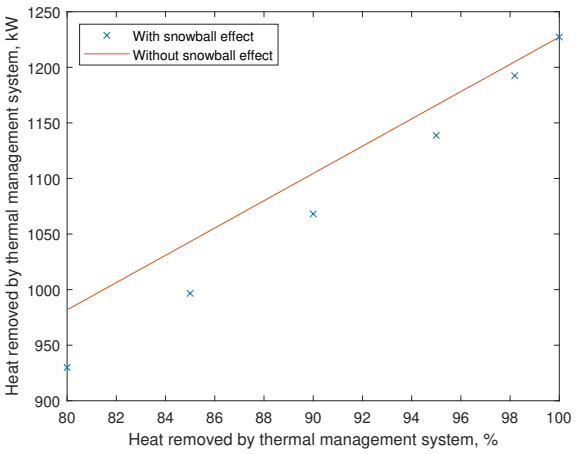

(a) Heat removed by thermal management system

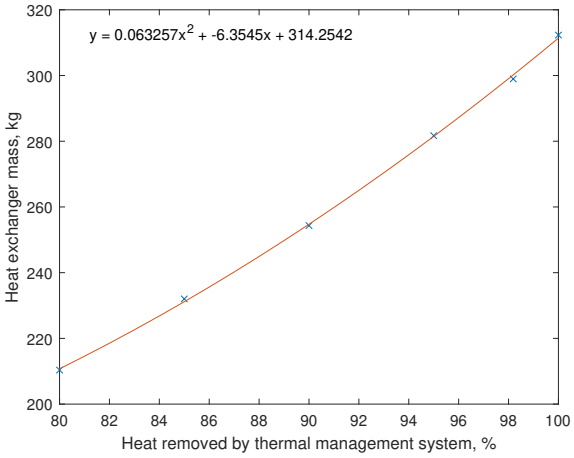

(b) Heat exchanger mass

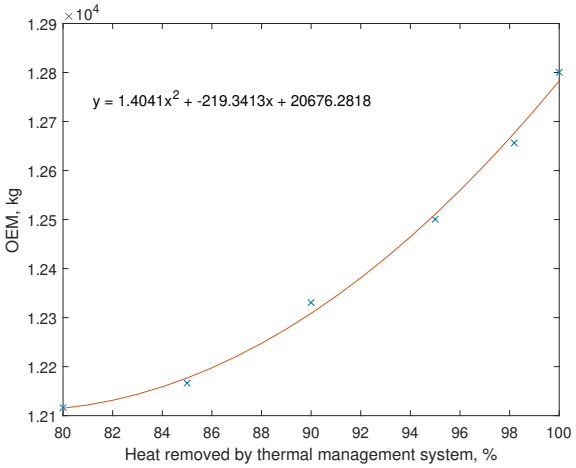

(c) Operating empty mass

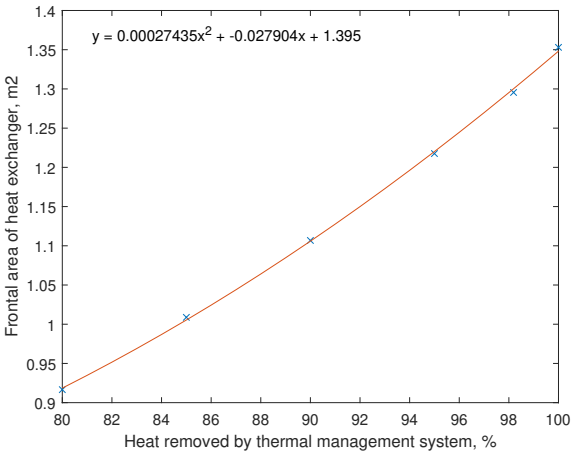

(d) Frontal area of heat exchanger core

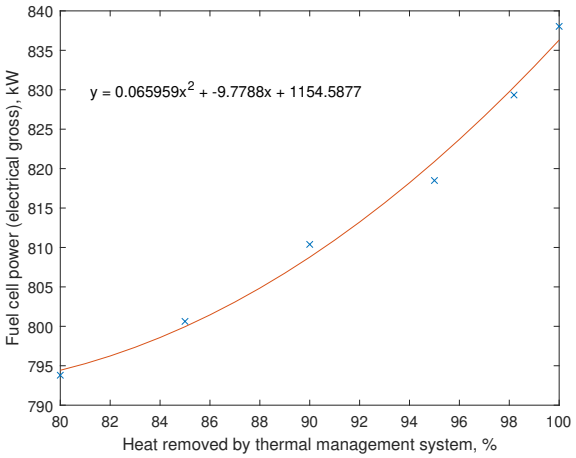

(e) Fuel cell system power (electrical gross)

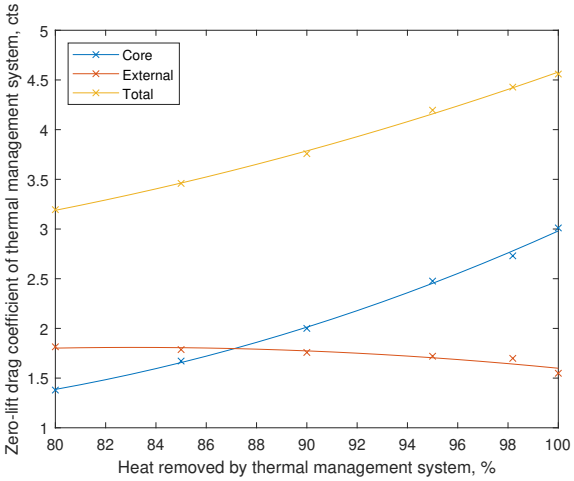

(f) Zero-lift drag coefficient of thermal management system

Figure IV.3.2: Selected plots from the sensitivity study of the percentage of stack heat removed by the thermal management system

$$y = \frac{x}{100}\dot{Q}_{TMS,all} \tag{IV.3.1}$$

Comparing the two sets of results it can be seen that at lower values of $\dot{Q}_{TMS}/\dot{Q}_{stack}$ the actual amount of heat removed is considerably lower than the expected amount of heat removed. This is in line with the expected impact of the snowball effect on the size of the fuel cell system. The difference between the two sets is shown to increase for decreasing $\dot{Q}_{TMS}/\dot{Q}_{stack}$ in line with expectations.

Analysing Figure IV.3.2f it is shown that with decreasing $\dot{Q}_{TMS}/\dot{Q}_{stack}$ the zero-lift drag coefficient of the thermal management system also decreases. This is shown to be predominately due to the decrease in the core component of the drag attributed to the thermal management system. The core drag is a function of the mass flow rate of air which is dependent on the frontal area of the heat exchanger core. From Figure IV.3.2d it can be seen that the frontal area decreases with decreasing $\dot{Q}_{TMS}/\dot{Q}_{stack}$. The external component is shown not to change considerably. This is because the width of the heat exchanger core (no-flow length) is not significantly affected by $\dot{Q}_{TMS}/\dot{Q}_{stack}$, changing only by around -4% from 100% to 80%.

IV.3.2.2 Heat exchanger design methodology inputs

The developed heat exchanger model presented in section III.IV.B has several inputs. Two of these are the allowable pressure drop on the air and coolant sides. This sensitivity study analyses the effect of these inputs on the heat exchanger size. Selected results are presented in Figure IV.3.3. The sensitivity study was performed using the input data into the heat exchanger model in the last iteration for the baseline configuration, referred to as configuration A in section III.VI.

Figure IV.3.3a shows that the volume of the heat exchanger depends predominantly on the air side pressure drop. The volume is the product of the heat exchanger height, length and width. These lengths are shown in Figures IV.3.3b-IV.3.3d. The airflow length is allowed to increase for increasing air side pressure drop. This was expected as the pressure drop is a function of among other things, the length of the passage as shown in Equation (III.20). The coolant flow length is however shown to not be influenced by the coolant pressure drop. Figure IV.3.3b shows a little variation in colour across the graph. Low allowable pressure drops on both fluid sides yield a very long heat exchanger height which considerably distorts the colour scale. The no-flow length is higher for low allowable air side pressure drops and decreases with increasing air side pressure drop. For low allowable air side pressure drops, the airflow length is restricted to small lengths. For the heat transfer to be balanced more air passages are required which increases the no-flow length. This also increases the frontal area of the heat exchanger core as is shown in Figure IV.3.3e. As the heat exchanger mass is closely related to the heat exchanger volume a very similar relation is seen in Figure IV.3.3f as in Figure IV.3.3a.

There is a considerable discontinuity in Figures IV.3.3a and IV.3.3f around a coolant side pressure drop of around 3,000 Pa. A similar but less pronounced discontinuity is also seen in Figures IV.3.3b-IV.3.3d. This discontinuity marks the point where the assumption for the balance of thermal resistances is invalid. The assumption, which is related to the individual side ntu was shown in Equations (III.11) and (III.12). Above the discontinuity the assumption is valid. Below the discontinuity the assumption and sensitivity study is invalid. To make the sensitivity study valid for coolant pressure drops below the current discontinuity a new calculation for the individual side ntu needs to be considered. Beyond an allowable air side pressure drop of around 18,000 Pa, the number of iterations exceeds the maximum set for this sensitivity study. Below an allowable air side pressure drop of around 4,400 Pa the check on the calculation of $\dot{Q}$ fails. This check compares $\dot{Q}$ calculated through Equations (III.4) and (III.30).

IV.3.3 Results of the Baseline Hybrid-Electric Aircraft Based on the Metro 23

Additional results of the aircraft configuration referred to as configuration A in section III.VI are presented. This aircraft configuration is referred to as the baseline aircraft from here forth. The baseline aircraft was sized for take-off at sea-level ISA conditions with a conventional thermal management system where all heat produced with the fuel cell stack is taken away by the thermal management system. The zero-lift drag coefficient breakdown of the baseline hybrid-electric aircraft is shown in Figure IV.3.4. The drag attributed to the thermal management system contributes 4.56 cts to the total zero-lift drag coefficient. This accounts for around 2.4% of the total zero-lift drag of the aircraft and includes both the core drag and external drag components. These individual components account for 66.0% and 34.0% respectively.

A comparison of the OEM for the baseline aircraft sized with and without considering the thermal

management system is shown in Figure IV.3.5. The weight shown in the figure is a class 2 weight estimation. The bar graph clearly shows the snowball effect of the thermal management system on the OEM of the aircraft. The OEM is increased by 26.0%. The thermal management system only accounts for 14.1% of the difference in OEM between the two conceptually sized aircraft.

Three additional views of the baseline hybrid-electric aircraft are shown in Figure IV.3.6. Within the fuel cell engine the electric motor is shown in green, the compressor in yellow, the humidifier in blue, the fuel cell stacks in grey and the heat exchangers in red. A close-up view of the fuel cell engine of this conceptual aircraft was previously shown in Figure IV.2.2a. The installation angle of the heat exchangers can clearly be seen in Figure IV.3.6c. In Figure IV.3.6a the liquid hydrogen tank can be seen in yellow in the rear and the batteries in green in the main wing.

IV.3.4 Answers to the Thesis Research Questions

The research questions that this thesis set out to answer were presented in Chapter II.7. Concise answers to these questions are given below.

A1. The parasitic drag, additional weight and parasitic power associated with air-based fuel cell thermal management systems can be taken into account through a number of interlinked models based on sizing methods proposed in literature. These models can be implemented into an aircraft sizing environment and verified and validated against literature.

- A1.1. The conventional air-based fuel cell thermal management system consists of a ducted heat exchanger mounted in the wake of the propeller and a water-cooling loop.
- A1.2. The proposed unconventional air-based fuel cell thermal management system is the same as the conventional system but uses nanofluids as the liquid coolant.
- A1.3. The core drag component of the parasitic drag associated with the thermal management system can be modelled through the momentum loss of air through the ducted heat exchanger and the external drag can be modelled by increasing the skin friction drag coefficient of the fuel cell engine nacelle.
- A1.4. The heat exchanger mass can be modelled using a sizing model based on the methodology proposed by Shah and Sekulić [90] and the coolant pump mass can be modelled through empirical relations based on off-the-shelf coolant pumps.
- A1.5. The parasitic power of the coolant pumps can be modelled using Equation (III.21) as proposed by Kandlikar et al. [96] and Cengel and Cimbala [97].
- A1.6. The developed models can be implemented into the Initiator by incorporating them into the class two weight estimation module and the parasite drag estimation module.
- A1.7. The developed models can be verified by comparing both intermediate and final results with expected values from literature and comparing figures of merit calculated through different approaches with each other. The heat exchanger model can be validated against EchTherm, the nanofluid model against experimental measurements and a large portion of sizing methodology against the HY4 fuel cell demonstrator aircraft.

A2. The additional mass of the air-based fuel cell thermal management systems considered in this thesis has a small direct but considerable indirect snowball effect on aircraft performance. The parasitic drag and parasitic power both have a small direct and indirect snowball effect on aircraft performance.

- A2.1. The drag attributed to the thermal management system as modelled in this thesis contributes around 3% to the total zero-lift drag coefficient which is increased by +0.7% compared to the same aircraft sized without considering a fuel cell thermal management system.
- A2.2. The mass of the thermal management system as modelled in this thesis contributes around 3% to the operating empty mass which is increased by +26.0% compared to the same aircraft sized without considering a fuel cell thermal management system.
- A2.3. The required power of the coolant pump as modelled in this thesis was found to be negligible compared to the electrical gross power output of the fuel cell system.
- A2.4. The developed thermal management system sizing methodology was able to size a air-based thermal management systems with for all four CS-23 commuter aircraft considered in this thesis. The developed sizing methodology when applied to a larger, CS-25 aircraft yielded an unrealistic aircraft design.

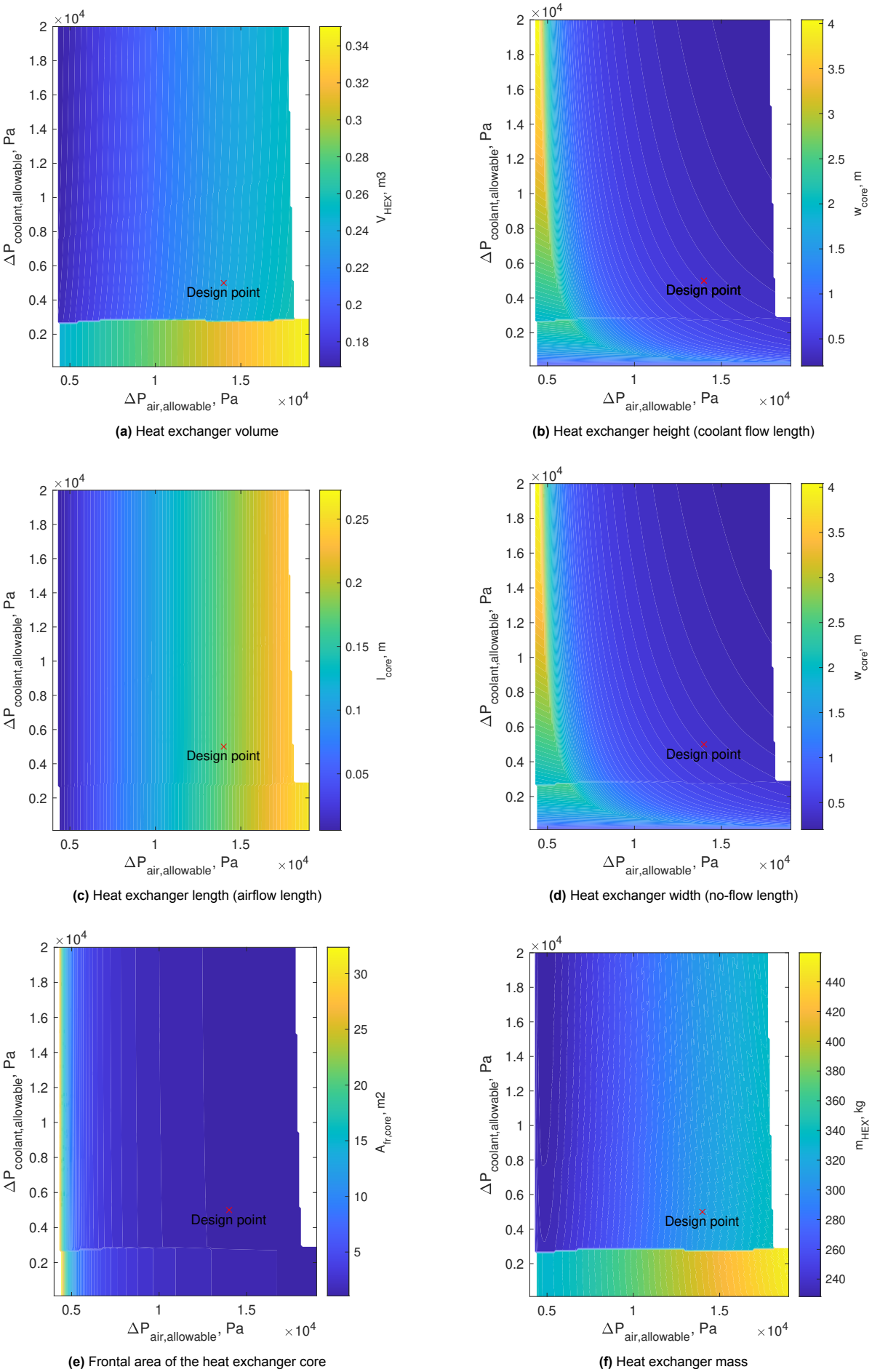

(a) Heat exchanger volume

(b) Heat exchanger height (coolant flow length)

(c) Heat exchanger length (airflow length)

(d) Heat exchanger width (no-flow length)

(e) Frontal area of the heat exchanger core

(f) Heat exchanger mass

Figure IV.3.3: Colour plots of heat exchanger properties as function of allowable pressure drops on air side during take-off and coolant side

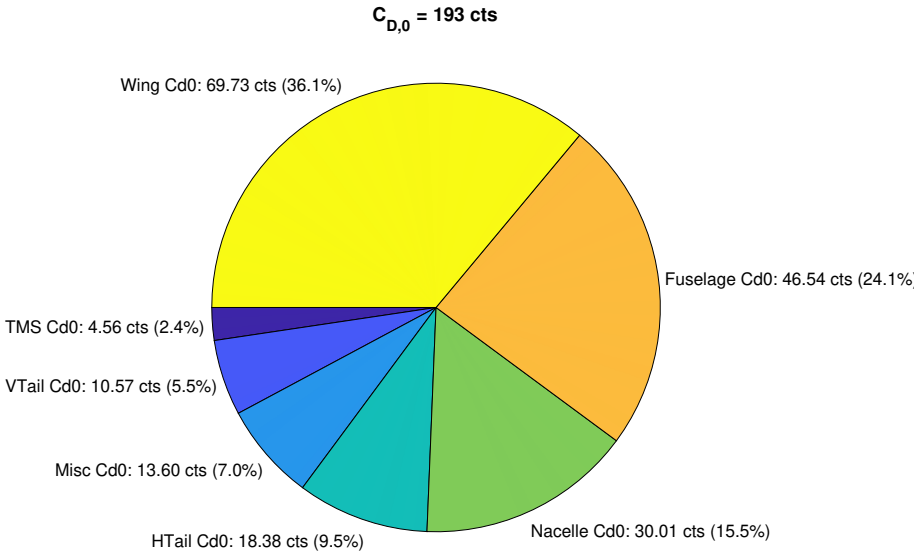

Figure IV.3.4: Zero-lift drag coefficient breakdown of the baseline hybrid-electric aircraft

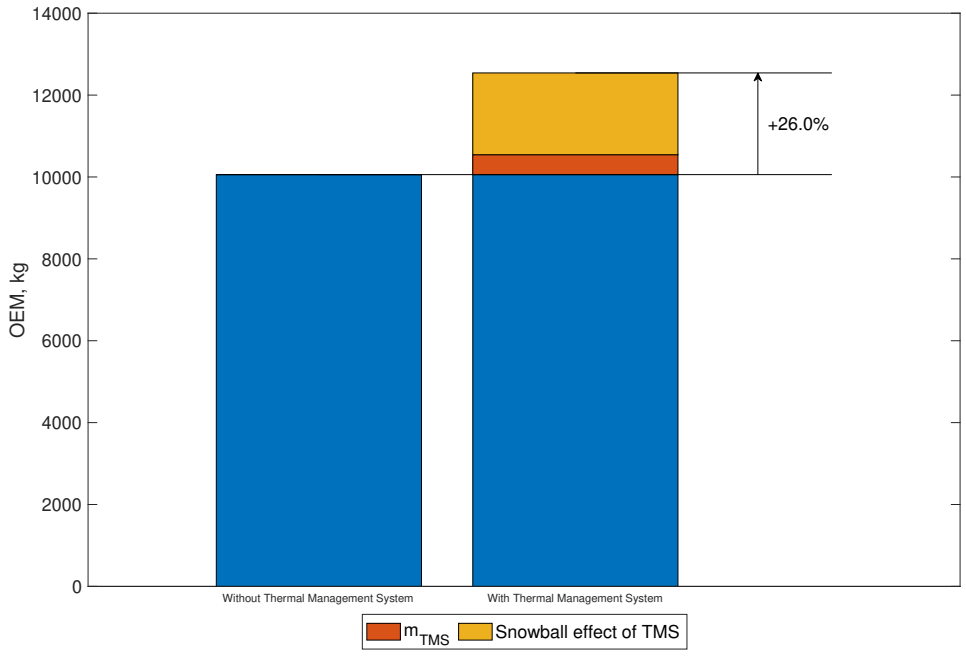

Figure IV.3.5: Comparison of OEM for the baseline aircraft sized with and without considering the thermal management system

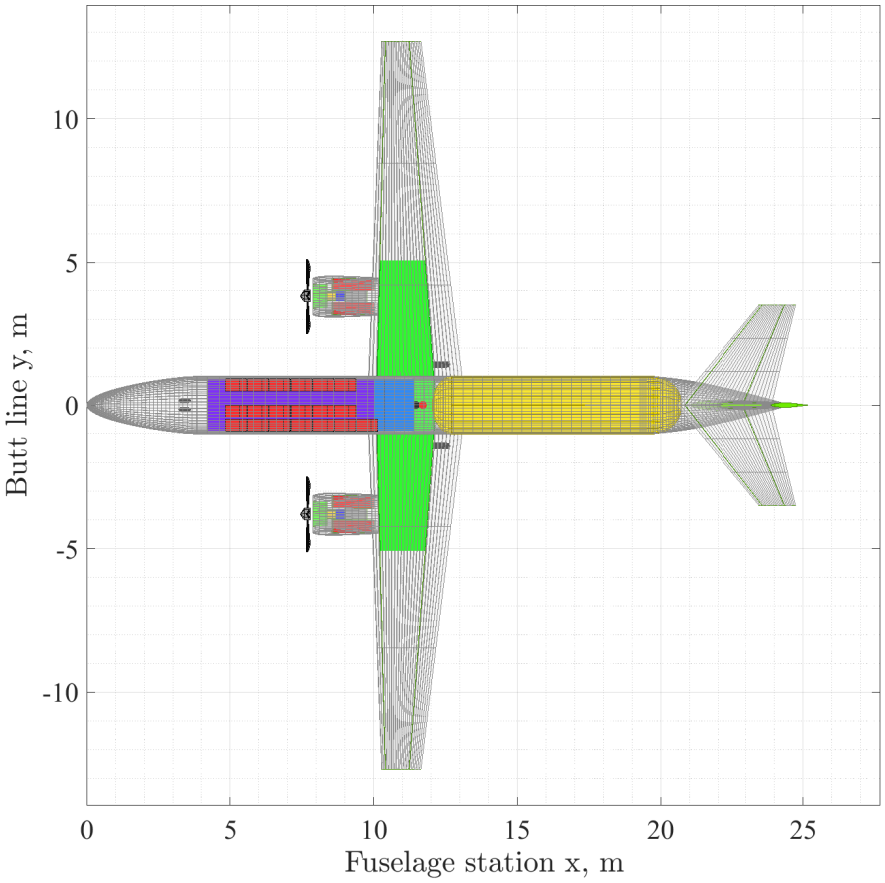

(a) Top view

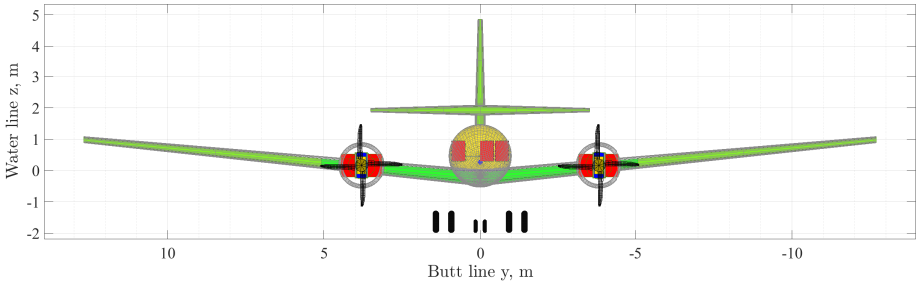

(b) Front view

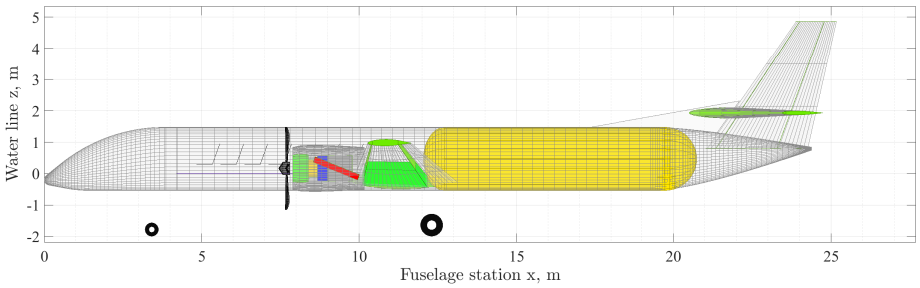

(c) Side view

Figure IV.3.6: Views of the baseline hybrid-electric aircraft based on the Metro 23 sized by the Initiator

References

[1] A.E. Scholz, J. Michelmann, and M. Hornung. “Fuel Cell Hybrid-Electric Aircraft: Design, Operational, and Environmental Impact”. In: *AIAA SciTech 2022 Forum*. Technical University of Munich. San Diego, California: AIAA, Jan. 2020. DOI: 10.2514/6.2022-2333.

[2] A.S.J. van Heerden et al. “Aircraft thermal management: Practices, technology, system architectures, future challenges, and opportunities”. In: *Progress in Aerospace Sciences* 128 (2022), p. 100767. DOI: 10.1016/j.paerosci.2021.100767.

[3] B.T. Schiltgen, J.L. Freeman, and D.W. Hall. “Aeropropulsive Interaction and Thermal System Integration within the ECO-150: A Turboelectric Distributed Propulsion Airliner with Conventional Electric Machines”. In: *AIAA Aviation Forum*. Washington, D.C.: AIAA, June 2016. DOI: 10.2514/6.2016-4064.

[4] D. Kožulović. “Heat Release of Fuel Cell Powered Aircraft”. In: *GPPS Chania20*. Hamburg University of Applied Sciences. Sept. 2020. DOI: 10.33737/gpps20-tc-99.

[5] S.F. Hoerner. *Fluid-Dynamic Drag*. 2nd ed. Bakersfield, CA: Hoerner Fluid Dynamics, 1965. ISBN: 978-9-99-119444-8.

[6] D. Guida and M. Minutillo. “Design methodology for a PEM fuel cell power system in a more electrical aircraft”. In: *Applied Energy* 192 (2017), pp. 446–456. DOI: 10.1016/j.apenergy.2016.10.090.

[7] C.A. Snyder et al. *Propulsion Investigation for Zero and Near-Zero Emissions Aircraft*. Tech. rep. NASA TM—2009-215487, 2009. URL: https://ntrs.nasa.gov/citations/20090023315.

[8] G. Inacio et al. “Feasibility Study of Using Liquid Hydrogen Tanks as Energy Carriers and Cooling Agents for a Small Aircraft Powered by PEMFCs”. In: *AeroTech® Digital Summit*. SAE International, Mar. 2022. DOI: 10.4271/2022-01-0009.

[9] E. Vredenborg and F. Thielecke. “Thermal Management Investigations for Fuel Cell Systems On-Board Commercial Aircraft”. In: *SAE 2013 AeroTech Congress & Exhibition*. Hamburg University of Technology. SAE International, Sept. 2013. DOI: 10.4271/2013-01-2274.

[10] A. Thirkell. “Systems study for fuel cell powered more electric aircraft”. PhD thesis. Loughborough, United Kingdom: Loughborough University, 2021. DOI: 10.26174/thesis.lboro.14758005.v1.

[11] D. Comincini. “Modular Approach to Hydrogen Hybrid-Electric Aircraft Design”. MA thesis. Milan, Italy: Politecnico di Milano, 2018. URL: https://www.politesi.polimi.it/handle/10589/143966.

[12] G.L.M. Vonhoff. “Conceptual Design of Hydrogen Fuel Cell Aircraft. Flying on hydrogen for a more sustainable future”. MA thesis. Delft, the Netherlands: Technische Universiteit Delft, Feb. 2021. URL: http://resolver.tudelft.nl/uuid:8bd63dec-b67b-496b-92bc-3d5c07ff859f.

[13] J.W. Chapman, S.L. Schnulo, and M.P. Nitzsche. “Development of a Thermal Management System for Electrified Aircraft”. In: *AIAA SciTech 2020 Forum*. NASA. Orlando, Florida, Jan. 2020. DOI: 10.2514/6.2020-0545.

[14] D. Juschus. “Preliminary Propulsion System Sizing Methods for PEM Fuel Cell Aircraft”. MA thesis. the Netherlands: Technische Universiteit Delft, Oct. 2021. URL: http://resolver.tudelft.nl/uuid:fdc14875-175e-4a4b-8cde-f2f4b6028194.

[15] A.L. Dicks and D.A.J. Rand. *Fuel Cell Systems Explained*. 3rd ed. Chichester, England: John Wiley & Sons Inc, 2018. ISBN: 978-1-11-870699-2. DOI: 10.1002/9781118706992.

[16] E.G. Waddington, J.M. Merret, and P.J. Ansell. “Impact of LH_2 Fuel Cell-Electric Propulsion on Aircraft Configuration and Integration”. In: *AIAA AVIATION 2021 FORUM*. University of Illinois Urbana-Champaign. AIAA, Aug. 2021. DOI: 10.2514/6.2021-2409.

[17] K.A. Friedrich et al. “Fuel Cell Systems for Aircraft Application”. In: *ECS Transactions* 25.1 (Sept. 2009), pp. 193–202. DOI: 10.1149/1.3210571.

[18] R. O’Hayre et al. *Fuel Cell Fundamentals*. 3rd ed. Chichester, England: John Wiley & Sons Inc, 2016. ISBN: 978-1-5231-1024-7.

[19] J. Ramousse et al. “Heat sources in proton exchange membrane (PEM) fuel cells”. In: *Journal of Power Sources* 192 (2009), pp. 435–441. DOI: 10.1016/j.jpowsour.2009.03.038.

[20] R. Singh, A.S. Oberoi, and R. Singh. “Factors influencing the performance of PEM fuel cells: A review on performance parameters, water management, and cooling techniques”. In: *Int J Energy Res.* 46 (2021), pp. 3810–3842. DOI: 10.1002/er.7437.

[21] J. Xu et al. “Progress and perspectives of integrated thermal management systems in PEM fuel cell vehicles: A review”. In: *Renewable and Sustainable Energy Reviews* 155 (2022), p. 111908. DOI: 10.1016/j.rser.2021.111908.

[22] A. Faghri and Z. Guo. “Challenges and opportunities of thermal management issues related to fuel cell technology and modeling”. In: *International Journal of Heat and Mass Transfer* 48 (2005), pp. 3891–3920. DOI: 10.1016/j.ijheatmasstransfer.2005.04.014.

[23] G. Zhang and S.G. Kandlikar. “A critical review of cooling techniques in proton exchange membrane fuel cell stacks”. In: *International Journal of Hydrogen Energy* 37 (2012), pp. 2412–2429. DOI: 10.1016/j.ijhydene.2011.11.010.

[24] S. Rashidi et al. “Progress and challenges on the thermal management of electrochemical energy conversion and storage technologies: Fuel cells, electrolysers, and supercapacitors”. In: *Progress in Energy and Combustion Science* 88 (2022), p. 100966. DOI: 10.1016/j.pecs.2021.100966.

[25] E. Afshari, N. Jahantigh, and S. Ali Atyabi. “Chapter 16 - Configuration of proton exchange membrane fuel cell gas and cooling flow fields”. In: *PEM Fuel Cells*. Ed. by G. Kaur. Elsevier, 2022, pp. 429–463. ISBN: 978-0-12-823708-3. DOI: https://doi.org/10.1016/B978-0-12-823708-3.00008-0.

[26] Y. Huang et al. “Thermal management of polymer electrolyte membrane fuel cells: A critical review of heat transfer mechanisms, cooling approaches, and advanced cooling techniques analysis”. In: *Energy Conversion and Management* 254 (2022), p. 115221. DOI: 10.1016/j.enconman.2022.115221.

[27] M.H.S. Bargal et al. “Liquid cooling techniques in proton exchange membrane fuel cell stacks: A detailed survey”. In: *Alexandria Engineering Journal* 59 (2020), pp. 635–655. DOI: 10.1016/j.aej.2020.02.005.

[28] Q. Chen et al. “Thermal management of polymer electrolyte membrane fuel cells: A review of cooling methods, material properties, and durability”. In: *Applied Energy* 286 (2021), p. 116496. DOI: 10.1016/j.apenergy.2021.116496.

[29] S.G. Kandlikar and Z. Lu. “Thermal management issues in a PEMFC stack – A brief review of current status”. In: *Applied Thermal Engineering* 29 (2009), pp. 1276–1280. DOI: 10.1016/j.applthermaleng.2008.05.009.

[30] T.H. Bradley et al. “Development and experimental characterization of a fuel cell powered aircraft”. In: *Journal of Power Sources* 171 (2007), pp. 793–801. DOI: 10.1016/j.jpowsour.2007.06.215.

[31] B. Shabani and J. Andrews. “An experimental investigation of a PEM fuel cell to supply both heat and power in a solar-hydrogen RAPS system”. In: *International Journal of Hydrogen Energy* 36 (2011), pp. 5442–5452. DOI: 10.1016/j.ijhydene.2011.02.003.

[32] I. Tolji et al. “Thermal management of edge-cooled 1 kW portable proton exchange T membrane fuel cell stack”. In: *Applied Energy* 257 (2020), pp. 1–19. DOI: 10.1016/j.apenergy.2019.114038.

[33] C.-Y Wen and G.-W. Huang. “Application of a thermally conductive pyrolytic graphite sheet to thermal management of a PEM fuel cell”. In: *Journal of Power Sources* 178 (2008), pp. 132–140. DOI: 10.1016/j.jpowsour.2007.12.040.

[34] K.A. Burke. “Advanced Fuel Cell System Thermal Management for NASA Exploration Missions”. In: *6th International Energy Conversion Engineering Conference (IECEC)*. 2008. DOI: 10.2514/6.2008-5795.

[35] R. Flückiger et al. “Thermal analysis and optimization of a portable, edge-air-cooled PEFC stack”. In: *Journal of Power Sources* 172 (2007), pp. 324–333. DOI: 10.1016/j.jpowsour.2007.05.079.

[36] S.M.H. Hasmi. “Cooling Strategies for PEM FC Stacks”. PhD thesis. Hamburg, Germany: Helmut-Schmidt-Universität / Universität der Bundeswehr Hamburg, 2010. URL: https://www.hsu-hh.de/thermodynamik/wp-content/uploads/sites/741/2017/09/Dissertation-Hashmi.pdf.

[37] A. Baroutaij et al. “Advancements and prospects of thermal management and waste heat recovery of PEMFC”. In: *International Journal of Thermofluids* 9 (2021), p. 100064. DOI: 10.1016/j.ijft.2021.100064.

[38] K.A. Burke, I. Jakupca, and A. Colozza. “Development of Passive Fuel Cell Thermal Management Technology”. In: *7th International Energy Conversion Engineering Conference* (2009), pp. 1–13. DOI: 10.2514/6.2009-4656.

[39] M.R. Islam et al. “The potential of using nanofluids in PEM fuel cell cooling systems: A review”. In: *Renewable and Sustainable Energy Reviews* 48 (2015), pp. 523–539. DOI: 10.1016/j.rser.2015.04.018.

[40] A.A. Hmad and N. Dukhan. “Cooling Design for PEM Fuel-Cell Stacks Employing Air and Metal Foam: Simulation and Experiment”. In: *Energies* 14.9 (2021), pp. 1–19. DOI: 10.3390/en14092687.

[41] A. Fly and R.H. Thring. “Temperature regulation in an evaporatively cooled proton exchange membrane fuel cell stack”. In: *International Journal of Hydrogen Energy* 40 (2015), pp. 11976–11982. DOI: 10.1016/j.ijhydene.2015.04.086.

[42] A. Fly and R.H. Thring. “A comparison of evaporative and liquid cooling methods for fuel cell vehicles”. In: *International Journal of Hydrogen Energy* 41 (2016), pp. 14217–14229. DOI: 10.1016/j.ijhydene.2016.06.089.

[43] Irnie Zakaria et al. “Thermal analysis of Al_2O_3-water ethylene glycol mixture nanofluid for single PEM fuel cell cooling plate: An experimental study”. In: *International Journal of Hydrogen Energy* 41.9 (2016), pp. 5096–5112. DOI: 10.1016/j.ijhydene.2016.01.041.

[44] S.C. Kim et al. “Performance evaluation of a stack cooling system using CO2 air conditioner in fuel cell vehicles”. In: *International Journal of Refrigeration* 32 (2009), pp. 70–77. DOI: 10.1016/j.ijrefrig.2008.07.003.

[45] M.R. Islam, B. Shabani, and G. Rosengarten. “Nanofluids to improve the performance of PEM fuel cell cooling systems: A theoretical approach”. In: *Applied Energy* 178 (2016), pp. 660–671. DOI: 10.1016/j.apenergy.2016.06.090.

[46] J.P. Meyers et al. “Evaporatively-Cooled PEM Fuel-Cell Stack and System”. In: *ECS Transactions* 3.1 (2006), pp. 1207–1214. DOI: 10.1149/1.2356240.

[47] A. Nag Srinath et al. “Thermal Management System Architecture for Hydrogen-Powered Propulsion Technologies: Practices, Thematic Clusters, System Architectures, Future Challenges, and Opportunities”. In: *Energies* 15.1 (2022), pp. 1–45. DOI: 10.3390/en15010304.

[48] U. Soupremanien et al. “Tools for designing the cooling system of a proton exchange membrane fuel cell”. In: *Applied Thermal Engineering* 40 (2012), pp. 161–173. DOI: 10.1016/j.applthermaleng.2012.02.008.

[49] Y. Nonobe. “Development of the Fuel Cell Vehicle Mirai”. In: *IEEJ Transactions on Electrical and Electronic Engineering* 12 (2017), pp. 5–9. DOI: 10.1002/tee.22328.

[50] J.W. Pratt et al. “Proton exchange membrane fuel cells for electrical power generation on-board commercial airplanes”. In: *Applied Energy* 101 (2013), pp. 776–796. DOI: 10.1016/j.apenergy.2012.08.003.

[51] J.K. Nøland et al. “Dual Use of Liquid Hydrogen in a Next-Generation PEMFC-Powered Regional Aircraft with Superconducting Propulsion”. In: *IEEE Transaction on Transportation Electrification* x (2022), p. x. DOI: 10.1109/TTE.2022.3170827.

[52] H. Kellermann et al. “Design and Optimization of Ram Air–Based Thermal Management Systems for Hybrid-Electric Aircraft”. In: *Aerospace* 8.1 (2021). DOI: 10.3390/aerospace8010003.

[53] D. Eržen et al. *UNIFIER19 D2.2: Final Concurrent Design Report*. Tech. rep. Pipistrel Vertical Solutions, Politecnico di Milano and Technische Universiteit Delft, July 2021. URL: https://www.unifier19.eu/wp-content/uploads/2021/07/D2.2_Final_concurrent_design_report_Open.pdf.

[54] B.J. Brelje et al. “Development of a Conceptual-Level Thermal Management System Design Capability in OpenConcept”. In: *NATO Research Symposium on Hybrid/Electric Aero-Propulsion Systems for Military Applications (AVT-RSY-323)*. NATO Research and Technology Organization. Trondheim, Norway, Oct. 2019. DOI: 10.14339/STO-MP-AVT-323. URL: https://www.sto.nato.int/publications/STO%5C%20Meeting%5C%20Proceedings/STO-MP-AVT-323/MP-AVT-323-21.pdf.

[55] M. Rütten, L. Krenkel, and M. Freund. “Parametric Design, Comparison and Evaluation of Air Intake Types for Bleedless Aircraft”. In: *39th AIAA Fluid Dynamics Conference*. AIAA, June 2009. DOI: 10.2514/6.2009-3902.

[56] L. Piancastelli, L. Frizziero, and G. Donnici. “The Meredith Effect: an efficient way to recover the heat wasted in piston engine cooling”. In: *Journal of Engineering and Applied Sciences* 10.2 (2015). ISSN: 5327–5333. URL: https://www.arpnjournals.com/jeas/research_papers/rp_2015/jeas_0715_2249.pdf.

[57] M.F. Ahlers. “Aircraft Thermal Management”. In: *Encyclopedia of Aerospace Engineering*. John Wiley & Sons, Ltd, 2011. ISBN: 978-0-47-068665-2. DOI: 10.1002/9780470686652.eae046.

[58] T. Theodorsen. “The Fundamental Principles of the N.A.C.A. Cowling”. In: *Journal of the Aeronautical Sciences* 5.5 (1938), pp. 169–174. DOI: 10.2514/8.566.

[59] H. Kellermann, A.L. Habermann, and M. Hornung. “Assessment of Aircraft Surface Heat Exchanger Potential”. In: *Aerospace* 7.1 (2020). DOI: https://doi.org/10.3390/aerospace7010001.

[60] T. Wang, P.B. Martin, and C.P. Britcher. “Surface Heat Exchangers for Aircraft Applications: a technical review and historical survey”. In: *37th Aerospace Meeting & Exhibit Sciences*. AIAA, Jan. 1999. DOI: 10.2514/6.1999-119.

[61] H. Kallath et al. “Computational Study on the Aerodynamics of a Surface-Heated Wing for Thermal Management”. In: *AIAA Journal* 58.10 (2020), pp. 4339–4356. DOI: 10.2514/1.J059220.

[62] J.L. Anibal, C.A. Mader, and J.R.R.A. Martins. “Aerodynamic shape optimization of an electric aircraft motor surface heat exchanger with conjugate heat transfer constraint”. In: *International Journal of Heat and Mass Transfer* 189 (2022). DOI: 10.1016/j.ijheatmasstransfer.2022.122689.

[63] N. Beck et al. “Drag Reduction by Laminar Flow Control”. In: *Energies* 11.1 (2018). DOI: 10.3390/en11010252.

[64] H. Kellermann et al. “Assessment of fuel as alternative heat sink for future aircraft”. In: *Applied Thermal Engineering* 170 (2020), p. 114985. DOI: 10.1016/j.applthermaleng.2020.114985.

[65] V.G. Gkoutzamanis et al. “Thermal Management System Considerations for a Hybrid-Electric Commuter Aircraft”. In: *Journal of Thermophysics and Heat Transfer* 36.3 (2022), pp. 650–666. DOI: 10.2514/1.T6433.

[66] M. Shi et al. “Design and Analysis of the Thermal Management System of a Hybrid Turboelectric Regional Jet for the NASA ULI Program”. In: *AIAA Propulsion and Energy 2020 Forum*. Georgia Institute of Technology. Aug. 2020. DOI: 10.2514/6.2020-3572.

[67] B. Abderezzak, M. Hinaje, and J. Leveque. “Experimental potential of exploiting PEMFCSs waste heat using TEG modules”. In: *Mediterranean Journal of Modeling and Simulation* 11 (2019), pp. 20–35. URL: https://oaji.net/articles/2019/1983-1570526992.pdf.

[68] G. Romeo et al. “Air Cooling of a Two-Seater Fuel Cell-Powered Aircraft: Dynamic Modeling and Comparison with Experimental Data”. In: *Journal of Aerospace Engineering* 25.3 (2012), pp. 356–368. DOI: 10.1061/(ASCE)AS.1943-5525.0000138.

[69] N. Lapeña-Rey et al. “The Boeing Fuel Cell Demonstrator Airplane”. In: *Aerospace Technology Congress & Exhibition*. Boeing. Los Angeles, California: SAE International, Sept. 2007. DOI: 10.4271/2007-01-3906.

[70] N. Lapeña-Rey et al. “Environmentally friendly power sources for aerospace applications”. In: *Journal of Power Sources* 181 (2008), pp. 353–362. DOI: 10.1016/j.jpowsour.2007.11.045.

[71] N. Lapeña-Rey et al. “First Fuel-Cell Manned Aircraft”. In: *Journal of Aircraft* 47.6 (2010). DOI: 10.2514/1.42234.

[72] P. Rathke et al. “Antares DLR-H2 – Flying Test Bed for Development of Aircraft Fuel Cell Systems”. In: *ECS Transactions* 51.1 (2013), pp. 229–241. DOI: 10.1149/05101.0229ecst.

[73] J. Kallo et al. “Fuel Cell Systems for Aircraft Application & Antares DLR-H2 All-Electric Flying Testbed”. In: *51st AIAA Aerospace Sciences Meeting including the New Horizons Forum and Aerospace Exposition*. DLR. Grapevine, Texas: AIAA, Jan. 2013. DOI: 10.2514/6.2013-936.

[74] S. Flade et al. “Comparison of Anode Configurations During Long Distance Flight in Fuel Cell Powered Aircraft Antares DLR-H2”. In: *AIAA SciTech Forum 52nd Aerospace Sciences Meeting*. DLR. National Harbor, Maryland: AIAA, Jan. 2014. DOI: 10.2514/6.2014-0530.

[75] G. Romeo et al. “Engineering Method for Air-Cooling Design of Two-Seat Propeller-Driven Aircraft Powered by Fuel Cells”. In: *Journal of Aerospace Engineering* 24.1 (2011), pp. 79–88. DOI: 10.1061/(ASCE)AS.1943-5525.0000055.

[76] G. Romeo et al. “ENFICA-FC: Design of transport aircraft powered by fuel cell & flight test of zero emission 2-seater aircraft powered by fuel cells fueled by hydrogen”. In: *International Journal of Hydrogen Energy* 38 (2012), pp. 469–479. DOI: 10.1016/j.ijhydene.2012.09.064.

[77] G. Correa et al. “Flight test validation of the dynamic model of a fuel cell system for ultra-light aircraft”. In: *Journal of Aerospace Engineering* 229.5 (2015), pp. 917–932. DOI: 10.1177/0954410014541081.

[78] M. Podlaski et al. “Initial Steps in Modeling of CHEETA Hybrid Propulsion Aircraft Vehicle Power Systems using Modelica”. In: *AIAA Propulsion and Energy 2020 Forum*. AIAA, Aug. 2020. DOI: 10.2514/6.2020-3580.

[79] W. Stautner, P.J. Ansell, and K.S. Haran. “CHEETA: An All-Electric Aircraft Takes Cryogenics and Superconductivity on Board: Combatting climate change”. In: *IEEE Electrification Magazine* 10.2 (2022), pp. 34–42. DOI: 10.1109/MELE.2022.3165948.

[80] D. Comincini and L. Trainelli. “A Powertrain Sizing Method for Hydrogen-Driven Aircraft”. In: *15th Pegasus-AIAA Student Conference*. Politecnico di Milano. Glasgow, United Kingdom: PEGASUS, Apr. 2019. URL: https://re.public.polimi.it/handle/11311/1082702.

[81] L. Trainelli et al. “Sizing and Performance of Hydrogen-Driven Airplanes”. In: *AIDAA XXV International Congress*. Politecnico di Milano. Rome, Italy: Italian Association of Aeronautics and Astronautics, Sept. 2019. URL: https://mahepa.eu/wp-content/uploads/2020/06/Sizing-and-Performance-of-Hydrogen-Driven-Airplanes.pdf.

[82] M. Drela. “Aerodynamics of Heat Exchangers for High-Altitude Aircraft”. In: *Journal of Aircraft* 33.2 (1996), pp. 176–184. DOI: 10.2514/3.46919.

[83] R.K. Shah and M.S. Bhatti. “Laminar convective heat transfer in ducts”. In: *Handbook of single-phase convective heat transfer* 3 (1987), pp. 1–137.

[84] J.E. Hesselgreaves, R. Law, and D. Reay. *Compact Heat Exchangers. Selection, Design and Operation*. Oxford, United Kingdom: Butterworth-Heinemann, 2016. ISBN: 978-0-08-100306-0.

[85] P. Vocale. “Influence of Thermal Boundary Conditions and Number of Channels on the Performance of Heat Sinks with Rectangular Minichannels”. In: *Micromachines* 13.8 (2022). DOI: 10.3390/mi13081236.

[86] R.K. Shah and A. L. London. *Compact Heat Exchangers*. Cambridge, MA: Academic Press, 1978, p. 477. ISBN: 978-0-12-020051-1.

[87] W. M. Kays and M. E. Crawford. *Convective Heat and Mass Transfer*. 2nd ed. McGraw-Hill New York, 1987, p. 420. ISBN: 978-0-07-033457-1.

[88] W. M. Kays and A. L. London. *Compact Heat Exchangers*. 3rd ed. New York: McGraw-Hill, 1984, p. 335. ISBN: 978-0-07-033418-2.

[89] F. P. Incropera et al. *Fundamentals of Heat and Mass Transfer*. 6th ed. John Wiley & Sons, 2007. ISBN: 978-0-471-45728-2.

[90] R. K. Shah and D. P. Sekulić. *Fundamentals of Heat Exchanger Design*. John Wiley & Sons, 2003. ISBN: 978-0-471-32171-2. DOI: 10.1002/9780470172605.

[91] Ian H. Bell et al. "Pure and Pseudo-pure Fluid Thermophysical Property Evaluation and the Open-Source Thermophysical Property Library CoolProp". In: *Industrial & Engineering Chemistry Research* 53.6 (2014), pp. 2498–2508. DOI: 10.1021/ie4033999. URL: http://pubs.acs.org/doi/abs/10.1021/ie4033999.

[92] VDI e. V., ed. *VDI Heat Atlas*. 2nd ed. Germany: Springer Berlin, Heidelberg, 2010. DOI: 10.1007/978-3-540-77877-6.

[93] American Society of Heating, Refrigerating and Air-Conditioning Engineers, Inc. (ASHRAE). *2021 ASHRAE® Handbook - Fundamentals (SI Edition)*. American Society of Heating, Refrigerating and Air-Conditioning Engineers, Inc. (ASHRAE), 2021. ISBN: 978-1-947192-90-4.

[94] A. Datta. *PEM Fuel Cell MODEL for Conceptual Design of Hydrogen eVTOL Aircraft*. Tech. rep. NASA CR-0284, Jan. 2021. URL: https://ntrs.nasa.gov/citations/20210000284.

[95] T. Tomažič. "Fuel Cell and Hydrogen Technologies in Aviation". In: Cham, Switzerland: Springer International Publishing, 2022. Chap. Fuel Cell–Powered Passenger Aircrafts, pp. 83–95. ISBN: 978-3-030-99018-3. DOI: 10.1007/978-3-030-99018-3_4.

[96] S. G. Kandlikar et al. *Heat Transfer and Fluid Flow in Minichannels and Microchannels*. 2nd ed. Butterworth-Heinemann, 2014. ISBN: 978-0-08-098346-2. DOI: 10.1016/C2011-0-07521-X.

[97] Y. A. Cengel and J. M. Cimbala. *Fluid Mechanics*. McGraw-Hill, 2004. Chap. Flow in Pipes, pp. 321–398. ISBN: 978-0-47-247236-3.